DESIGN AND CHARACTERIZATION OF MULTIWAVELENGTH FIBER LASER IN O-BAND TRANSMISSION WINDOW

SITI FATIMAH BINTI NORIZAN

THESIS SUBMITTED IN FULLILMENT OF THE REQUIREMENTS FOR THE DEGREE OF PHILOSOPHY

DEPARTMENT OF PHYSICS

FACULTY OF SCIENCE

UNIVERSITY OF MALAYA

2015

Abstract

This thesis presents the research work that has been carried out on O-band transmission windows as support to the saturated optical fiber transmission windows. O-band is selected based on advantages it offer including operational cost effectiveness, low absorption coefficient, low dispersion wavelength range and operated with existence system. The aim of this research work is to investigate the components that could be used in developing O-band as transmission windows. The components studied in this research work are the optical amplifiers and multiwavelength fiber laser as the transmitter. The optical amplifiers are Bismuth doped fiber amplifier (BiDFA), O-band Raman fiber amplifier (RFA) and Booster optical amplifier (BOA). The BiDFA produce low amplification (~2 dB) but high nonlinearity coefficient measured to be 13.98 W^{-1} km^{-1} utilizing the four wave mixing (FWM) effect. The RFA was tested with 4 different types of fiber, where dispersion compensated fiber (DCF) shows the highest amplification performance with gain of 12 dB for single pass configuration and 14 dB for double pass at 1330 nm signal wavelength. The BOA is an improved version of semiconductor optical amplifier (SOA) capable to amplify up to 28 dB and 31 dB at 1350 nm for single pass and double pass configuration respectively. The optical amplifier is not only use as the amplifier but also to support the process of generating multiwavelength fiber laser (MWFL). Three techniques demonstrated in this thesis include; multiwavelength Brillouin fiber laser (MWBFL), Sagnac loop mirror (SLM) and Fabry Perot Interferometer. The MWFL was demonstrated by various configurations to investigate the performance including its peak power flatness and tune ability. The MWBFL generated from nonlinear effect of stimulated Brillouin scattering (SBS). The Brillouin threshold power required to generate SBS in O-band is less than threshold of C-band. The MWBFL demonstrated in 2 different cavites namely linear cavity and ring cavity. Both cavities produce 4 Stokes with the linear cavity giving a

closed spacing of 12.5 GHz while ring cavity 25 GHz. Inserting BOA in the multi pass linear configuration induce nonlinearity and hence produces 3 anti-Stokes signals. The flatness of MWBFL achieved via 2 techniques namely by in cooperate the BiDF in the cavity to provide FWM effects and by relocating the BOA. The spacing tunability for MWBFL is limited to two spacing 12.5 GHz and 25 GHz. Sagnac loop mirror were also demonstrated in linear and ring cavity, where the linear cavity provide stable and more number of channels (~16). The uniformity of MWFL via SLM was provided by the nonlinearity of BIDF. The tunability of the SLM is controlled by the length of polarization maintaining fiber (PMF). The FPI was only demonstrated in linear configuration. The spacing generated was double of SLM with the same length of PMF. The uniformity of peak power was also improved by the incorporation of BiDF. The tunability is achieved by controlling the polarization state. The spacing varied from 5.0 nm to 1.25 nm with 4 m PMF.

Abstrak

Tesis ini membentangkan kerja-kerja penyelidikan yang telah dijalankan ke atas O-band penghantaran tingkap sebagai sokongan kepada tingkap penghantaran tepu. O-band terpilih berdasarkan kelebihan ia menawarkan keberkesanan operasi termasuk kos, pekali penyerapan rendah, pelbagai serakan panjang gelombang rendah dan dikendalikan dalam sistem kewujudan. Tujuan penyelidikan adalah untuk menyiasat komponen yang boleh menjadi kegunaan dalam membangunkan O-band seperti penghantaran tingkap. Komponen dikaji dalam penyelidikan ini adalah penguat optik dan serat multiwavelength laser sebagai pemancar. Penguat optik termasuk Bismut gentian terdop penguat (BiDFA), O-band Raman serat penguat (RFA) dan Booster penguat optik (BOA). The BiDFA menghasilkan penguatan rendah (~ 2 dB) tetapi pekali ketaklelurusan tinggi diukur menjadi 13,98 W^{-1} km^{-1} menggunakan empat gelombang mencampurkan (FWM) kesan. RFA diuji dengan 4 jenis serat, di mana penyebaran serat pampasan (DCF) menunjukkan prestasi penguatan yang paling tinggi dengan keuntungan sebanyak 12 dB untuk konfigurasi pas tunggal dan 14 dB untuk lulus dua di 1.330 nm panjang gelombang isyarat. BOA ini adalah versi semikonduktor penguat optik (SOA) berjaya untuk menguatkan sehingga 28 dB dan 31 dB pada 1350 nm pas tunggal dan konfigurasi pas dua masing-masing. Penguat optik bukan sahaja menggunakan sebagai penguat tetapi juga untuk menyokong proses menjana laser gentian multiwavelength (MWFL). Tiga teknik ditunjukkan dalam tesis ini termasuk; multiwavelength serat Brillouin laser (MWBFL), Sagnac gelung cermin (SLM) dan Fabry Perot interferometer. The MWFL ditunjukkan oleh pelbagai konfigurasi untuk menyiasat prestasi termasuk kuasa kebosanan kemuncaknya dan keupayaan lagu. The MWBFL dijana daripada kesan tak lelurus dirangsang penyerakan Brillouin (SBS). Kuasa ambang Brillouin diperlukan untuk menjana SBS dalam O-band adalah kurang daripada C-band. The MWBFL menunjukkan dalam 2 rongga rongga yang berbeza dan

cincin iaitu linear rongga. Kedua-dua rongga menghasilkan 4 Stokes dengan rongga linear memberikan jarak 12.5 GHz manakala cincin rongga 25 GHz. Masukkan BOA dalam konfigurasi linear pas berbilang mendorong ketaklelurusan dengan itu menghasilkan 3 anti-Stokes. Kebosanan MWBFL dicapai melalui 2 teknik iaitu dengan bekerjasama dalam yang BiDF dalam rongga untuk meletakkan kesan FWM dan menempatkan semula oleh BOA itu. The tunability jarak untuk MWBFL adalah terhad kepada dua jarak 12.5 GHz dan 25 GHz. The Sagnac cermin gelung juga menunjukkan dalam rongga linear dan cincin, di mana linear yang memberikan jumlah yang stabil dan lebih saluran (~ 16). Keseragaman MWFL melalui SLM menyediakan oleh ketaklelurusan daripada BIDF. The tunability daripada SLM adalah kawalan oleh panjang polarisasi mengekalkan serat (PMF). FPI hanya ditunjukkan dalam konfigurasi linear. Jarak dijana adalah dua daripada SLM dengan panjang sama PMF. Keseragaman kuasa puncak juga bertambah baik dengan bekerjasama yang BiDF. Tunability ini dicapai dengan mengawal keadaan polarisasi. Jarak yang berbeza dari 5.0 nm kepada 1.25 nm dengan 4 m PMF

Acknowledgement

All Praise to God Almighty, I would like to express my special appreciation and thanks to my advisor Professor Dr. Harith Ahmad and Dr. Zamani Zulkifli, you have been a tremendous mentor for me. I would like to thank you for encouraging my research and for allowing me to grow as a research scientist. Your advice on both research as well as on my career have been priceless.

A special thanks to my family. Words cannot express how grateful I am to my my mother, father, and siblings, for all of the sacrifices that you've made on my behalf. Your prayer for me was what sustained me thus far. I would also like to thank all of my friends; especially Amirah, Azura, Haniza and Ahya, who supported me in writing, and incanted me to strive towards my goal. At the end I would like express appreciation to my beloved husband Zarma Nurhaidan, who spent sleepless nights with and was always my support in the moments when there was no one to answer my queries.

Contents

List of Tables

List of figures

Acronyms

ASE	Amplified spontaneous emission
BiDF	Bismuth doped fiber
BiDFA	Bismuth doped fiber amplifier
BOA	Booster optical amplifier
BP	Brillouin pump
C	Coupler
C-band	Conventional band
CPM	Cross phase modulation
DCF	Dispersion compensated fiber
DP	Double pass
DWDM	Dense wavelength division multiplexing
EDF	Erbium doped fiber
EDFA	Erbium doped fiber amplifier
FWM	Four wave mixing
FWHM	Four width half maximum
FPI	Fabry perot interferometer
FTTH	Fiber to the home
FUT	Fiber under test

L-band	Long band
MFD	Mode field diameter
MWBFL	Multiwavelength Brillouin fiber laser
MWFL	Multiwavelength fiber laser
NF	Noise figure
O-band	Original band
OC	Optical circulator
OCS	Optical channel selector
OL	Objective lens
OPM	Optical power meter
OSA	Optical spectrum analyser
PC	Polarization controller
PCF	Polarization crystal fiber
PMF	Polarization maintaining fiber
RFA	Raman fiber amplifier
RP	Raman pump
S-band	Short band
SBS	Stimulated Brillouin scattering
SLM	Sagnac loop mirror

SMF	Single mode fiber
SNR	Signal to noise ratio
SOA	Semiconductor optical amplifier
SP	Single pass
SPM	Self phase modulation
SRS	Stimulated raman scattering
TLS	Tunable laser source
TWF	True wave reach fiber
WDM	Wavelength division multiplexing
ZDW	Zero wavelength dispersion

Nomenclature

$\Delta\beta$	Phase mismatching
Δv_B	Brillouin pump line width
Δv_p	Pump line width
A_{eff}	Effective core area
D	Displacement of electric field
E	Electric field intensity
f_s	Stokes frequency
G	Signal gain
g_B	Brillouin gain coefficient
$g_B(v_B)$	Center of Brillouin gain coefficient
g_R	Raman gain coefficient
G_R	Raman gain spectrum
I_p	Brillouin pump intensity
I_s	Stokes intensity
L_{eff}	Effective length
n	Refractive index
NA	Numerical aperture
P	Polarization state

P_{FWM}	Power of FWM signal
P_p	Brillouin Pump power
P_s	Signal power
P_{th}	Threshold power
α	Absorption coefficient
β	Birefringence coefficient
γ	Nonlinear coefficient
δ_{FPI}	Phase changes for FPI
δ_{SLM}	Phase changes for SLM
ε_o	Permittivity
η	Efficiency of FWM
λ_p	Pump wavelength
λ_s	Stokes wavelength
v_a	Acoustic velocity
χ_e	Electric susceptibility
ω	Frequency of optical signal

Chapter 1 Introduction

1.1 Overview of fiber optic communication

Optical fiber is important for modern communication world especially in the development of ultra-fast networking system. Rapid networking system through optical communication started with the development of optical fiber with high attenuation of 1000 dB/km @1550nm (Charles, 1970) due to contamination in the fiber glass. Eliminating the impurities of the material reduced the loss to 20dB/km (Kapron, et al. 1970) and not long after with further reduction to only 0.2dB/km (Miya, 1980) and continue to improve. The improvements are not only on the fiber attenuation but also against the quality of the signals such as chromatic dispersion. Optical fiber is a strain of elliptical glass that transmitted light through total internal reflection (TIR) principle (Bates, 2001).The imperfection of the fiber divides the signal into numbers of modes, which disperse along the device. Step index fiber is proposed to overcome the chromatic dispersion effect fiber with different layers of reflective index coating which controls the propagation of the light can transmit single modes light by controlling the size of fiber core is called as single mode fibre (Sanferrare, 1987).

Revolution of optical fiber technology leads to others inventions to support the technology including the transmission source. The frequency of the transmitted signal is around 800 nm and quite recently has improved to 2.0 μm due to current development in the fiber technology. During the first generation of optical fiber communication, the 800 nm signal was used that utilized the GaAs semiconductor laser as transmitter. Then it was replaced by the 1300 nm signal or is called as original window transmission (O-band). The selection is made due to low absorption coefficient of the optical fiber around this region which reduce optical electric (O/E) repeater. Furthermore, based on the zero dispersion curves, the 1300 nm region provide lowest dispersion compared to

other available transmission wavelength. The improvement of absorption coefficient to 0.2 dB/km and the increment of bit rate up to 10 Gb/s has introduced the optical communication to conventional window (C-band) operating at 1550 nm. The conversion of the amplifier from electrical/optical to fully optical has increased the speed of the optical communication and also extends the distance of access transmission. The development of Erbium doped fiber leads to utilization of wavelength division multiplexing which allows multiple signals to be transmitted and amplify simultaneously.

As the traffic demand continue to grow the bit rates also rising in numbers of generations starting with 45 Mbps in 1975 to 100 Tbps in 2010 which multiply the speed almost 10 times for every 4 years. Therefore, proactive measures should be taken to accommodate user needs. One of the measures is to maximising the use of all transmission windows available which consists of expanding the optical amplifier bandwidth, more efficient transceiver/receiver and also improves of optical fiber.

1.2 Demands on expanding telecommunication capacity

The demand for faster and wider capacity of transmission signals has contributed to the fiber optics evolution. Therefore numerous studies have been carried out to find alternatives to cater the demands. There are a number of alternatives to overcome the issue including, increasing the channel bit rate (D. Hillerkuss, 2011), reducing the channel spacing between existing channels to maximize the transmission window utilization, or by exploring a new transmission windows (T. Kasamatsu, 2002). Between these options, the extension of current transmission window is the only options that utilize the existing optical and electrical technologies which minimize the transformations cost. The C-band dominated most of optical communication system due to the performance of EDFA. However, the capacity starts to saturate where it is

approaches the maximum capacity of 100 GHz. Thus, researchers began to explore new transmission windows. Instead of exploring for new transmission windows, it is also possible to extend the operation of existing windows. One of the potential windows that can be extended is O-band operating at wavelength region 1260 nm to 1360 nm. This window has a reliable background as transmission medium before the era of Erbium doped fiber amplifier (E. Desurvire, 1987). There are various advantages of using O-band as the transmission windows including; low fiber absorption coefficient, high potential to be used in wavelength division multiplexing (WDM) system, and also the zero dispersion for standard ITU fiber that makes it a highly potential windows to be use in the long haul transmission system.

1.3 Demand on the improve transmitters

Operating in new transmission windows requires supporting components that have to be compatible with operating wavelength including its transmitter and signal amplifier. Current system is uses semiconductor laser to produce single channel wavelength. The technology is convenience for small bandwidth but due to exponential growth of capacity demand, the system requires high operational cost. Larger space is needed to occupy large number of semiconductor laser for each channel. Moreover, cooling system must be included since the laser diode produces heat and operates at certain temperature. Therefore the transmitter must be improved together with the expansion of transmission window so that the optical system operates effectively.

Optical fiber allows multiple wavelength signals to be transmitted in one single fiber without interfering with each other. This gives a promising solution to the high capacity demands. During 1990s, the exponential growth of the data speed is contributed by the use of the WDM. The WDM is a component that multiplex and demultiplex the signals according to their wavelengths when the signal enters or exit the

fiber optic cable. The technology enables simultaneous data transfer. The WDM is identified using its spacing between adjacent signals.

One of the solutions to minimize the expenses of O-band transmission system is by producing multiwavelength fiber laser (MWFL). The MWFL is a system sequence of lasers at different wavelength which can be used as individual channels. There are various techniques of producing multiwavelength lasers including Fabry Perot interference, multiple fiber Bragg grating, Sagnac loop mirror, and nonlinear effect like Brillouin or four wave mixing effect. Each one has its own characteristic. This thesis focuses on the design and characterization of MWFL using nonlinear techniques and interferometers

1.4 Demands on the new optical amplifier.

The development of optical amplifiers has spawned new generation of telecommunication systems starting with the EDFA for 1.55 μm signal. Optical amplifiers can reduce the dependency on optical-electrical-optical (O/E/O) repeater; it also shortens the time of data transmission since the O/E/O repeater is time consuming. Optical amplifier helps to improve the distance requirement between repeaters from 50 km to 160 km.

Over the years the optical amplifier has undergone several upgrades in terms of type of amplifiers, wavelength ranges, and the quality of the output signal. There are 3 types of optical amplifiers; rare-earth doped optical fiber amplifier, semiconductor optical amplifiers, and also amplifiers generated from manipulating the nonlinearity effects of optical fibers.

Extending the transmission windows required modifications of optical amplifier to ensure the performance of optical communication system. The optical amplifier is not only being used as an amplifier, but it is also been acknowledged to be used as an

optical gain block, optical linear repeater, preamplifier for the weak signal and also as signal seed for fiber laser. In terms of generating fiber lasers, the optical amplifier is one of the important components in many fiber laser demonstrations. It is either used as optical amplifier, signal seeding or both.

In O-band region there are various amplifiers known including Neodymium Doped Fiber Amplifier (NdDFA), Dysprosium Doped Fiber Amplifier (DDFA), Raman Fiber Amplifier (RFA), and Semiconductor Optical Amplifier (SOA). Each of the above amplifiers has its own characteristic, advantages and disadvantages. This thesis will discuss on the characteristic of three amplifiers used in the making of multiwavelength fiber laser. These three amplifiers are a new Bismuth doped fiber amplifier (BiDFA) which is believed to cater amplification for most of the available transmission windows from O-band (1260 nm) to L-band (1620 nm); O-band Raman fiber amplifier (RFA), and integrated circuit amplifier called as O-band Booster optical amplifier (BOA).

1.5 Research Methodology

The research procedure for this research project is described as the flow map in figure 1.1. The research methodology starts with the study of existing optical amplifiers for O-band region and the techniques that are used to generate fiber lasers. The O-band amplifiers were tested to find suitable optical amplifiers to be use in the research work. The research continues with generation of multiwavelength fiber laser by utilizing selected optical amplifier. Then, multiwavelength fiber laser was degenerated using three different methods; nonlinear stimulated Brillouin scattering effect, interferometer techniques including Sagnac loop mirror and Fabry Perot interferometer. The developed lasers are improved in terms of its stability, flexibility, and bandwidth range. This thesis is concluded by suggesting new future works that can be done to improve the performance of this research.

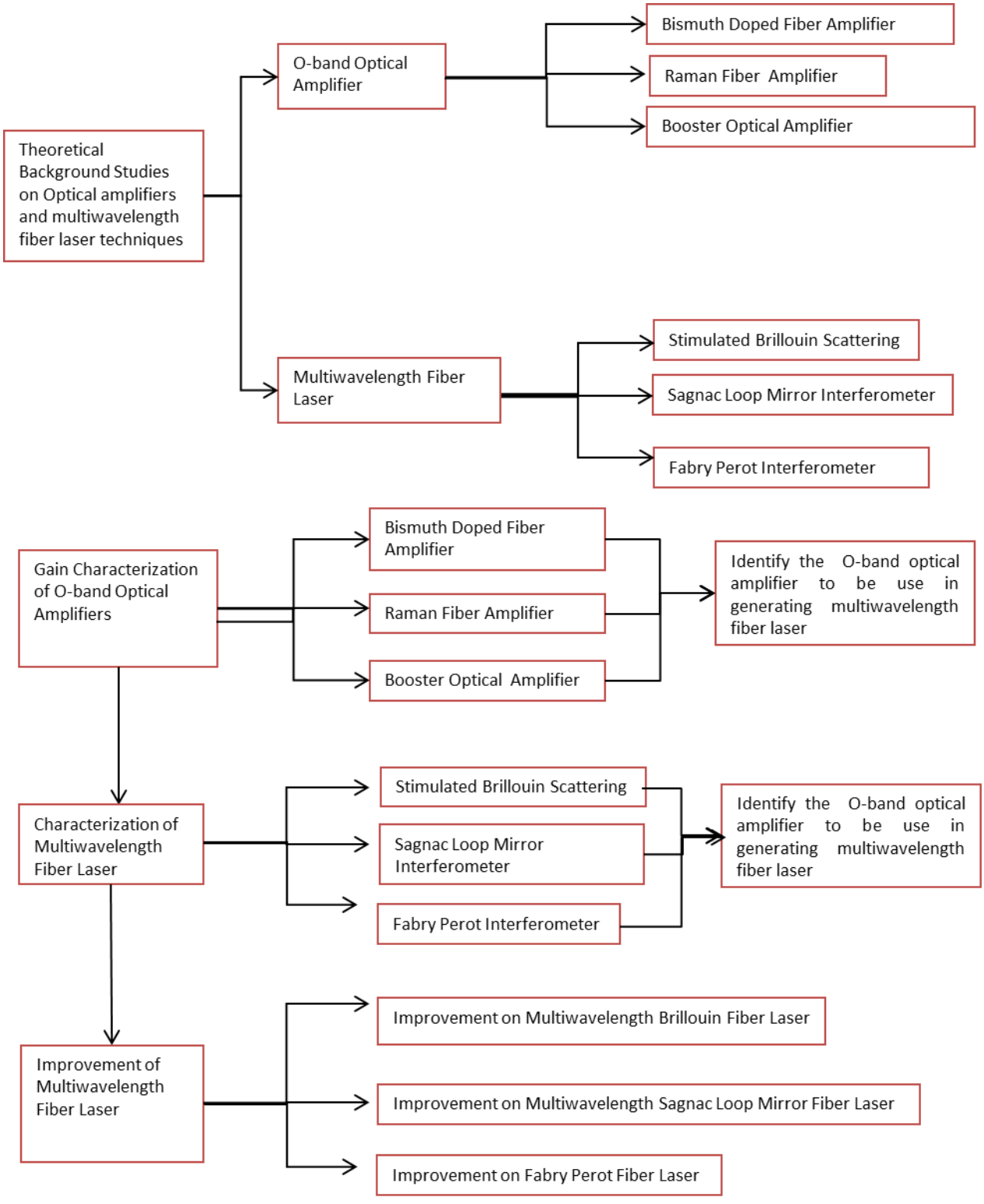

Figure 1.1 Flow chart of research methodology

1.6 Objective of the thesis

Main objective of the research works are;

1) Characterizing the existing O-band amplifier and identifying suitable amplifiers to be used in the generation of multiwavelength fiber laser
2) Designing and characterizing the multiwavelength O-band fiber laser
3) Identify the deficiency of generated O-band multiwavelength fiber laser and to improve the work.
4) Identify the multiwavelength fiber laser techniques that are suitable to be used in WDM system for O-band transmission windows.

1.7 Thesis overview

In this thesis, the focus is given to the development of O-band transmission windows. O-band transmission windows was chosen because of its many advantages mentioned in section 1.2, where the system provides less coefficient absorption and near zero dispersion in ITU standard SMF-28 fiber which minimize the need of optical amplifier. It also requires no extra compensating fiber to be used to suppress the dispersion during transmission. Therefore, the cost expenses to improve from conventional fiber optic communications system can be reduced as compared to other current available transmission windows.

The knowledge on the new transmission windows are not only beneficial to fiber optics communication but can also improve many other applications like development of high power fiber laser, and remote sensory system.

The thesis consists of six chapters where chapter 1 is the introduction to the thesis. Apart from the introduction, three types of optical amplifiers for O-band region are demonstrated in chapter 2, where the characteristics such as gain, noise, stability and

other properties are studied. From the study, the best optical amplifier was chosen according to the requirements needed to develop the O-band multiwavelength fiber laser. In chapter 4, multiwavelength fiber laser are produced by demonstrating three techniques to generate multiwavelength fiber laser, including nonlinear technique which is Stimulated Brillouin Scattering technique, two interferometer techniques one is Sagnac Loop mirror and also Fabry Perot interferometer. From the demonstration, we indicate the techniques that represent certain properties and have different advantages. In the chapter 5, improvements are made to overcome issues such as uneven peak power, unstable output channels and also flexibility on the channels availability. The summary and the future work of this research work are outlined in chapter 6.

Chapter 2 Theoretical Background

2.1 Introduction

Optical fiber technology was not designed solely for application of optical communication, but many other applications including sensor system, navigation system, and a lot more. The use of optical fibers in other fields has stimulated photonic research field including the laser technology. By propagating the laser into the fiber, data communication can be send throughout the world. In early days, the light emitting diode (LED) is used as the transmitter, but due to the increase of the data capacity, LED is no longer an ideal transmitter since its broad emission spectrum limits the ability to increase the transmission capacity. Therefore, the laser is an ideal solution due to its coherence properties, mobility, compact and availability in various frequencies. Laser can be found in many forms like gas laser, semiconductor laser and also optical fiber laser. Optical fiber laser have numerous advantages compared to the others including ultra-narrow emission spectrum, that is useful especially for high precision technologies. The first pulsed optical fiber laser was discovered in 1973, (Stones, 1973) and continuous wave was discovered shortly after.

A part of optical fiber laser, multiwavelength fiber laser also generates interest especially towards improving the wavelength division multiplexing (WDM) system. The multiwavelength lasers have been demonstrated in various techniques including increasing the capacity of the transmission windows. This development has forced and enabled the O-band transmission windows to be reactivated, since the research in this area is less active since the emergence of the Erbium doped fiber amplifier (EDFA) in 1980 that boosted the use of C-band transmission window.

2.2 Multiwavelength Fiber Laser by Nonlinear Effect

2.2.1 Nonlinear effect on optical material

Nonlinear effect is defined as phenomena that depend on the intensity of electric field (Digonnet, 1993). Nonlinearity could be understood through study of dielectric material. Dielectric is typically used to describe materials with high polarity, where whenever the electric field enters the material, the electric charges will not flow through the material as in conductor material. Instead, it will rearrange so that positive charges are displaced toward the field and negative charges shift in the opposite that causes dielectric polarization. Optical fiber is one of the examples of dielectric material, where by making the optical fiber dependent on the intensity of the electric field.

In linear optics, the displacement of electric field, *D* is defined by the equation 2.1;

$$D = \varepsilon_0 E + P \tag{2.1}$$

where *P* represents the polarization induced in the optical medium. In linear and isotropic optical media, the polarization is linearly proportional to the *E* field and is in the same direction as *D*

$$P = \varepsilon_0 \chi_e E \tag{2.2}$$

where the permittivity is represented by ε_0 in vacuum and χ_e is the electric susceptibility. Under small intensity the electrons oscillates with the same frequency as the incident field, therefore the conditions optical properties of the medium (e.g refractive index and absorption coefficient) are independent of the light intensity. However, high intensity electric field rearrange the electron to form an-harmonic motion that makes P satisfies frequencies that does not include the incident frequency

(Boyd, e al. 2003) as given by equation 2.3 as well as linear and nonlinear interactions are illustrated by figure 2.1.

$$P = \varepsilon_0(\chi^1 E + \chi^2 E^2 + \chi^3 E^3 + \cdots) \quad (2.3)$$

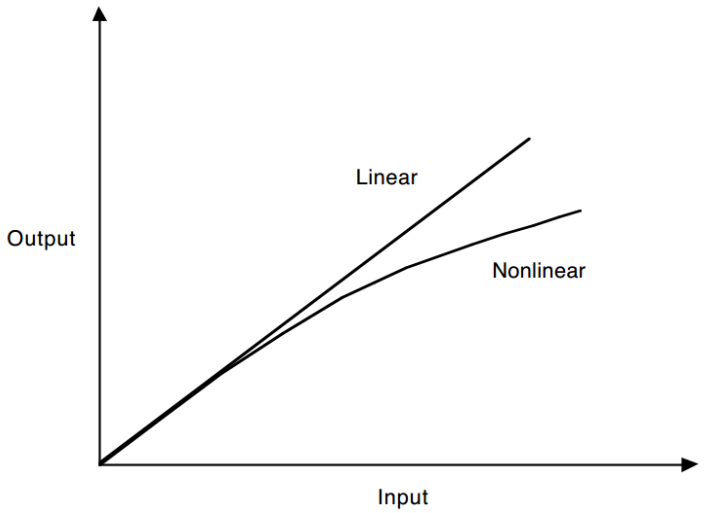

Figure 2.1 Illustration of linear and nonlinear interaction

The relation can be explained through equation of polarization with numbers of susceptibility parameters. The dominant parameters in the equation 2.3 are χ^1 the χ^2 that contributed by the second harmonics generation and sum of frequency generation. Meanwhile, the lowest-order nonlinear effect is contributed by the third susceptibility coefficient, χ^3. The quantity in parentheses indicates that the susceptibility changes with light intensity. In fact, this relation is far a material with a refractive index and absorption coefficient that is intensity dependent. High electromagnetic field in optical fiber may change the orientation of the molecules which results as many implacable such as nonlinear refractive index and inelastic scattering as illustrated in figure 2.2. The nonlinear effect in optical fiber is divided into two categories, which is in nonlinear refractive index effects and inelastic scattering effects.

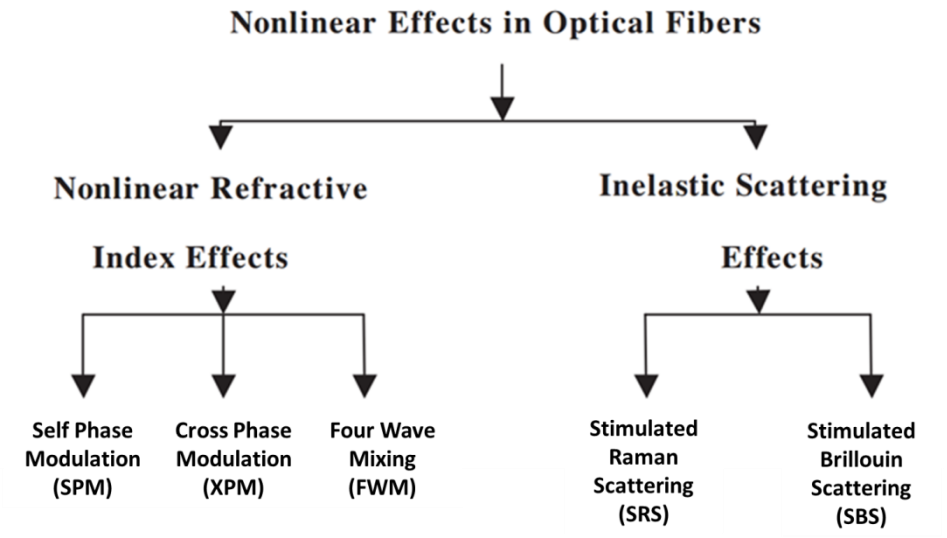

Figure 2.2 Fraction of nonlinear effects

The nonlinear refractive index is an effect when the refractive index changes with the intensity of electric field. This effect includes self-phase modulation (SPM), cross phase modulation (XPM), and four wave mixing (FWM), which is depends on the type of electric field source. Meanwhile, the inelastic scattering effects are generated when the signal channels collides with phonon that stimulate scattering. The stimulated Raman scattering (SRS) is an example of incident electric field that collides with optical phonon while the stimulated Brillouin scattering (SBS) is the collision with acoustic phonon. The intensity of scattered power increases exponentially after the electric field exceeds the threshold value. Brief explanations on each nonlinear effect are summarized below;

(i) Self-Phase Modulation (SPM)

The refractive index depends on the intensity of electric field. If pulse of electric field is used, the leading edge of the source will have different refractive index with the trailing edge. Therefore, it results in temporally varying indexes which leads to temporally varying phase change. This nonlinear phenomenon of self-induced phase modulation is called as Self Phase Modulation (SPM).

(ii) Cross Phase Modulation (XPM)

SPM is a major problem in single channel optical communication. In multiple channels optical communication system, nonlinear effect leads to another problem. Whenever two of more optical pulse propagates in single optical fiber simultaneously, the SPM is generated not only by the modulation of refractive index of the channels but also is affected by other channels. By having multiple numbers of channels in the optical system, another nonlinear phenomenon called Cross Phase Modulation (XPM) is generated. The XPM are twice effective than the SPM with the same amount of electric field intensity.

(iii) Four Wave Mixing (FWM)

All nonlinear effects will generate new channels and suppressing other except for SPM and XPM effect. The FWM generated through the third susceptibility coefficient (χ^3) where whenever there are three different channels propagating in the medium, this (χ^3) will generates the fourth channels that have frequency equals to the frequency sum of all three channels. Meanwhile the power of three initial channels will be suppressed. Detail on FWM effect will be discussed on section 2.2.3.

(iv) Stimulated Raman Scattering (SRS)

Phonon is an excitation of quantum atomic cell at an early stage. Whenever the unit cell contains more than one atom as in optical fiber, two types of phonon will be generated, namely optical phonon and acoustic phonon. Optical phonon is generated when the positives and negatives ions swing against each other. The collision of incident electric field generates SRS. The power of initial high intensity electric field will be transferred into different frequency. Brief explanation is in section 3.3.

(v) Stimulated Brillouin Scattering (SBS)

The collision between incident signal and acoustic phonon generates phenomena which is called as stimulated Brillouin scattering (SBS). The acoustic phonon is produce by the shift of positive and negatives ions that swing together like a moving grating due to the propagation of the electric field. Any photons that collide with this acoustic phonon will generate signals with different frequency. The generated frequency depends on the difference of incident frequency with acoustic phonon frequency which is around 12 THz depending on various parameters of medium and electric field source. Section 2.2.2 will briefly explain the process of stimulated Brillouin scattering.

Previously all these effects are avoided in the optical communication system. However, recent demands on the advanced optical communication technology have encouraged the research towards nonlinear properties of optics. Researches have brought up various applications that have been commercially used today such as multiwavelength fiber laser. The research works here cover the multiwavelength fiber laser generation in the O-band region.

The nonlinear effects that are used to generate the O-band multiwavelength fiber laser are SBS and FWM. The selections are made due to low development cost and minimum adjustment of current system.

2.2.2 Principles of Stimulated Brillouin Scattering

Stimulated Brillouin scattering is generated through an electrostriction process of dielectric medium. High electric field rearranges the refractive index of the medium that changes it into an acoustic phonon and acts like a moving grating. The resulting scattering from collision between the incident light and the acoustic wave is called as Brillouin scattering which moves in backward direction of the incident light as depicted by figure 2.3.

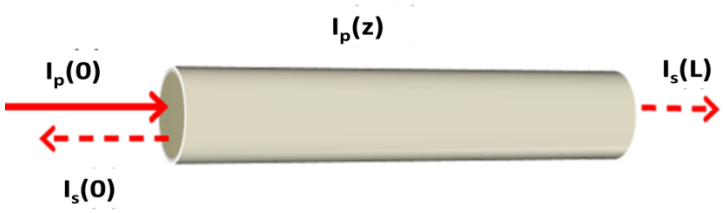

Figure 2.3 Depletion of Brillouin pump and generation of Stokes signal process

The intense light source that trigger the nonlinear effect is defined as Brillouin Pump (BP) while the backscattered signal that is generated is called as Stoke or anti Stokes depending on the frequency shift. The nonlinear interaction between the Brillouin pump and the Stokes wave can be governed by these following coupled equations:

$$\frac{dI_p}{dz} = -g_B I_p I_s - \alpha I_p \tag{2.4}$$

$$\frac{dI_s}{dz} = -g_B I_p I_s + \alpha I_s \tag{2.5}$$

Where I_p and I_s are the intensity of Brillouin pump and Stokes respectively, g_B represent the Brillouin gain coefficient. The process continues until the intensity of the current Stokes power is insufficient to generate a new Stokes. This continuous process generates multiple signals that have slightly different frequency f_s from its Brillouin pump frequency, f_{BP} and is given by equation 2.6,

$$f_s = 2ncv_a/f_{BP} \tag{2.6}$$

Where n is a group refractive index, c as light velocity, and v_a is an acoustic velocity. Multiwavelength Brillouin fiber laser have been demonstrated in many transmission windows (Shirazi, et al. 2008).

2.2.3 Principles of Four Wave Mixing

Four waves mixing (FWM) is one of the nonlinear refraction effects originating from third order susceptibility. The FWM is an intermodulation phenomenon whereby the interaction between two signals generates a third signal called an idler. There are two type of FWM which are non-degenerate and degenerate FWM. Whenever three optical signals with frequencies ω_1, ω_2, and ω_3, propagate inside the fiber simultaneously, (χ^3) generates a fourth field with frequency ω_4, which is related to other frequencies by the relation $\omega_4=\omega_1\pm\omega_2\pm\omega_3$, these frequencies are non-degenerate FWM as shown in figure 2.4 (a). Meanwhile the degenerated FWM is presented by three components that interact and are related by $\omega_3= \omega_1+\omega_1-\omega_2$ shown in figure 2.4 (b). Comparing both types of FWM, it is much easier to produce the idler using non-degenerate FWM.

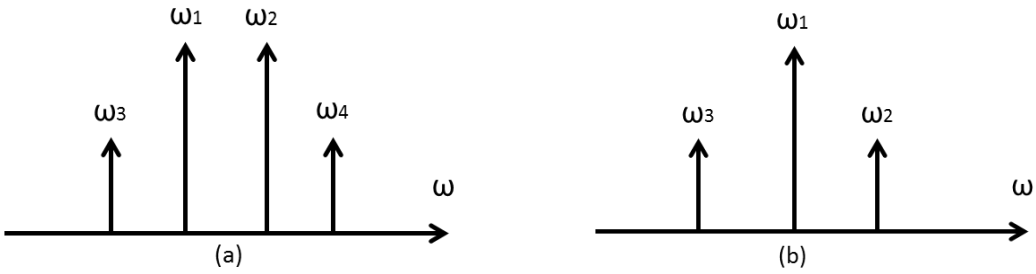

Figure 2.4 Four wave mixing with (a) non degenerate and (b) degenerate.

The non-degenerate FWM consists of two wavelengths known as the pump and the signal. The power of the generated extra signal is also known as FWM signal, P_{FWM} (Inoue, et al. 1992 and Yamamoto, et al. 1997) is represented by equation 2.7.

$$P_{FWM}(L,\Delta\beta)=\eta(\Delta\beta)\gamma^2 L_{eff}{}^2 P_P^2 P_S \exp(-\alpha L) \tag{2.7}$$

where γ is the nonlinear coefficient, L_{eff} is the effective length of the fiber, which is given by

$$L_{eff} = \frac{1}{\propto}(1 - e^{-\propto L}) \tag{2.8}$$

The α represent as absorption coefficient, L length of fiber, and P_s, P_p are power for signal and pump respectively, while $\eta(\Delta\beta)$ is the efficiency of FWM in terms of phase mismatching $\Delta\beta$. The FWM efficiency is a ratio of FWM power over FWM power at $\Delta\beta$ equal to zero, $\eta(\Delta\beta)=\frac{P_{FWM}(\Delta\beta, L)}{P_{FWM}(\Delta\beta = 0, L)}$. Another definition of $\eta(\Delta\beta)$ is written as in equation 2.9.

$$\eta(\Delta\beta) = \frac{\alpha^2}{\alpha^2 + \beta^2}\left[1 + \frac{4\exp(-\alpha L)\sin^2(\Delta\beta L/2)}{\alpha^2 L_{eff}^2}\right] \tag{2.9}$$

The $\Delta\beta$ is given by the difference between the propagation constant $\beta_{FWM} + \beta_S - 2\beta_P$ and $\beta_{FWM,}\ \beta_S$ where β_P are phase for FWM, the signal and propagation constant respectively. When there is no phase mismatching, $\Delta\beta$ is equal to zero which makes $\eta(\Delta\beta)$ to be maximum 1. By replacing the value into equation 2.7 the nonlinear coefficient can be determined. Another solution for phase mismatching is shown in equation 2.10.

$$\Delta\beta = 2\pi\,\Delta f^2\,\frac{\lambda_p^2}{c}\left[(f_p - f_o)\frac{\lambda_p^2}{c}\frac{dD_c}{d\lambda}\right] - \gamma(2P_p - P_s) \tag{2.10}$$

where λ_p is pump wavelength, f_o, f_p and f_s are represented as zero dispersion, pump and signal frequency respectively, $\Delta f = f_{p-} f_s$, and $\frac{dD_c}{d\lambda}$ is the dispersion slope. The term $\gamma(2P_p - P_s)$ represents the nonlinear phase matching factor $\Delta\beta_{NL}$ which is small and can be neglected (Mollenauer, et al. 1996 and Vinegoni, et al. 2002). The four wave mixing is proven technique in producing multiwavelength fiber laser

2.3 Multiwavelength Fiber Laser by Interferometer techniques

2.3.1 Introduction on Interferometer

An interferometer technique is a technique that employs the superposition of electromagnetic waves. The technique is used in many applications including; telecommunication number of sensor applications, military defends, astronomical and also medical. There are number of categories in utilizing this technique, which differ in terms of the properties that includes the properties of EM waves, the propagation path and also the method of splitting and combining the waves.

The properties of EM waves describe the sources that have been used in the interferometer technique. If the waves that superposition have same wavelength it is called as Homodyne otherwise it is called as Heterodyne. The interferometer by Homodyne techniques will affect the intensity and also the pattern of the outgoing signals, where else Heterodyne can be used to generate new wavelength and also to amplify weak signals.

The propagation properties describe the paths that the waves travel before the interference take place. Interferometer process that makes the beams to travel in different paths is called as double paths for example as is Michelson interferometer. Meanwhile, if the beams travel on the same path and interfere between the path it is called as common path. Common path have numbers of example configuration including the Sagnac Loop Mirror, Fabry Perot and gyroscope.

Last categories of interferometer technique are method of splitting and combining waves. If the splitting involving only the amplitude waves it called as amplitude splitting; such as Mach Zehnder, Fabry Perot and Michelson interferometer. The technique is different with the splitting of wave front called as wave front splitting;

Young slit experiment and also Lloyd mirrors. Generating multiwavelength fiber laser utilizing these techniques has been demonstrated through number of experiment.

This project explored 2 interferometer techniques namely, Sagnac Loop mirror and Fabry Perot Interferometers. The selection of these techniques is based on its advantages including; the compactness, low cost expenses, tunability, and possible of future implementation. Furthermore, generating MWFL with the Mach-Zehnder and Michelson interferometer experience polarization induce fading (PIF) effect from propagation into 2 different medium that varies the state of polarization of incident light in an unpredictable manners and leads to interferometric optical mixing efficiency and loss of interference source (Stowe et al. 1982)

2.3.2 Principles of Sagnac Loop Mirror (SLM)

Named after the French physicist Georges Sagnac, Sagnac loop mirror is under a category of homodyne interferometer with a common path way. It also represents interferometer phenomenon that depends on the polarization of light. The effect is generated from one beam source that is spliced into two identical beams and propagates in direction opposite to each other and travel in a ring shape as shown in figure 2.5.

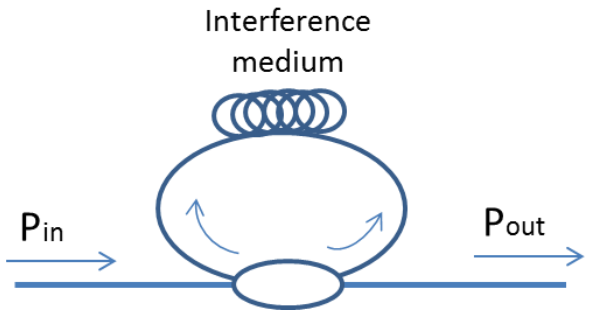

Figure 2.5 Sagnac loop mirror

Initially identical beams travel in the same distance path but due to rotation of the ring, both beams experience changes of phase which can be determined according to equation 2.11

$$\delta_{SLM} = \frac{2\pi}{\lambda} BL \tag{2.11}$$

The birefringence coefficient, *B* is the product of the difference between effective indices of fast and slow modes. The interference between two beams occurs at the point of entry. The product of the interference is in fringe pattern that has periodic spacing. The Sagnac loop mirror provides many advantages including high sensitivity on rotation which makes it favourable for sensor application.

2.3.3 Principles of Fabry Perot Interferometer

The Fabry-Perot Interferometer (FPI) is composed of superposition of incident and reflected beams caused by partially reflected mirror or end face of fiber or both. The reflection can be inside or outside the cavity which is called as intrinsic and extrinsic respectively. The intrinsic FPI is performed by building up the reflector inside the fiber such as fiber Bragg grating as shown in figure 2.6 (a). Therefore, this type of FPI needs special fabrication. The extrinsic FPI is built by just having end face of fiber or partial reflection mirror to create reflection as illustrated in figure 2.6 (b).

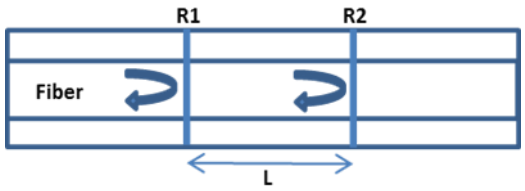

(a)

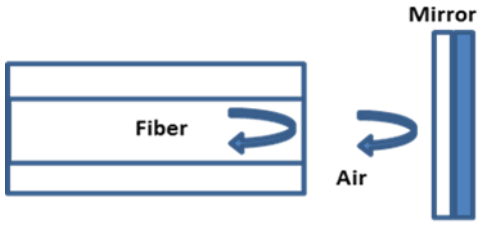

(b)

Figure 2.6 (a) intrinsic and (b) extrinsic Fabry Perot Interferometer

Similar to the Sagnac loop mirror interferometer, the result of the superposition of FPI could also be described by the intensity modulation of incident beams which is caused by the phase difference of incident and reflection beams as described in equation 2.12.

$$\partial_{FPI} = \frac{2\pi}{\lambda} B2L \tag{2.12}$$

2.4 O-band Optical amplifiers

Modern optical amplifier technology can be divided into a numbers of groups. The amplifiers that have been investigated include the one using rare earth fiber amplifier (FOA), nonlinear optical amplifier (NOA) and also solid state gain medium (semiconductor optical amplifier, SOA). The optical amplifier in FOAs and SOAs categories operate on the same principles as the stimulated emission but with different external energy, which provides the population inversion state. Through the process of stimulated emission, the external energy is converted to create population inversion which amplifies the propagating input light signals (Miya et al. 1979). In FOAs, rare earth-doped fibers are the gain medium where rare earth ion is the active ions. Meanwhile, for SOA the gain medium is a semiconductor material and external current injection is the external energy. The NOA operates based on the nonlinear optical principle. The next sub section will shortly explain the properties and ability of each

amplifier, and will determine suitable amplifier to be utilized in generating multiwavelength O-band fiber laser.

2.4.1 Rare earth doped fiber amplifier (FOA)

The amplification source for FOA is an external optical laser source which is different for every fiber depending on their absorption wavelength. The absorption wavelength is the wavelength region where the energy is similar or equal to the energy gap of the active ions that excites to the next energy level. Usually the wavelength of external laser source is lower than the wavelength of the generated signal. Sufficient power of external laser source will generate a population inversion which is the phenomenon that describes higher energy level that has more active ions compared to its lower level. At this stage, the incoming photon from the external laser source will collide with the excited ions and generates another photon with coherence properties as the photons strike it. This process is called as stimulated emission amplification, where the generated photons will collide with the rest of the excited photons and multiply the numbers of coherent photons instantly, therefore created an amplification effect.

The important parameters to determine good optical amplifier are high signal gain, lower noise figure, high signal to noise ratio, high power conversion efficiency and wide wavelength range.

Signal gain of an optical amplifier can be described as ratio of output power, P_{out} over input power, P_{in} as shown in equation 2.13

$$G = \frac{P_{out}}{P_{in}} \tag{2.13}$$

Noise figure determine the level of noise in the signal. It is represent as input signal to noise ratio, SNR_{in} over output signal to noise ratio, SNR_{out} describe equation 2.14

$$NF = \frac{SNR_{in}}{SNR_{out}} \tag{2.14}$$

The signal to noise ratio (SNR) is another way to determine the noise level in the signal by differentiating the signal power to the noise power generated by amplified spontaneous emission (ASE). The ASE spectrum is photons generated when the excited ions decay to the lower ground without any external energy because the ions already exceeded their half lifetime. Meanwhile the power conversion efficiency measures the generated amplified power in comparison to the power from external laser source. The wavelength range is simply the range of wavelength covered by amplifier.

Rare earth doped fiber amplifier or often call as fiber optical amplifier (FOA) was first discovered in Optoelectronic Research Center, Southampton University of London, where the active medium used is trivalent Erbium which amplified mostly in the C-band region (1530 nm-1580 nm). Until now the modified Erbium doped fiber manages to amplify up to 360 nm which cover most of available transmission windows except for O-band. As for O-band there are numbers of rare earth fiber that have been tested with hope it can supply the amplification needs for the future optical telecommunication demand as good as Erbium doped fiber to C-band region. These include Praseodymium Doped Fiber Amplifier (PdDFA), Neodymium Doped Fiber Amplifier (NdDFA), and Dysprosium Doped Fiber Amplifier (DDFA).

Recently, there has been another doped fiber optical amplifier which is proposed through modelling that claims to amplify most of the transmission windows starts from O-band till L-band using Bismuth ions (Chun, 2009). However, until now there are still no demonstration on Bismuth doped fiber that can amplify all transmission windows as claimed. In the case of Bismuth doped fiber, active ion are still undetermined and suggested its contributed by number of other ions.

2.4.2 Nonlinear effect amplifier (NOA)

As described by the title, this type of amplifier utilizes the nonlinear optical effect as the amplification principle. Most of the nonlinear effect can generate amplification but most have efficiency obstacle, where high power is required to produce even a small amplification. However, there are nonlinear effect that can produce exceptional amplification including Raman fiber amplifier (RFA) and also optometric amplifier.

The Raman fiber amplifier (RFA) is a nonlinear effect amplifier that manipulates the stimulated Raman scattering (SRS). The scattering resulted from collision between the photon and the phonon that generates new photons at a lower energy. The rest of the energy will be transferred as non-radiate waves called as phonon. The amplification of RFA, P_o can be described by equation 2.15

$$P_o = \varepsilon_0(\chi^1 + \chi^3 E_{pump}^2)E_{signal} \tag{2.15}$$

The ε_o is the permittivity of fiber, χ^1 and χ^3 first and third susceptibility respectively also electric field of pump and signal represent as E_{pump} and E_{signal} respectively. The pump changes the absorption coefficient of the material, making it negative and producing gain at the signal frequency. The advantage of utilizing this type of amplifier is that the amplification can happen at any frequency depending on the frequency of the pump as long as the pump intensity exceeds its threshold. The spacing between the pump frequency and amplification frequency vary with different type of optical fibers.

2.4.3 Semiconductor optical amplifier

Semiconductor optical amplifier (SOA) is integrated circuit generated amplification through similar operation of rare earth optical amplifier except the medium is a semiconductor material.

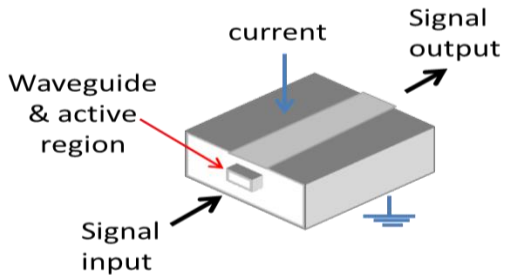

Figure 2.7 Cross section of semiconductor optical amplifier

In the semiconductor laser diode, p-type (rich in hole) and n-type (rich in electron) treated silicon is pile together. The injected current pumps the electrons in the n-type. As the electron flows to the p-type it combined with holes and release photons. The generated photon bounces back and forth in the microscopic junction between slices of P-type and n-type. The continuous process called as stimulated emission process that produces laser effect. The wavelength of light produces through this stimulated transition process subjected to the band gap energy. The development of energy has been supported by 2 high reflected mirrors placed at both ends.

Semiconductor optical amplifier has similar structure with the laser diode except that instead of having 2 mirrors at both ends figure 2.7, it is replaced by anti-reflection coating that prevents the optical feedback and helps it operate below threshold region. Stimulated emissions by the decaying photon create ASE. High intensity of electron injected creates the population inversion crucial for the amplification process. New generated photon is coherence with the input signal. Together with the decayed photon,

the signals travel though the SOA and producing more stimulated emission and if the amount of photon emitted from the process is more than its absorption (generated from reabsorption of signal by valance band), the signal will be amplified.

The performance of SOA depends on two factors; SOA design (facet reflectivity) and gain medium. The SOA design affect the ripple generated from amplification process meanwhile the gain medium gives effect on its gain, noise figure and ASE pattern.

Chapter 3 Characterization of O-band Optical Amplifiers

3.1 Introduction

There have been tremendous studies on the multiwavelength fiber laser since 1980's. Through that, various amplifiers systems are used either to amplify the seeding signal (Al-Mansoori, et al. 2009) or as seeding signal source itself (Ahmad, et al. 2009). Optical amplifier can be divided into two categories, namely fiber optic based and integrated circuit based amplifier. The properties of optical amplifier for generating multiwavelength fiber laser include providing high gain, low noise figure and also able to amplify multiple signal simultaneously (Nusinsky et al., 2004) without being suppressed.

In the case of C-band multiwavelength fiber laser, an EDFA is the widely used amplifier where it can produce high gain of over 30dB. Unfortunately, the signal dependency of gain characteristic and profile has causing problem in cascading the EDFAs (Mrinmay et al., 2007). Another choice is to use integrated circuit amplifier like C-band SOA. Gain mode competition does not occur in SOA since it is inhomogeneous gain medium (Wang, et al. 2003), but with its high noise figure and low gain characteristic it might pose a problem.

In O-band region, there are a numbers of commercialized amplifiers including, Raman Fiber Amplifier (RFA) (Dianov, et al. 1994), Semiconductor Optical Amplifier (SOA) (Assadihagni et al. 2008) and fiber optical amplifier (FOA) such as Neodymium Doped Fiber Amplifier (Naftaly, et al. 2000) and Praseodynium Doped Fiber Amplifier (Ohishi, et al. 1991). Unfortunately none can be as efficient as EDFA for C-band amplification. Most of the FOA, for O-band require high pumping power, meanwhile

the SOA suffer from high noise figure and low gain. This chapter will discuss the characteristic of three amplifiers for multiwavelength fiber laser.

Recently another new fiber is believed that to be able to provide amplification to most of the available transmission windows from 1260nm to 1620nm which is Bismuth doped fiber (BiDF). First broad emission of Bismuth silica glass was discovered by (Fujimoto et al. 2001). In section 3.2, the performance of Bismuth doped fiber is studied by characterizing its absorption spectrum, ASE, and gain. The double pass configuration was used to study the improvement in its gain properties. Apart from general studies of amplifier parameters, the nonlinear coefficient value is also included in that section.

As discussed earlier, the nonlinear effect can be manipulated and used as an amplifier such as stimulated Brillouin scattering or stimulated Raman scattering. The stimulated Raman scattering is proven to produce better performance among nonlinear amplifier, therefore O-band Raman fiber amplifier (RFA) was included and discussed in next section. O-band RFA has high dependency on fiber nonlinear value and length, hence different fibers and length are used to study the Raman gain coefficient value. The final section of this chapter will discuss on the improvement of integrated circuit amplifier, which is called Booster optical amplifier (BOA). The gain and noise figure characteristics of BOA is measured together with the performance of polarization dependent gain (PDG). Multiple pass amplification happens during the process of generating multiwavelength fiber laser. Hence, the performance of BOA with double pass configuration is also demonstrated.

3.2 The performance of Bismuth Doped Fiber Amplifier

Bismuth was first used in the optical fiber to overcome the quenching effect of Erbium doped fiber amplifier and to improve the amplification in the L-band (Cheng, et al. 2009), where bandwidth have improve to 90 nm (1530 nm to 1620 nm). Bismuth was next used as the nonlinear medium, which was doped on the oxide base optical fiber (Lee, et al. 2006). The highest nonlinear coefficient recorded for Bismuth-oxide nonlinear fiber was 1360 $W^{-1}km^{-1}$ (Sugimoto, et al. 2004). Meanwhile, infrared luminescent from bismuth-doped silica glass was first discovered (Fujimoto et al. in 2001) that show wide luminescent from 1000nm to 1600nm.

The Bismuth doped fiber (BiDF) used for the following experiments is obtained from the Optical Research Center (ORC), Southampton University, UK and is labelled as L30157-T0220. The Bismuth fiber is doped together with alumina, germanium oxide, phosphate and bismuth as an active ion ($BiSiO_2GeO_2P_2O_5$).

3.2.1 Absorption Spectrum

The absorption spectrum provides information on absorption losses along the operating wavelength and also clues on available pumping wavelength for the respective fiber amplifier. The cut back method is a commonly uses to measure the attenuation loss due to the absorption of active ion. By inserting a broad spectrum of white light source into 1m of BiDF that connected with connectors at both ends, the spectrum of the loss is gathered. Next the 1m BiDF will be cut into 5cm pieces to ensure that no absorption takes place is other than the splicing loss. The spectrum from the 1 m BiDF will be deducted with the 5 cm BiDF spectrum to show the actual absorption loss. The absorption coefficient is shown in figure 3.1.

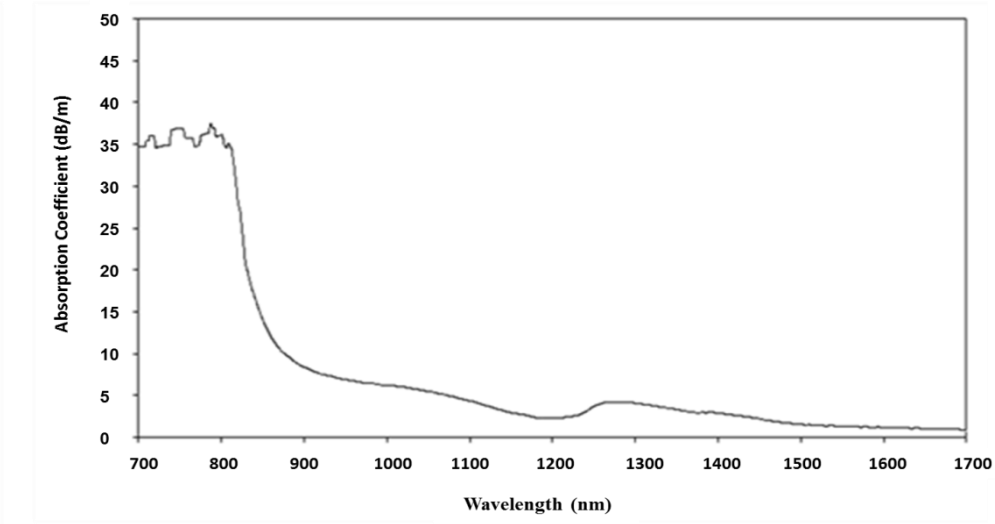

Figure 3.1 The absorption spectrum of BiDF

Due to the limitation of optical spectrum analyzer (OSA) the spectrum can only be analyzed from 600 nm to 1700 nm, high absorption spectrum was observed from 600 nm to 850 nm which is around 35 dB/m and 5 dB/m for the aimed region of 1310 nm. The absorption spectrum shows a broad selection of pump wavelengths. The broad absorption spectrum is caused by the multiple active ions present in the fiber (Omenetto, et al. 2006).

3.2.2 ASE at different excitation wavelength

A broad pumping wavelength is an advantage as a variety of pump wavelength could be used to excite the doped ion in the fiber. Therefore in this section, the BiDF is tested with various pump wavelengths to observe the efficiency of the pumping scheme.

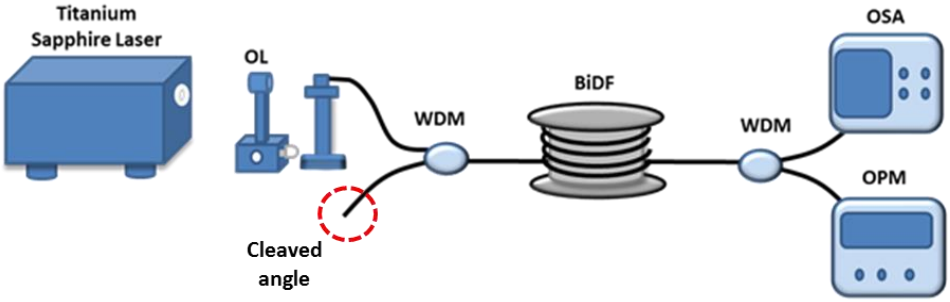

Figure 3.2 Experimental setup for collecting ASE of the BiDF

Experimental configuration in figure 3.2 consist of the Ti:Sapphire laser used to generate tuneable wavelength with ranges from 800 nm to 890 nm and the power output is up to 1.0 W for each selected wavelength. The excitation source output is directly coupled into the input of the WDM using a 20X magnification objective lens (OL). The direct coupling of the excitation source into the WDM minimizes fibre mode mismatch which may occur if a separate fibre is used for coupling. The free space – fibre coupling efficiency measured to be more than 60%. The laser then enters the BiDF system through 800/1300 wavelength division multiplexer (WDM) with 1 dB loss. The power coupled into the BiDF is around 390 mW. The ASE spectrums were extracted at the WDM signal output and analysed using OSA which was fixed to be at a resolution of 2.0 nm (Seongwoo, et al. 2009).

The study of optimum length of BiDF is important due to ASE spectral profile dependency on the active medium length. The spectral power level of the ASE with different BiDF lengths is shown in Figure 3.3. The pump power use in the measurement is 270 mW at 840 nm.

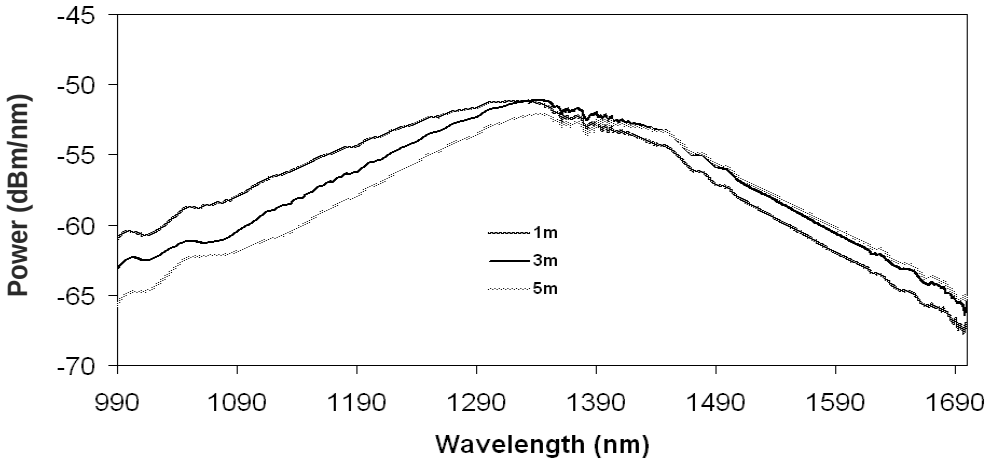

Figure 3.3 The Bi-DF ASE at different length.

ASE spectral power in the wavelength range from 990 nm to 1390 nm reduces with longer Bi-DF length. On the other hand, for wavelength range from 1390 nm to

1690 nm, ASE spectral power for 1 m of Bi-DF is lower compared to the of 3 m and 5 m length. These characteristic is similar to Erbium-doped fibre in which, by utilizing a longer length fiber, the ASE spectrum power shift to the longer wavelength. This condition is due to re-absorption of the signal at a shorter wavelength by the BiDF followed by re-emission at longer wavelengths. This effect is proportional to the length of BiDF used as higher re-absorption rate occurs in a longer active fiber length (Seongwoo, et al. 2009).

The figure 3.3 illustrated that 3m BiDF gives the highest and stable ASE. Therefore in the case of studying the effects of different excitation wavelength, 3 m fiber was used. The effect of different excitation wavelengths power on ASE generation by BiDF is observed by fixing the tuneable Ti-Sapphire laser to 270 mW and tuned from 820 nm to 870 nm with 10 nm increment and the length of BiDF is fixed at 3 m. The corresponding ASE spectra is measured and analysed.

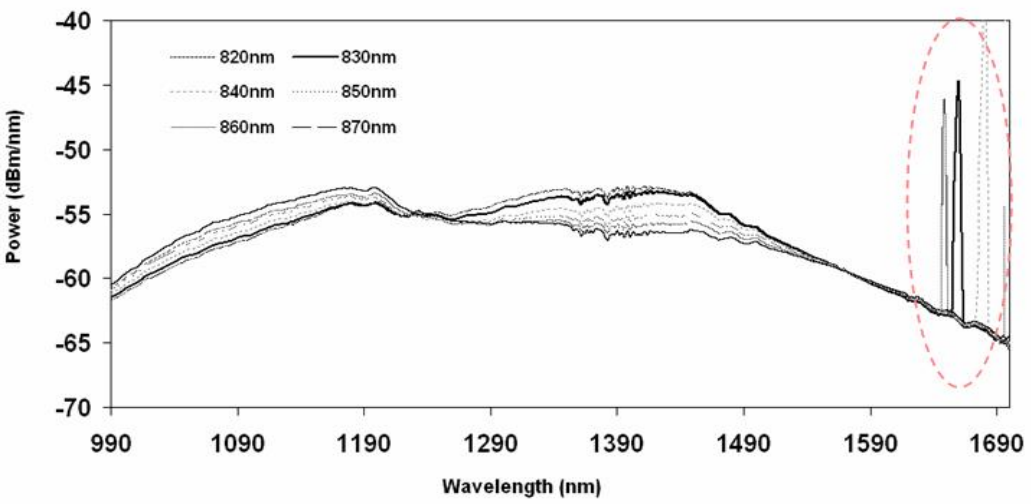

(a)

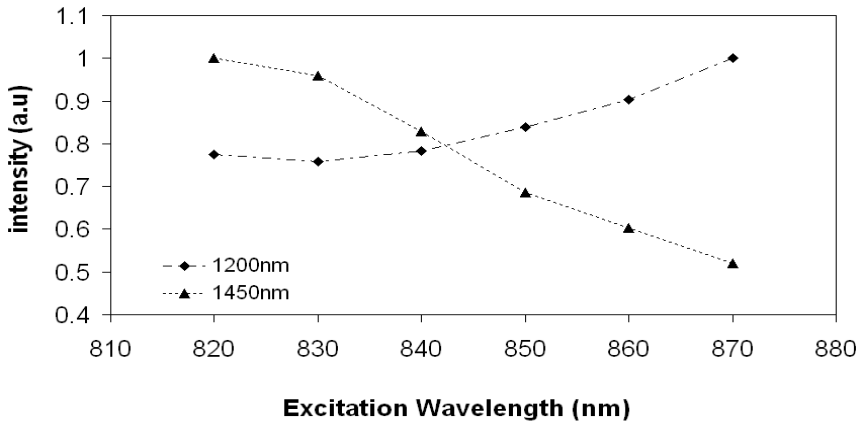

(b)

Figure 3.4 (a) ASE spectrum and (b) intensity of signal at wavelength 1200nm and 1450nm at different excitation wavelength

Figure 3.4(a) shows the ASE spectra of BiDF when excited with different excitation wavelengths. The peaks at the end of the spectrum in figure 3.4(a) are the harmonics of the excitation source. The spectra show visible changes of the ASE spectrum when different excitation wavelengths are used. The ASE power level at longer wavelength range (1245 nm – 1560 nm) decreases when longer excitation wavelengths are used, while at shorter wavelength range (950 nm – 1245 nm), the ASE power level increases with increasing excitation wavelengths. Spectral power at 1200nm (representing shorter wavelength range) and 1450 nm (representing longer wavelength range) when excited with different excitation wavelengths are shown in Figure 3.4(b). The figures show an increase in spectral power at 1200 nm when longer excitation wavelength is used. At 1450 nm, the spectral power decreases towards longer excitation wavelength. This condition is caused by the presence of different active centre sites in the BiDF with slightly different transition energy levels. This observation is believed to be similar to that reported by (Gumenyuk et al.2011), where signal at shorter wavelength is higher when longer excitation wavelengths in the absorption band were used. Spectral power level of the two wavelengths is observed to be the same

when the excitation wavelength is set at 840 nm, indicating a relatively uniform spectrum profile when 840 nm optical source is used for excitation.

3.2.3 Gain characterization

The gain performance of optical fiber amplifier is defined as the positive signal difference after propagating through the BiDF. The signal that enters the BiDF will be amplified by the bismuth ion excited from the energy of the pump. The conventional setup to examine the gain is similar with the previous experimental setup of ASE measurement except an unoccupied port of WDM was continued to tuneable laser source as shown in figure 3.5. The tuneable laser source (SANTEC-510) has wavelength range from 1260 nm to 1360 nm. Signal gain of BiDFA is measured by comparing the signal power with and without the presence of excitation source. The gain is calculated by the relation $G = \log_{10}(P_o / P_i)$ where P_o is the output signal power with pump excitation and P_i is the input signal power without pump excitation (Young-Seok, et al. 2009). The fundamental experimental configuration of BiDFA utilizes the co pumping scheme where the O-band tuneable laser source (TLS) and the excitation pump propagate in the same direction. Both signals are coupled by the wavelength division multiplexer (WDM) into the BiDFA. The excitation source is a Titanium Sapphire laser operating at a wavelength 840 nm with the maximum excitation power of 270 mW.

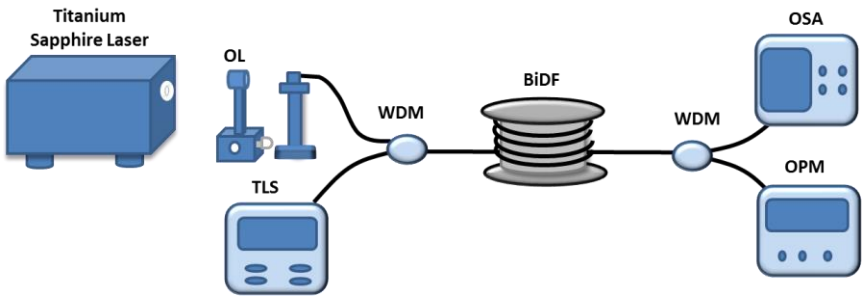

Figure 3.5 Experimental setup for gain charaterization of BiDF with co pumping scheme

The performance of BiDF for single-pass configuration with co pumping scheme is shown in figure 3.6. The experiment was repeated for 3 different fiber lengths namely 1 m, 3 m, and 4 m. Input signal power and excitation power are set at -30 dBm and 270 mW, respectively for both configurations.

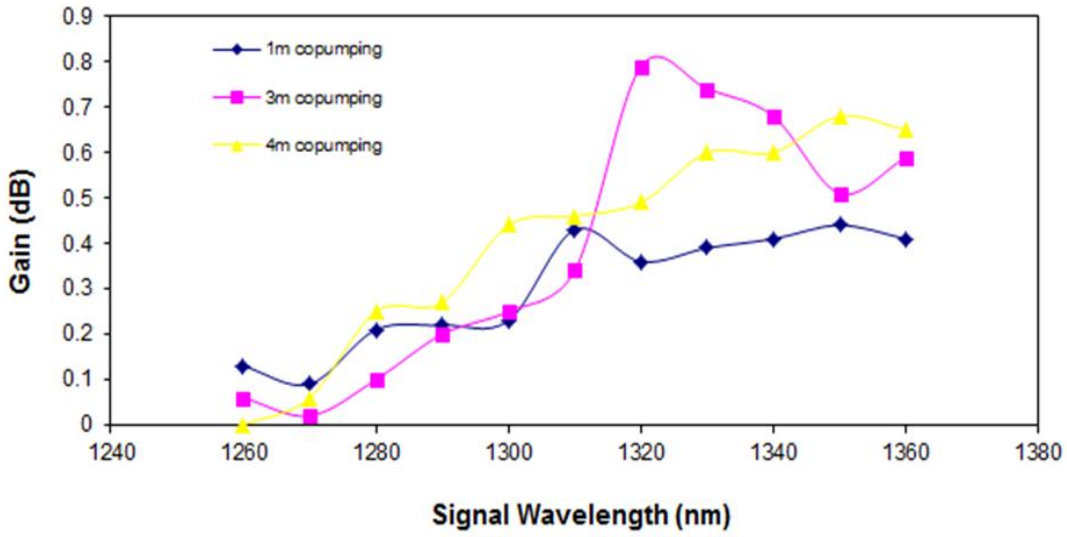

Figure 3.6 Gain performance of co pumping BiDFA

The co pumping scheme shows better performance for the 3 m length compared to that 4 m due to insufficient pumping power to pump the overall 4 m length of BiDF which resulted in the absorption of the generated signal. To overcome this issue and to provide more power into the fiber, bidirectional pumping scheme is used.

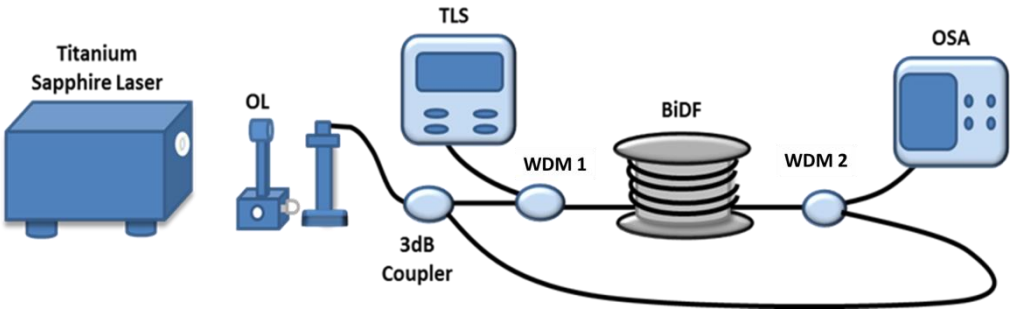

Figure 3.7 Experimental setup for gain charaterization of BiDFwith bidirectional pumping scheme

As illustrated in figure 3.7 the bidirectional pump can be achieved by placing a 3 dB coupler before the WDM1. The fiber is pumped from both ends. The signal is amplified at the start of the fiber and has a loss in the middle of fiber due to insufficient pump power but later the signal is amplified again at the end of the fiber.

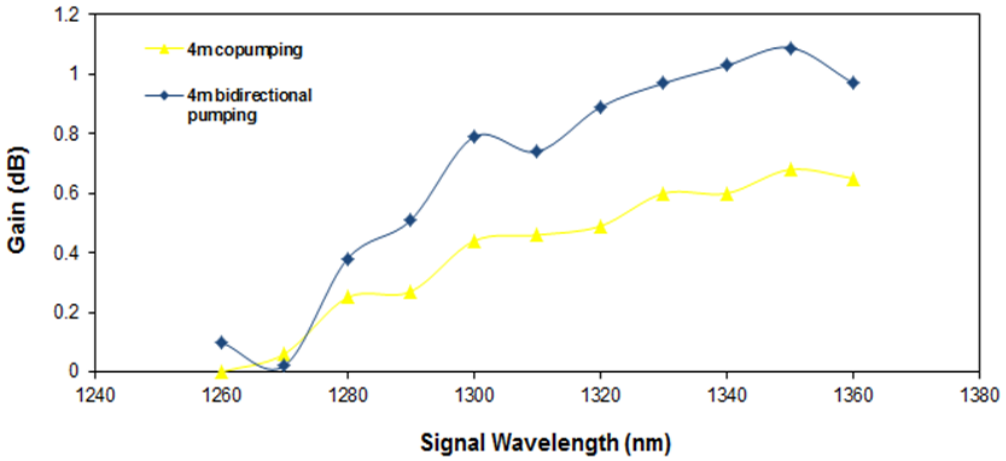

Figure 3.8 Gain performance of bidirectional pumping of BiDFA

Figure 3.8 shows an increase of 50% in gain from the co-pumping configuration. Unfortunately the gain generated from both pumping scheme, are still very low to act as the O-band amplifier. Hence double-pass configuration is demonstrated as it has been one of the methods commonly used in improving signal amplification for the S-band (Roselem, et al. 2005), C-band (Nishi, et al. 1990), and L-band (Harun, et al. 2003, Aozasa, et al. 2002) amplifiers. The solution is also cost effective and a compact solution to amplifier performance gain as no additional active fibre length or excitation source is required.

3.2.4 Gain improvement by double-pass configuration

Due to low amplification in single pass configuration, the double pass technique was proposed. Double pass configuration is a basic technique to increase the gain of an amplifier. It still resembles the fundamental fiber amplifier setup except with an

additional optical circulator (OC2) at the end of the BiDF fiber as shown in figure 3.9 that act as mirror to create double pass.

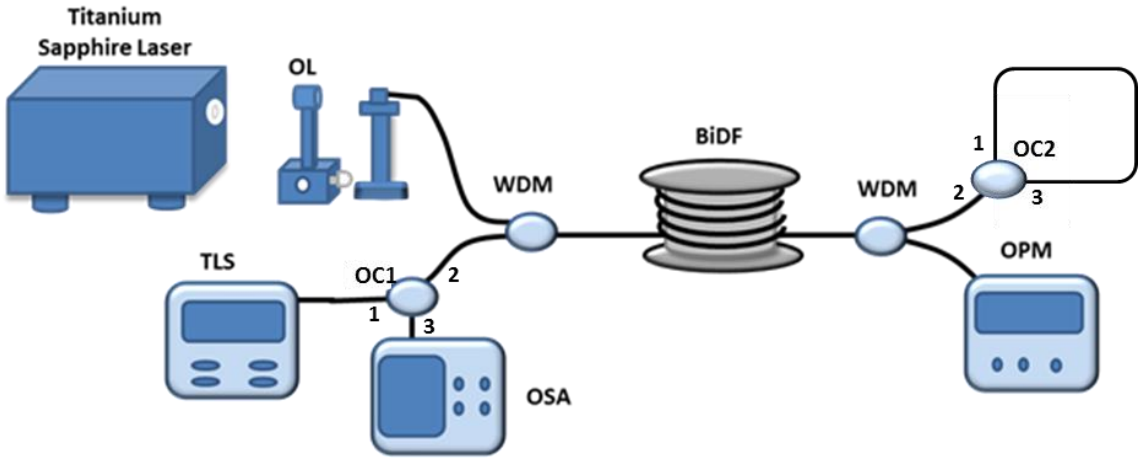

Figure 3.9 Experimental setup of Bismuth doped fiber amplifier with double-pass Bi-DFA configuration

The extra OC2 bounces the amplified signal back into the BiDF by connecting its port 1 and port 3. Due to 1dB insertion loss induced by OC2, reflection by the optical circulator is limited to 80%. The amplified signal emerging from port 3 of OC1 is analysed using the optical spectrum analyser.

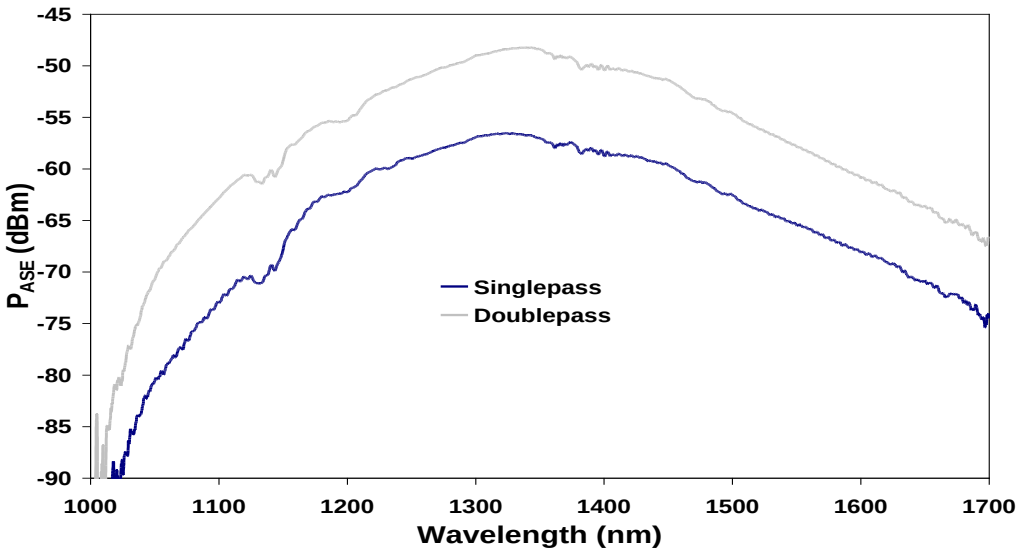

Figure 3.10 The spectrum of amplified spontaneous emission of single-pass and double-pass BiDFA.

An improvement of ASE spectra of double-pass as compared to single-pass BiDFA is as shown in figure 3.10 by having the excitation power fixed at the same power as the single-pass configuration (270 mW). Both single- and double-pass configurations exhibit similar ASE profile, with a peak level of -48 dBm at 1340 nm for the double-pass BiDFA. The ASE level for the double-pass BiDFA increases by 8 dB at 1340 nm over that of the single-pass BiDFA. The ASE enhancement between 7 dB - 8 dB is observed throughout the measured wavelength range. The ASE 3 dB bandwidth for double-pass BiDFA is 188 nm. The ASE bandwidth is limited by the 1310 nm optical circulator which has a spectral transmission window that reduces towards the shorter (1100 nm) and longer (1700 nm) wavelength range being measured. The 3dB bandwidth of the ASE is expected to be wider if optical circulators with broader flat transmission range are used.

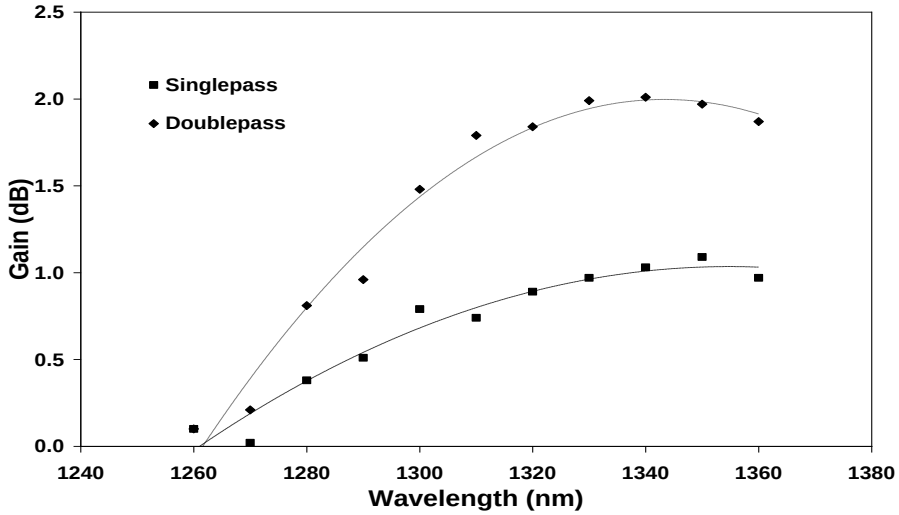

Figure 3.11 Signal gain for single- and double-pass BiDFA with different signal wavelengths.

Signal gain for single- and double-pass BiDFA at different signal wavelengths is shown in Figure 3.11. By keeping the parameter the same as for single pass configuration the maximum signal gain is obtained at 1340 nm with 1.0 dB for single-pass and 2.0 dB for double-pass BiDFA. Double-pass BiDFA shows a 25% gain

improvement over single-pass BiDFA between 1310 nm to 1360 nm. A longer measurement wavelength range is limited by the tuneable laser source which has tuning range from 1260 nm to 1360 nm only. Gain enhancement below 1310 nm reduces towards 1260 nm. This is due to the higher loss at this wavelength range induced by OC2. Whereas in a single-pass BiDFA the input signal only passes through OC1 once, the signal in a double-pass BiDFA need to pass through OC1 and OC2 twice. Therefore, gain enhancement in the shorter wavelength is limited by the transmission bandwidth of the components used in the configuration.

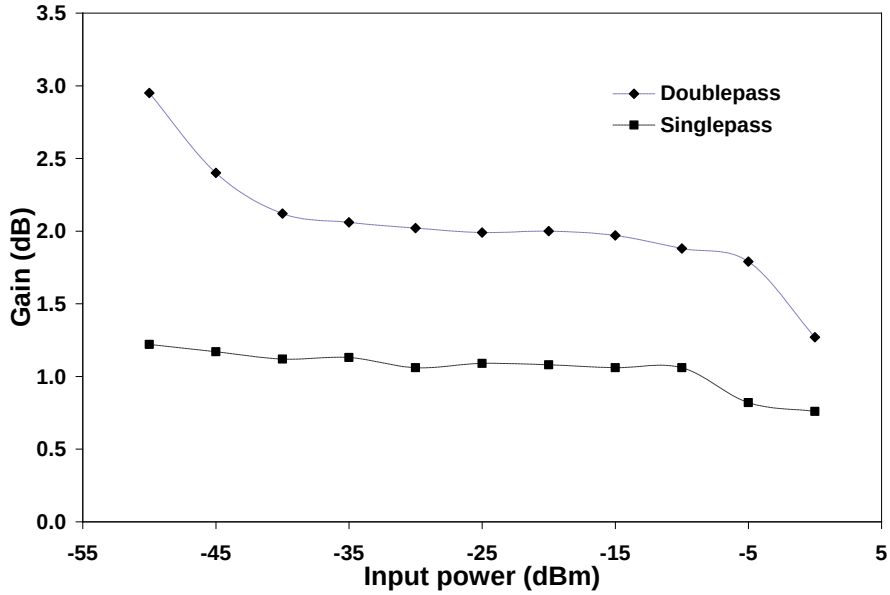

Figure 3.12 Signal gain of single- and double-pass BiDFA at different input power.

The study of gain characteristic at different input power levels is important to understand the dynamic behaviour of BiDFA. Signal gain of BiDFA at different signal input power is shown in Figure 3.12.The signal wavelength is set at 1340 nm. The signal gain enhancement in the double-pass BiDFA is around 25% for the input signal levels between -40 dBm and -10 dBm. For smaller signal power, gain enhancement is observed to increase to 48% for input signal level of -50 dBm. While gain enhancement reduce to 12% when input signal power is increased to 0 dBm. The larger gain

enhancement for small signal is due to low extraction of energy from the gain medium in the single-pass BiDFA and hence higher population inversion is available for signal amplification for double-pass BiDFA. On the other hand, gain enhancement reduces towards the large input signal region as BiDFA reached gain saturation with high input signal power.

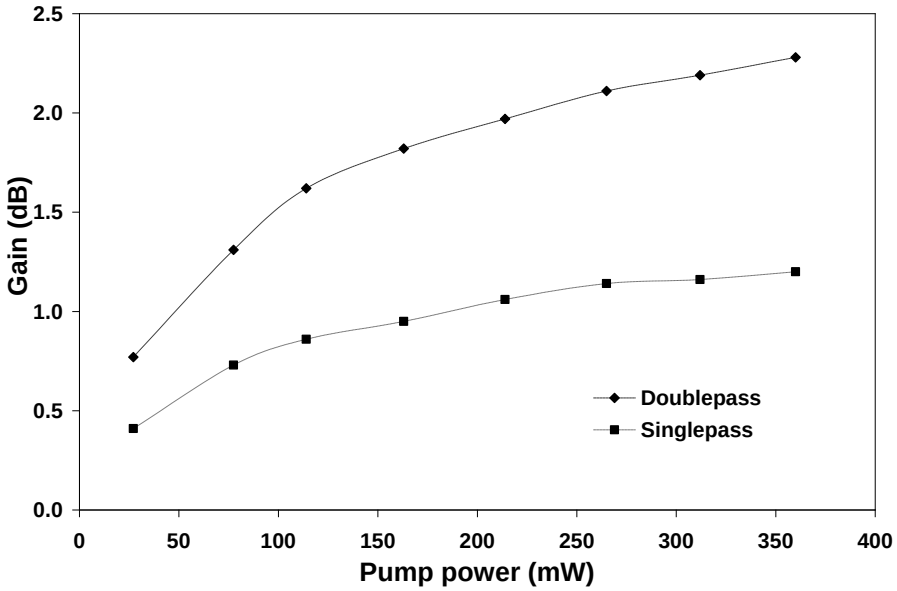

Figure 3.13 Signal gain as a relation of pump power.

Figure 3.13 shows the signal gain variation with pump power. The input signal wavelength is set at 1340nm with input power of -30dBm. Gain enhancement increases with increasing pump power from 0.4 dB to 1.1 dB with pump power of 270 mW and 360 mW, respectively. Gain efficiency for single-pass and double-pass BiDFA are 5.9 dBW^{-1} and 10.0 dBW^{-1}, respectively. Gain enhancement is believed to be higher if a longer length of bismuth-doped fiber is used as reported by other research groups (Mridu, et al. 2009). Another area that requires research attention to realize ultra-broadband fiber amplifier is the improvement of transmission bandwidth for optical components used to construct BiDFA. Nevertheless, results obtained in this work are

evidence that signal gain in the O-band using BiDFA can be enhanced with double-pass amplifying technique.

3.2.5 Determination of nonlinear coefficient of BiDF

In order to increase the amplification, longer lengths of BiDF are proposed. Longer fiber results in generating greater nonlinear effects. Therefore the study of nonlinearity of BiDF is required. It was reported Bismuth based fiber (BiBF) shows high nonlinearity up to 1360 $W^{-1}km^{-1}$(Sugimoto, et al. 2004), probably due to the Bismuth ion. Third order optical nonlinearity of glass material strongly depends on linear refractive index (Miller's rule) (Hasegawa, et al. 2006). High nonlinearity can be obtained by applying high refractive index glass as a nonlinear medium. Bismuth has an average reflective index of 2.55 (Gospodinov,et al. 1989) which is high enough to produce a high nonlinearity effect. Therefore in this section, the Bismuth doped fiber nonlinear coefficient value was measured by utilizing the Four Wave Mixing (FWM) effect. The FWM technique was chosen due to its mobility and less complex. As described by Inoue, et al. 1992, the FWM effect supposed to be operated effectively at a region close to its zero dispersions wavelength (ZDW). When the pump wavelength is equal to zero dispersion wavelengths, $\Delta\beta$ will be zero. Hence, determining the nonlinear coefficient using four wave mixing technique requires knowledge of the zero dispersion region of the fiber. Unfortunately, the ZDW for BiDF is unknown.

A numerical study was done on highly nonlinear fiber (HNLF) to show the relationship between FWM power distribution with spacing of signal wavelength and ZDW. The HNLF properties: zero dispersion wavelength at 1531 nm, dispersion slope of 0.007 $km.ps/nm^2$, with length of 100m, and nonlinearity coefficient of 10.71 W^{-1} km^{-1}. The result of the simulation is shown in figure 3.14, where the signal wavelength is fixed at 7 different wavelengths across C-band region which is 1525 nm.

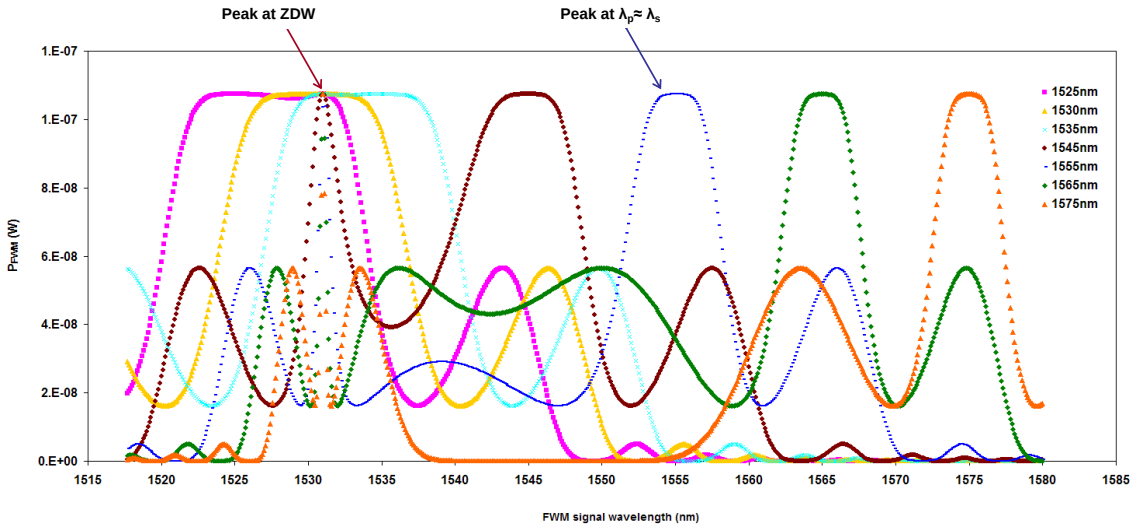

Figure 3.14 The simulation of FWM power over FWM signal wavelength

The simulation indicates that the power of FWM are maximum at two peaks as shown in figure 3.14, where the first peaks is when the pump wavelength is at the ZDW ($f_p \approx f_0$). It is also observed that at the second peak, the P_{FWM} generates a wider bandwidth towards the ZDW. In summary, of the P_{FWM} bandwidth is as depicted in figure 3.15.

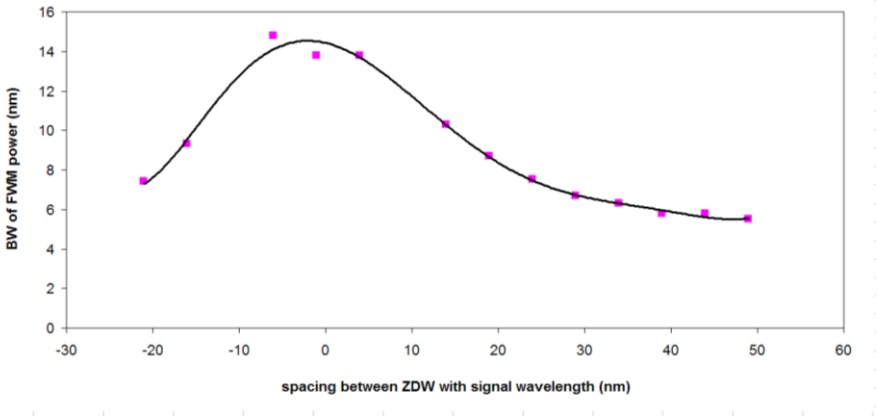

Figure 3.15 Bandwidth of the P_{FWM} against the spacing between ZDW and signal wavelength

According to the simulation result, it shows that the ZDW can be measured by observing the bandwidth of P_{FWM} whenever the wavelength of the pump and the signal

are closely spaced. The experiment was done to measure the ZDW of BiDF. The FWM nonlinearity measurement setup is illustrated in figure 3.16

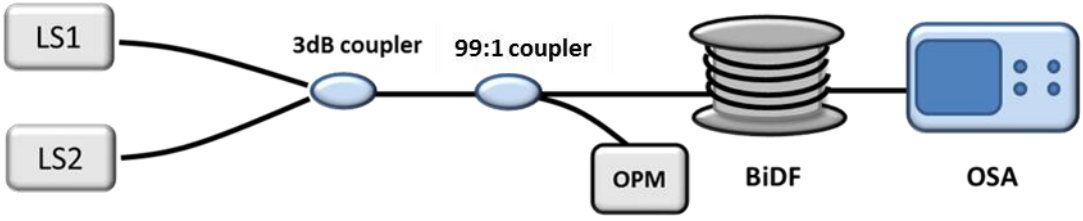

Figure 3.16 Four wave mixing ZDW nonlinearity measurement setup.

The measurement was conducted in 2 wavelengths regions, O and C band. Two external laser source (LS) is use as the pump and signal. The signal source is fixed at one wavelength with power of 11 dBm (LS1) or mark as signal while the pump source is a tuneable laser source with power of 12 dBm (LS2) marked as pump as refer to figure 3.17. The signals are coupled into the Bismuth doped fiber (BiDF) by using a 3 dB coupler. The power of both LS1 and LS2 was observed by the optical power meter (OPM) thru tapping 1% of its power by the 99:1 dB coupler. The FWM power can be observed from the FWM spectrum by OSA at the end of BiDF. By measuring the bandwidth of FWM signal for each different signal wavelength, the zero dispersion wavelength (ZDW) can be obtained.

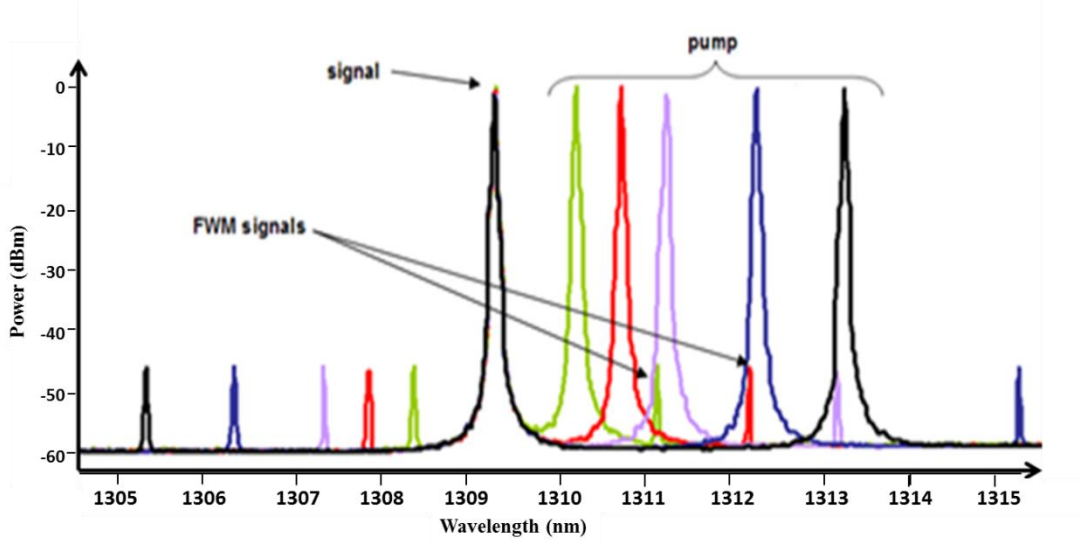

Figure 3.17 Spectrum of four wave mixing by the BiDF

In the case of BiDF, due to the limitation of the second tuneable laser source at the O-band region, the bandwidth can only be fully observed at the C-band region. As for the O-band region the signal source is extracted from the fiber laser which is adjusted to have similar properties as the other tuneable laser source. The fixed laser sources for the O-band region were at 1300 nm, 1308 nm, 1310 nm and 1340 nm using the FBG technique

An example of FWM power distribution against the spacing of signals and pump wavelength is as shown in figure 3.18, where the signal wavelength is fixed at 1550 nm and the pump signals are varied with an increment of 0.1 nm. The bandwidth of the distribution was measured by taking the width at half of the maximum intensity which is 0.39 nm wide.

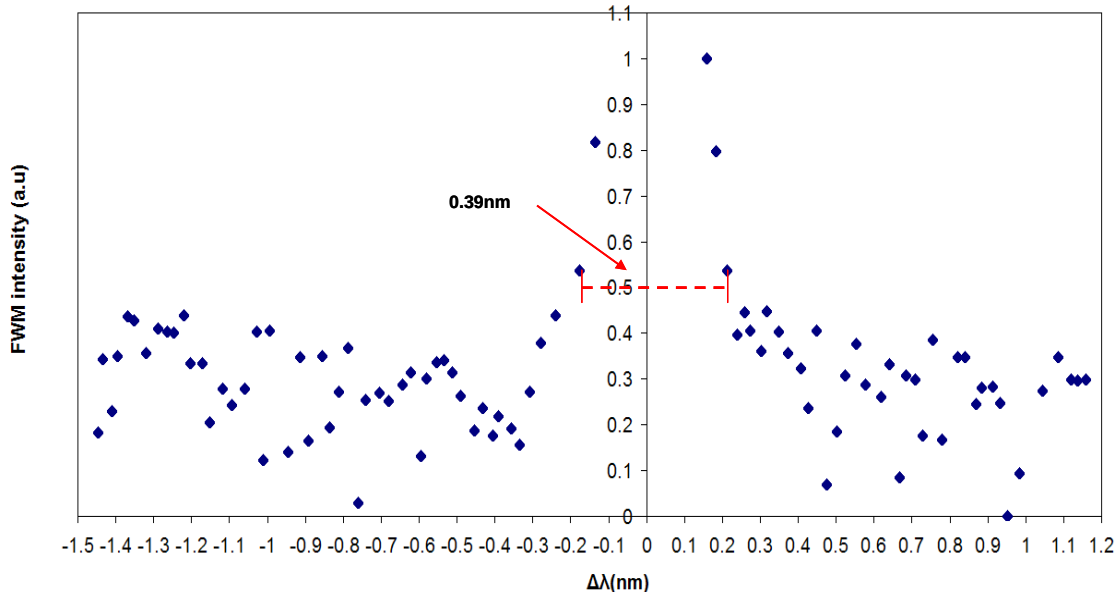

Figure 3.18 The distribution of FWM intensity over wavelength spacing of pump and 1550 nm signal

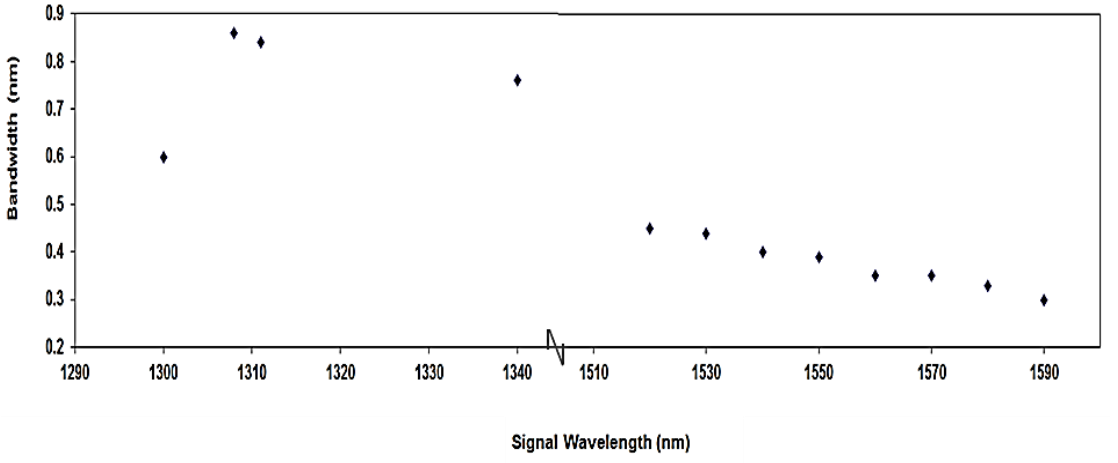

Figure 3.19 The bandwidth of FWM power distribution against signal wavelength.

A summary of the bandwidth collected at available O and C-band region is as shown in figure 3.19. The bandwidth collected from the available signal source shows that O-band region has a higher reading compared to the C-band region. The maximum reading was taken when the signal source is at 1308nm which is 0.84 nm. Hence, the zero dispersions wavelength determined to be approximately at 1308 nm.

The experimental setup for the measurement of nonlinear coefficient measurement is same as experiment for measuring ZDW. Referring to equation 2.7, the measurement can be conducted by taking the zero dispersions wavelength to be 1308 nm. The signal wavelength is fixed at 1308 nm while the pump is scanned through a 4 nm span as shown in figure 3.20.

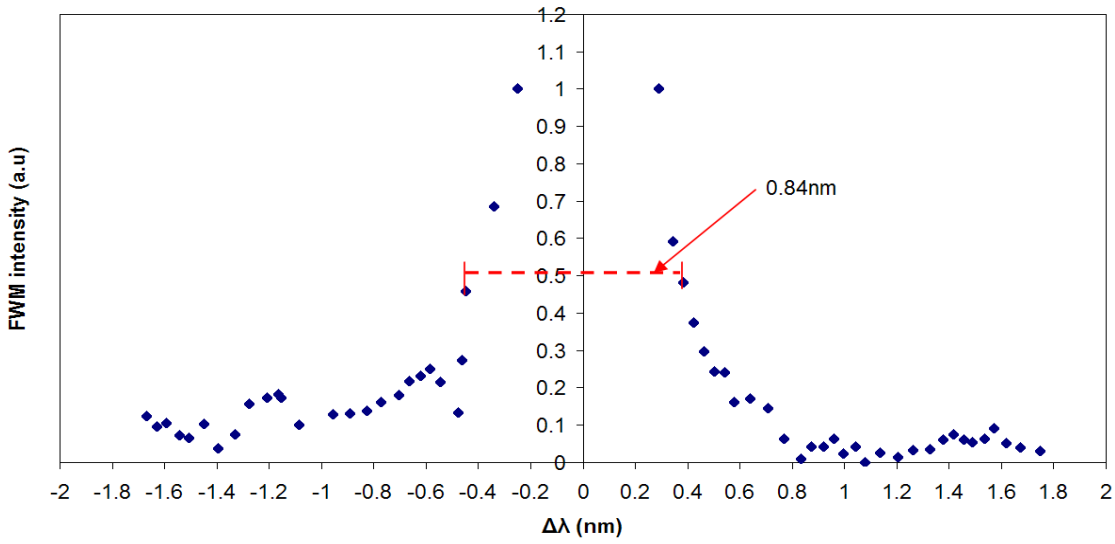

Figure 3.20 The P_{FWM} distributions at signal wavelength of 1308nm

The maximum P_{FWM} is measured at 0.23 nm from the signal wavelength taken at the point where the nonlinear efficiency, $\eta(\Delta\beta)$ is maximum 1. From the calculation made from equation 2.7, by replacing the value $\eta(\Delta\beta)$ to 1 the calculated nonlinear coefficient is proposed to be at 13.98 W^{-1} km^{-1} which is higher compared to a highly nonlinear fiber.

From equation 2.9, another way to get $\Delta\beta$ to be nearly equal to zero is when λ_p and λ_s are closely spaced. Meaning that, the nonlinear coefficient can also be calculated at a wavelength further than ZDW. The nonlinear coefficient is also calculated when the signal wavelength at 1550 nm as depicted at in figure 3.18. The calculated nonlinear coefficient is 10.92 W^{-1} km^{-1}, which shows that the value is not far from the nonlinear coefficient at ZDW.

According to equation 2.10, the value of chromatic dispersion slope $\frac{dD_c}{d\lambda}$ is proportional to the $\Delta\beta$ which affects the power of FWM. The simulation of FWM power at various value of $\frac{dD_c}{d\lambda}$ is shown in figure 3.21. The perfect match for chromatic dispersion slope value is at 0.079 ps.nm/km. The chromatic dispersion value is vital because high chromatic dispersion will reduces the FWM effects as the signals losses coherence

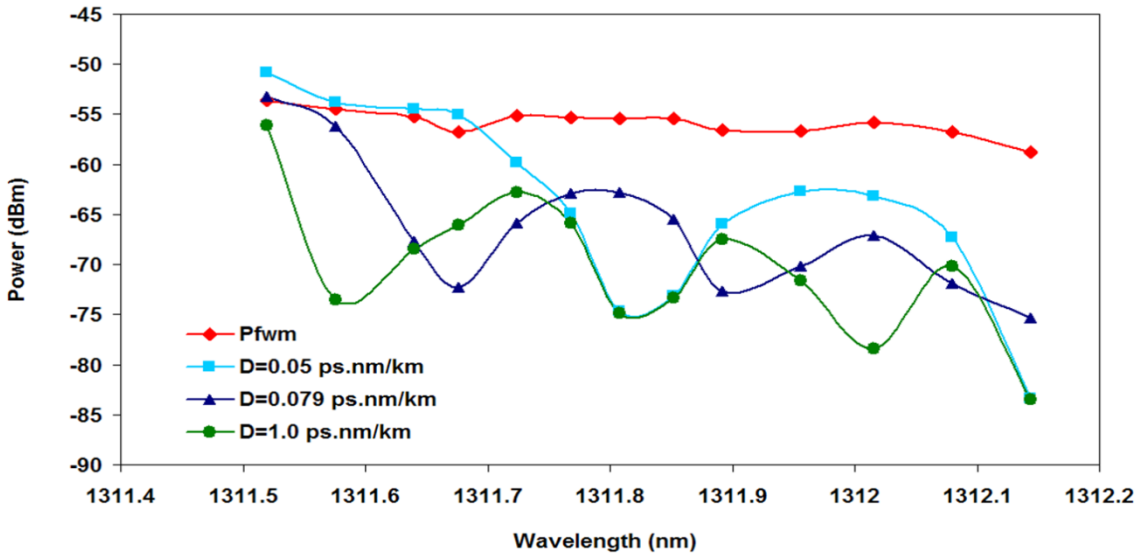

Figure 3.21 Fluctuation of P_{FWM} at different dispersion slope

The responsible nonlinear refractive index n_2 that causes the nonlinear refractive related to nonlinear coefficient is given by;

$$\gamma = \frac{n_2 \omega}{cA_{eff}} \tag{3.1}$$

where c is speed of light, ω is the frequency of propagation optical field and A_{eff} is the effective cross section of fiber used and is given by;

$$A_{eff} = \frac{\pi(MFD)^2}{4} \tag{3.2}$$

The MFD, which represent mode field diameter is given by;

$$MFD = 2\omega_o = \frac{2\alpha}{\sqrt{lm\, V}} \tag{3.3}$$

with V is the number taken to be $V = \frac{2\pi\alpha(NA)}{\lambda}$, NA is a numerical aperture $NA = \sqrt{n_2^2 - n_1^2}$ or from the measured value of 0.25. Meanwhile α represent the radius of the fiber core which is given as 5 μm. Hence give the MFD at wavelength 1310 nm is 7.9 μm and the A_{eff} is 50.09 μm^2. By taking γ to be 13.98 $W^{-1}km^{-1}$, and ω is to be at 0.229 THz, so the n_2 is calculated to be $0.917x10^{-20}$ m^2/W.

3.3 The performance of O-band Raman Fiber amplifier

Another optical amplifier tested in this chapter is Raman fiber amplifier (RFA). As discussed in chapter 2, the RFA is an amplifier generated from the nonlinear effect of the optical fiber, where a portion of the energy is transferred from the pump signal to the new generated signal. Like any other nonlinear effect, a high intensity of the light is needed to trigger the nonlinear effect. For RFA, the pump wavelength depends on the target signal region. Raman scattering effect is the result of the incident of light collides with the optical phonon (vibration of molecule), resulting in the transfer of energy that causes the incident light to lose some of its power. Hence, new shorter wavelength is generated call as Stokes. The new wavelength generated will have an absorption coefficient of be negative value, thus providing gain to the incoming signal. The frequency difference between the incident or pump wavelength with the new generated signal is around 100 nm@13 THz depending on the material of the nonlinear medium.

3.3.1 Determining the Raman Threshold

The power needed for a pump to generate Raman effects is called Raman threshold. It is defined as the power of the pump at which the Stokes power equals

pump power at the output ends $P_s(L) = P_O \exp(-\alpha_p L)$. The Raman threshold can be approximated as

$$P_{th} = \frac{16\, A_{eff}}{g_R L_{eff}} \tag{3.4}$$

where g_R represents Raman gain coefficient, which depends on the dopant of the fiber. The g_R can also be measured by analysing the backscattering ASE of RFA (Zhao, et al. 2010). The technique requires measuring the ASE of the RFA before and after the stimulated emission occurs.

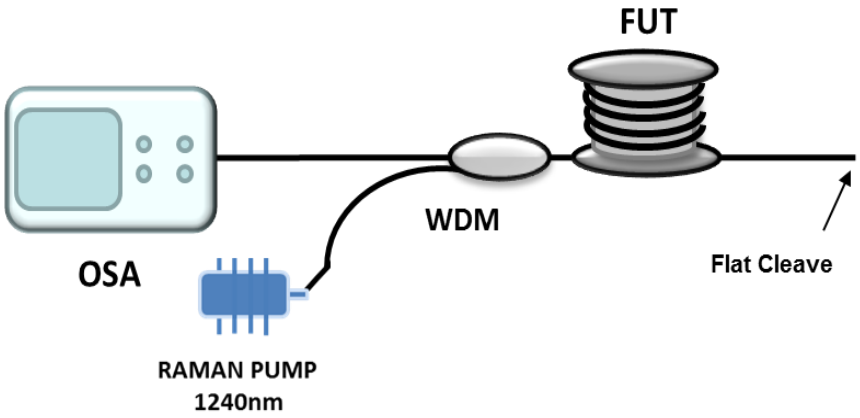

Figure 3.22 Experimental setup of backscattering RFA

The simple setup of backscattering ASE measurement is shown in figure 3.22. The Raman gain spectrum can be obtained by measuring the ratio between the backscattering ASE at low pump power and high pump power. This was tested with different fiber under test (FUT). The ratio between both spectrums is defined as G_R and is given by;

$$G_R = exp \frac{g_R P_p L_{eff}}{A_{eff}} \tag{3.5}$$

Where P_p represent the pump power. By obtaining the Raman gain spectrum the Raman gain coefficient can be obtained mathematically.

The Raman gain coefficient was measured for 4 types of fiber with different length which are 7.7 km Dispersion Compensated Fiber (DCF), 20 km True Wave Reach Fiber (TWF), 50 km Single Mode Fiber (SMF), and 100 m Photonic Crystal Fiber (PCF).

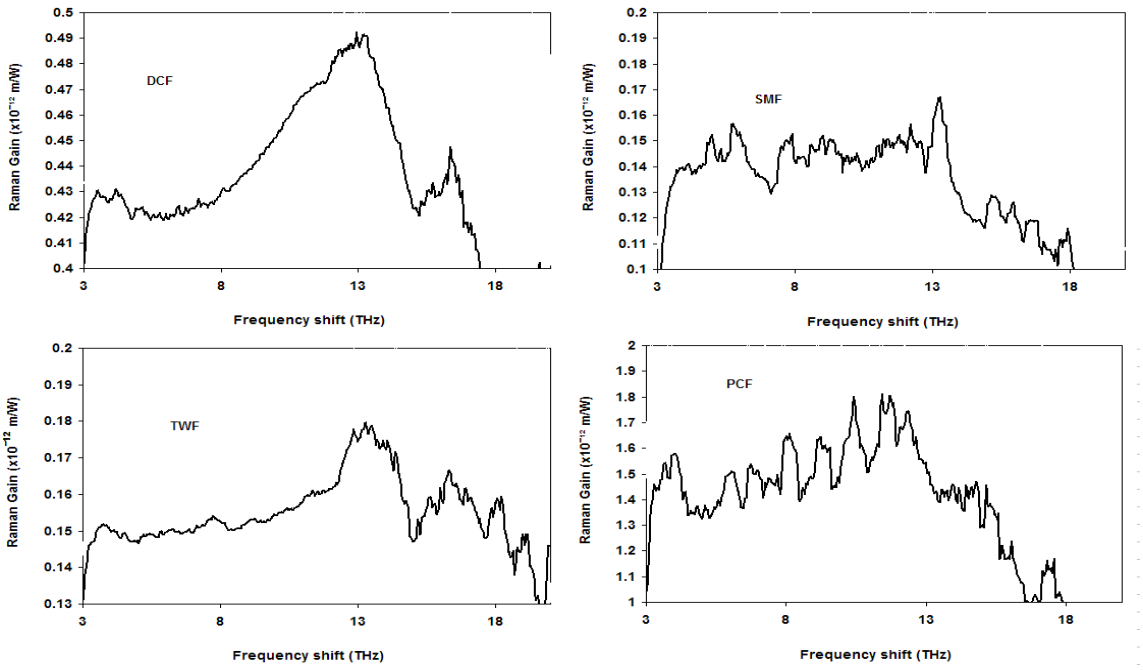

Figure 3.23 Raman gain coefficient for different types of fibers

Figure 3.23 shows the Raman gain coefficient for every tested fiber. The highest Raman gain is obtained at frequency shift around 13.2 THz except for PCF where it gives highest Raman gain of 1.8 x10^{-10} mW at 12 THz. By utilizing the value of Raman gain coefficient obtained from this experiment the Raman threshold is calculated as listed in table 3.1.

Beside the gain coefficient, equation 3.4 also shows that Raman threshold is inversely proportional to the effective length of the fiber. Longer fiber lengths make it more efficient to produce Raman amplifier. The dependency clearly shown by PCF where even possessing high $g_{R,}$ the P_{th} for PCF is high due to the limitation of it length.

The DCF requires the lowest power to initiate the Raman scattering effect.

Table 3.1 The parameters for Raman fiber amplifier

Optical Fiber Type	**A_{eff} (μm^2)**	**L_{eff} (km)**	**g_R ($x10^{-12} m/W$)**	**P_{th} (dBm)**
Single Mode Fiber (SMF)	69.40	12.56	0.17	15.05
Dispersion Compensated Fiber (DCF)	16.62	5.76	0.49	7.69
Photonic Crystal Fiber (PCF)	63.17	0.03	1.8	42.58
True Wave Reach Fiber (TWF)	55.42	10.00	0.18	14.87

3.3.2 Gain Characterization of Raman Fiber Amplifier

Raman amplifier is a reliable choice for optical amplifier due to its advantages of its ability to generate amplification in any fiber. As a result, it can minimize the upgrading cost, and it can provide a flat gain spectrum which depends on the pump distribution and the RFA can also have gain in entire transmission region. This section describes a demonstration of O-band Raman fiber amplifier for different types of fibers.

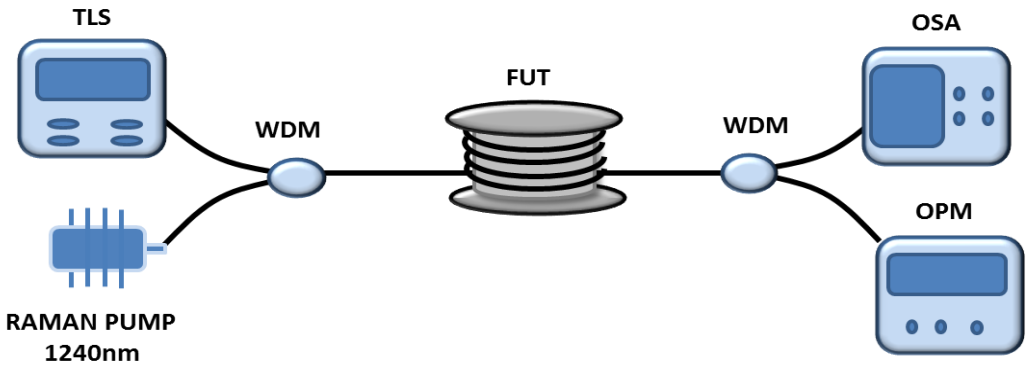

Figure 3.24 Experimental setup of Raman fiber amplifier

To generate the amplification at the O-band region, a 1240 nm Raman pump with 280 mW was used. By utilizing the fundamental experiment setup of FOA with addition of RP, the RFA can be characterized as shown in figure 3.24. The gain characteristic was done by analysing the on/off gain, which is the gain is ratio between the signals of pumped fiber over the signal of the un-pumped fiber.

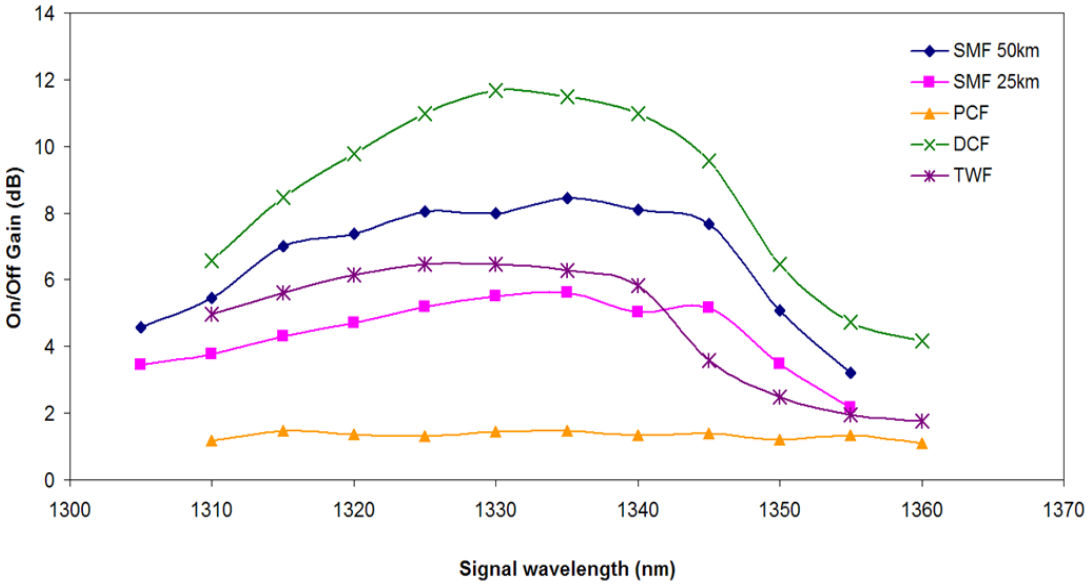

Figure 3.25 Performance of RFA against signal wavelength

The performance of the on/off gain against the signal wavelength is shown in figure 3.25. From the figure, the DCF shows the highest gain even though PCF gives the highest g_R. Unfortunately due to the limitation of the PCF length, high gain cannot be obtained. Besides that, the P_{th} of DCF of length 7.7 km is the lowest among all the tested fiber.

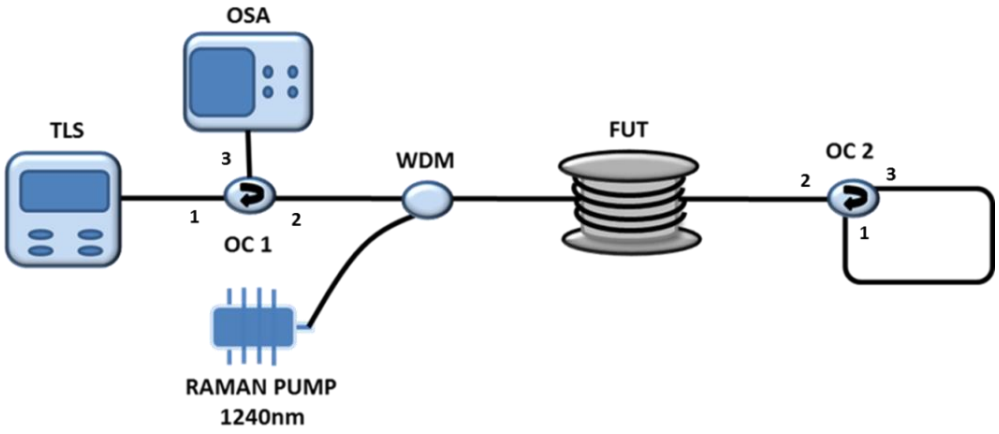

Figure 3.26 Double-pass configuration of RFA

The RFA has also tested with double pass configuration where the tested fiber is chosen to be 7.7 km DCF. Additional to two optical OC are inserted in the RFA configuration; one as the reflector (OC2) and another (OC1) to drop the spectrum to be analysed as in figure 3.26. The increment of nearly 4.5 dB from previous configuration is obtained with signal wavelength at 1330 nm, -30 dBm and maximum Raman power (280 mW) refer to figure 3.27.

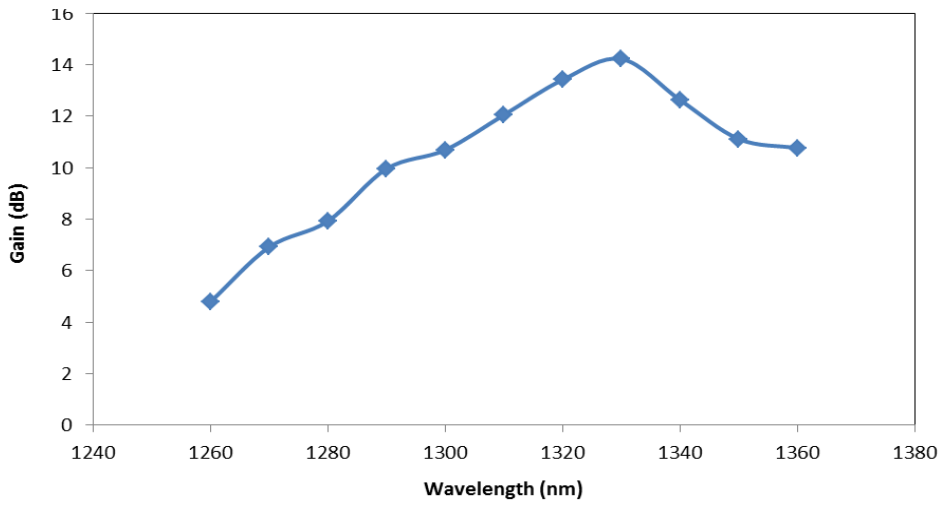

(a)

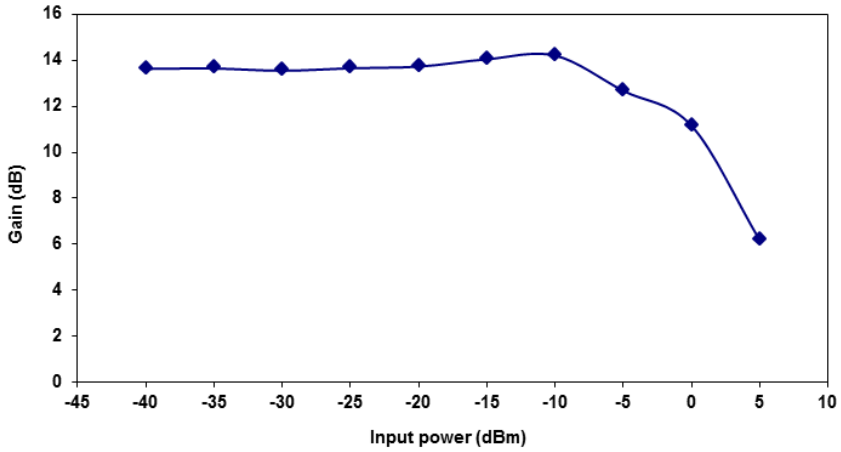

(b)

Figure 3.27 Gain performance of double-pass RFA over (a) signal wavelength (b) signal power

3.4 The performance of O-band Booster Optical Amplifier (BOA)

As mentioned previously, optical amplifiers can be divided into two categories, namely generated from fiber optics and those generated from the integrated circuit. Both types of amplifiers fall under the category of fiber optic amplifier (FOA). The semiconductor optical amplifier (SOA) is generated from integrated circuit where the amplification process of SOA is similar with that of conventional FOA; however instead of using light as the pump source, an external current is used in the process of generating population inversion state. The current injection excites the electrons from the conduction band into the valence band. Simultaneously that leaves the holes in conduction band, which is similar to the inversion population of the FOA process. The band gap energy defines the wavelength region of amplification, therefore the signal frequency need to coincide with the energy of the band gap. The signal enters the medium of SOA to generate amplification through the process of stimulated emission.

The performances of the SOA characteristic depends on two factors namely, the design of the SOA and the material used as the gain medium. The SOA design determines on the reflectivity of the whole SOA chip to avoid gain ripple. Meanwhile

gain medium material affects the performance of the gain and noise figure. By experimenting on the material, the manufacturer (COVEGA) managed to fabricate the SOA with an improved gain and called it as Booster optical amplifier (BOA) in O-band region.

In this section the comparison is made between conventional semiconductor optical amplifier (SOA) and proposed BOA. The BOA used in this experiment is model QBOA1310 by COVEGA. It operates within the region 1260 nm to 1360 nm.

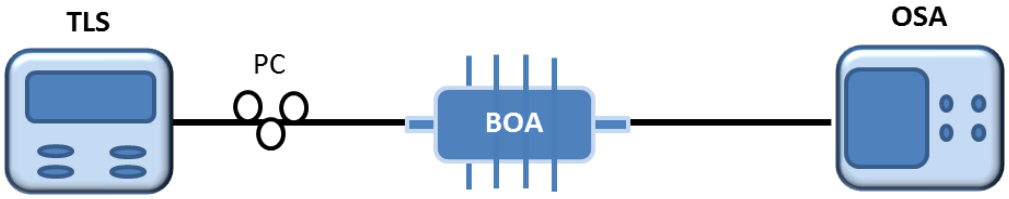

Figure 3.28 Experimental setup of single pass BOA

The conventional setup of measuring the performance of BOA is shown in figure 3.28. It consists of a tuneable laser source (TLS), Booster optical amplifier polarization controller (PC) and OSA. The PC is used is to change the polarity of the signal to maximise the electric field entering the BOA structure. The ASE performance of BOA at its maximum injected current (450 mA) is shown in figure 3.29. The ASE spectrum shows maximum power at 1340 nm and full width half maximum of nearly 60 nm from 1310 nm to 1370 nm.

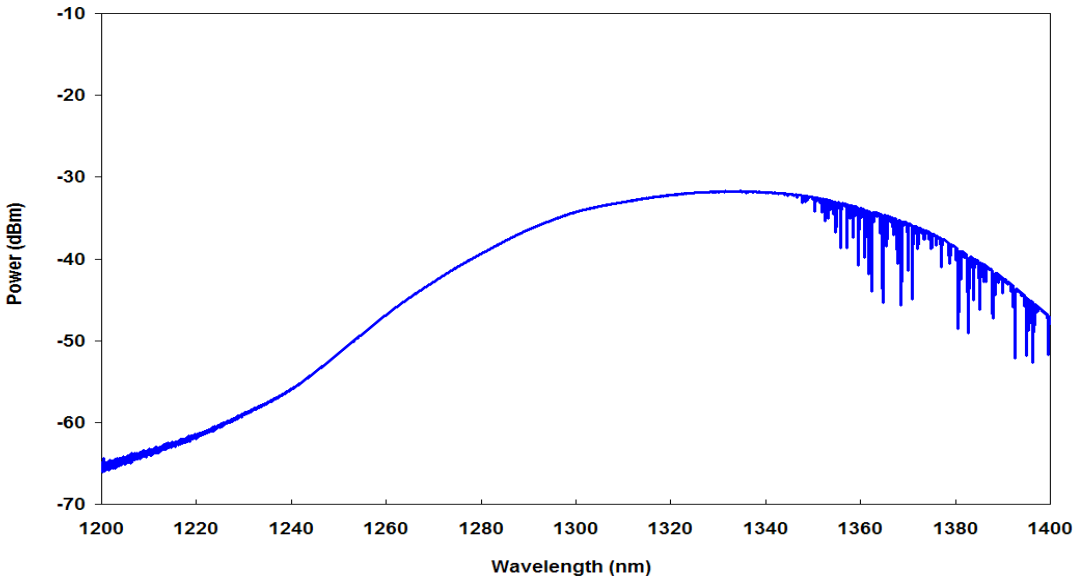

Figure 3.29 The ASE of O-band BOA

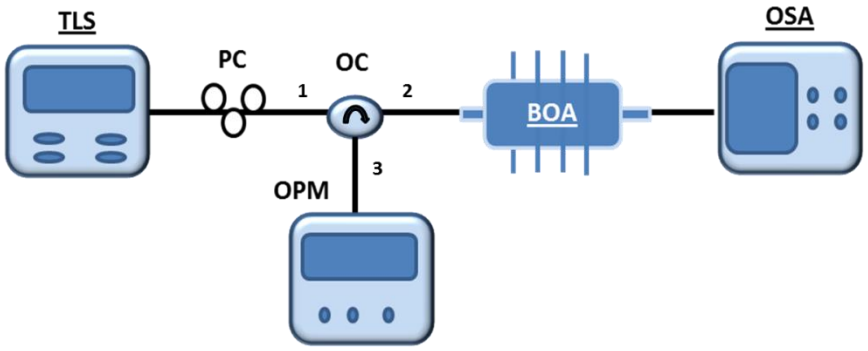

Figure 3.30 Characterization setup of ORP

The QBOA1310 operated bi-directionally. The spontaneous emission spectrum emitted at both ends of the configuration gives a high unwanted reflection. This unwanted reflection or called optical return power (ORP) affects the amplification performance where the BOA amplifies the signals together with the spontaneous emission which increases the noise figure. The ORP is observed by extracting the reflecting power by placing optical circulator before the signal enters the BOA, as depicted in figure 3.30. The ORP obtained at different current values and different wavelength is plotted in figure 3.31.

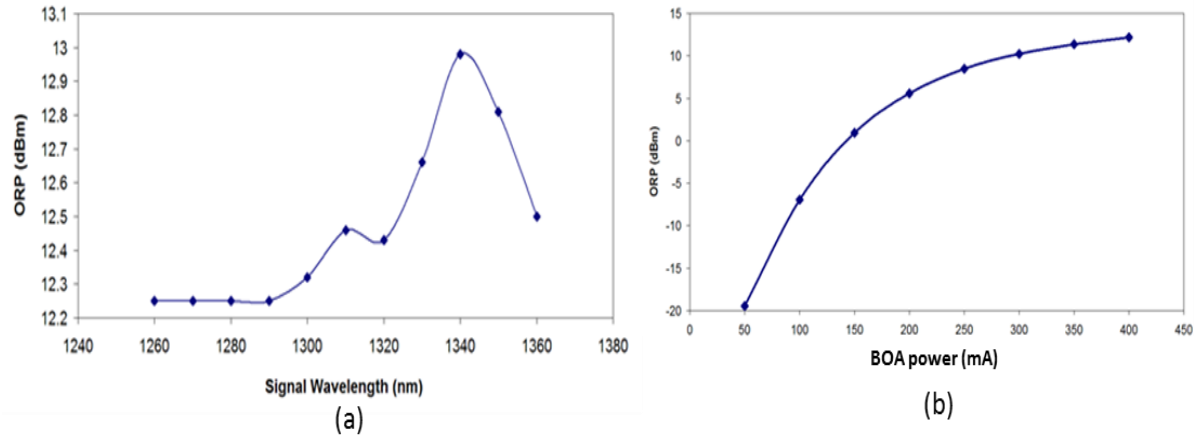

Figure 3.31 Optical return power for BOA (a) at varies wavelength (b) at varies operating current

In order to prevent the ORP, additional components were included in the setup. An isolator or an angle cleave connector is used. The isolator creates a unidirectional path and here the isolator is placed at both ends of the BOA. Meanwhile angle connectors prevent the Fresnel reflection at the air gap of the connector. The reflection of the ASE increases the NF of BOA, therefore all flat connector replaced by angle connector. The effects of the isolator and the angle connector on the gain and noise figure for various wavelengths are as shown in figure 3.32.

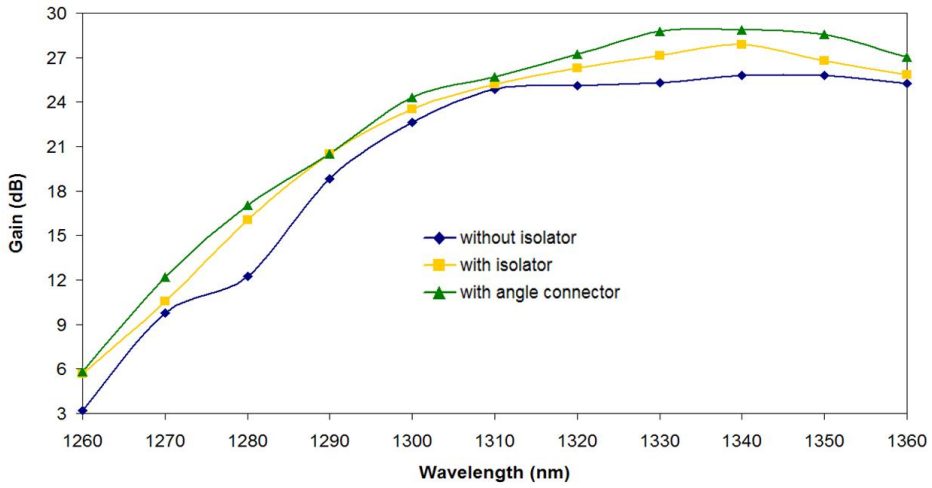

(a)

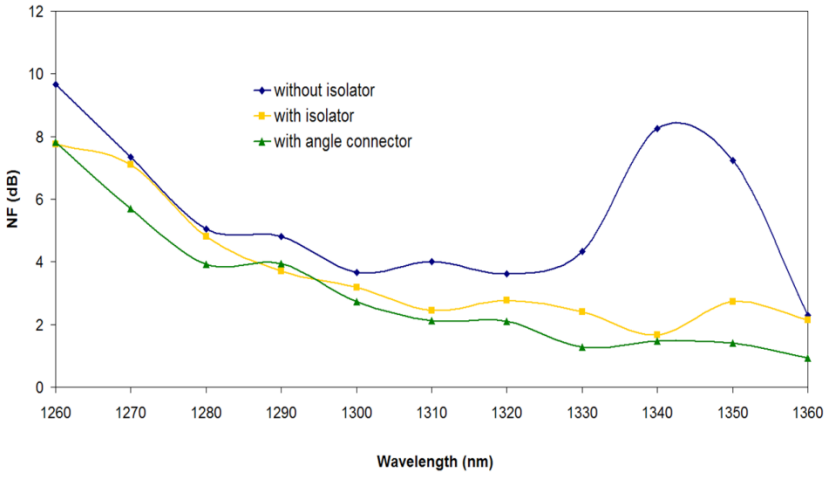

(b)

Figure 3.32 Characterization of BOA with unidirectional device (a) gain and (b) NF

By setting the power of the signal to be as small as -30 dBm and BOA power at 400 mA, gain improvement of 3 dB was obtained when the angle cleaved connector is used in the system as in figure 3.32. Meanwhile, only 2 dB is obtained when an isolator is used, probably due to the insertion loss of the isolator itself that is approximately 1 dB. The noise figure shows an average reduction of 3dB for BOA system with the isolator and the cleave angle connector.

The performance of BOA improved by utilizing the additional components, therefore the following experiment will be conducted by using this type of connector. The performance of BOA against feedback current is shown in figure 3.33. The current threshold for the BOA shows positive gain at 100 mA. After 250 mA the gains appears to be saturated with an increment of 4 dB.

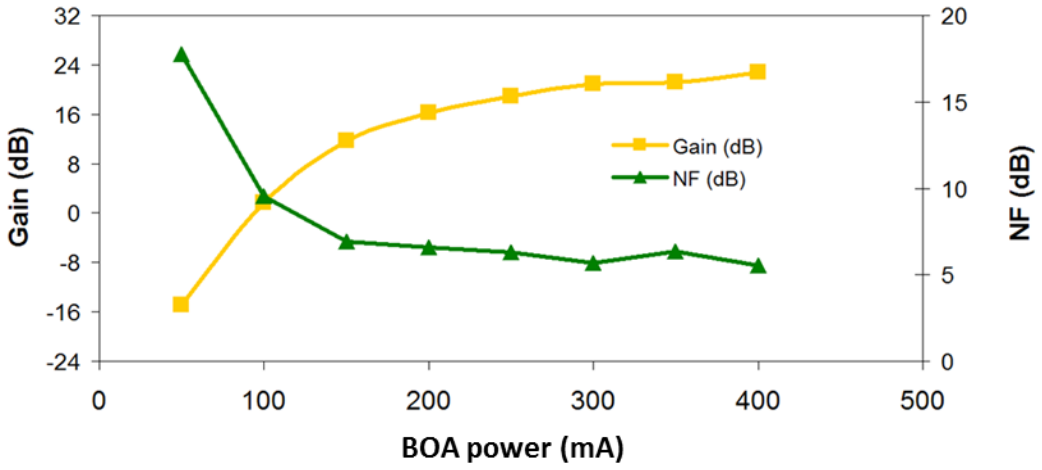

Figure 3.33 BOA characterization over operating current

As a comparison to the BOA, the performance of the conventional SOA for different signal wavelengths is shown in figure 3.34. Between the conventional SOA and BOA, BOA shows better performance including higher gain (28 dB @ 1350 nm), wider operating wavelength at 1270 nm till 1360 nm (90 nm) and generate extremely lower noise figure (~6 dB) as illustrated in figure 3.35. As for conventional SOA, it can amplify at limited wavelength range of 1300 nm-1335 nm (35 nm) at a maximum value of 15 dB and large value of noise figure ~20 dB was obtained.

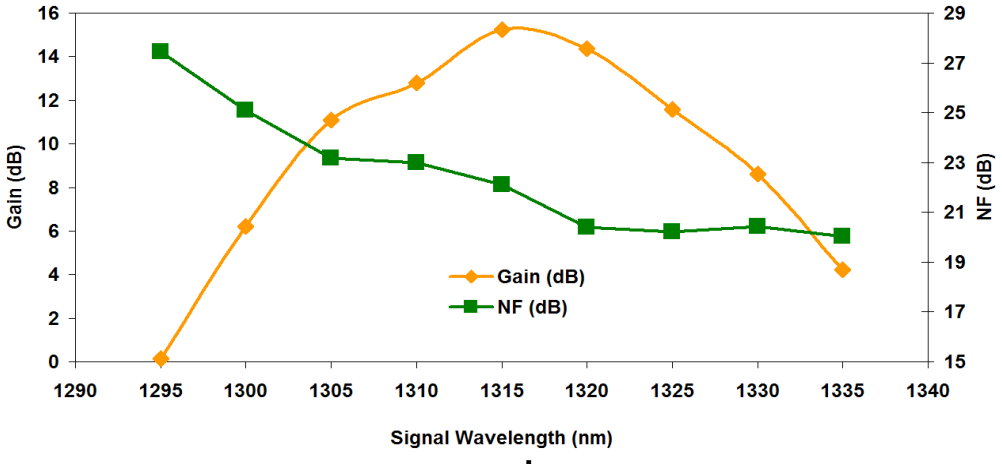

Figure 3.34 The performance of conventional SOA against signal wavelength

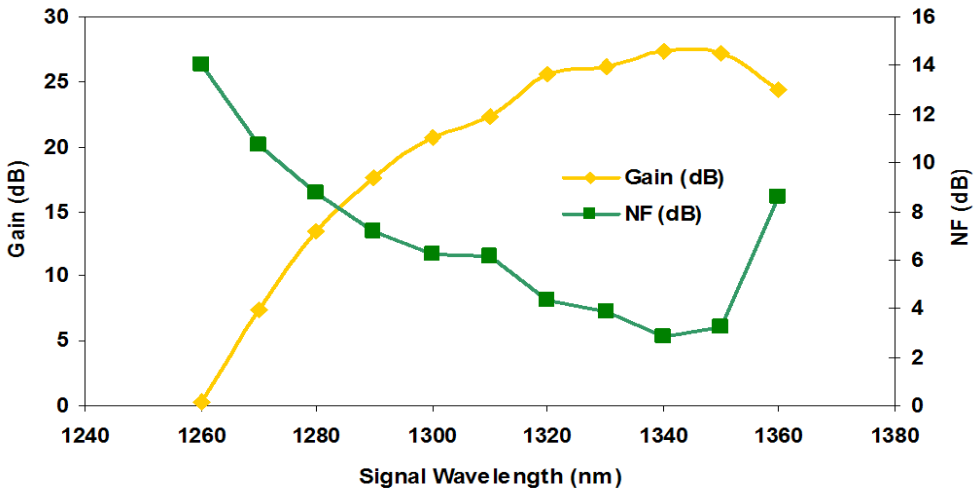

Figure 3.35 The performance of BOA against signal wavelength

The gain performance against signal input power is important to predict the maximum input power before it reaches its saturated point. Referring to the figure 3.36, saturated point of BOA occurs when the input power is at -10 dBm @ 1340 nm, at which spectrum gain decrease gradually. If the input power is higher than -10 dBm it will experience a small amplification from the BOA due to the lack of active ion (electrons) to reacts with all the photon that enters the medium.

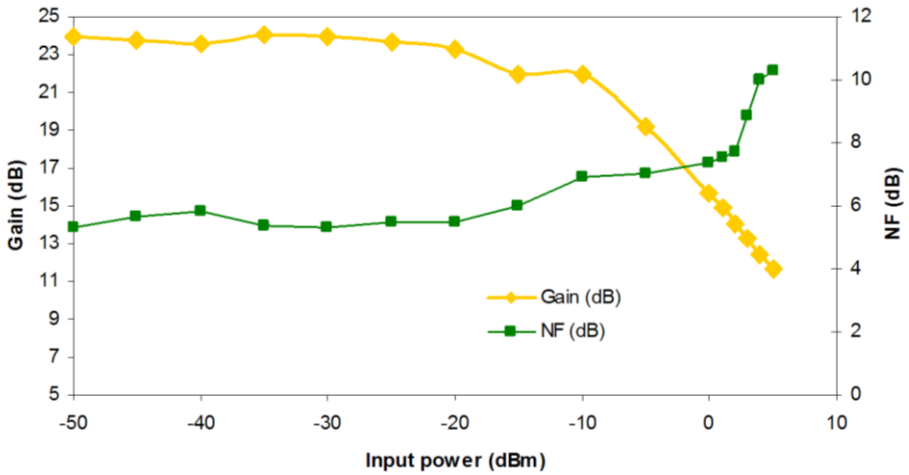

Figure 3.36 Characterization of BOA over the signal input power

As discussed in chapter 2, SOA experience a polarization dependent of gain (PDG). The PDG is defined as the difference between minimum and maximum gain obtained when the polarization of the system. Due to the same structure, BOA inherit

the same properties. Since optical fiber random polarizer and the BOA provide different gain for each TM and TE modes, the differences obtained is large. In this case, the maximum and minimum gain obtain can be observe at figure 3.37.

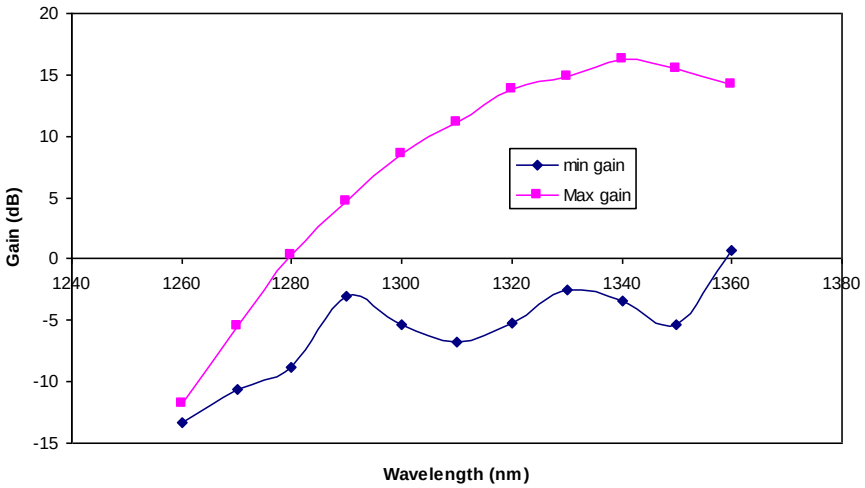

Figure 3.37 The gain performance at ar various polarization state

The maximum gain obtained is the same as the previous result shown in figure 3.35 . Certain polarization not only reduce the gain but also cause negative gain where the signal experience losses instead of amplification due to components attenuation. This greatly affect the generation of multiwavelength fiber laser. The polarization of the system need to be observed to generate better multiwavelength fiber laser performance.

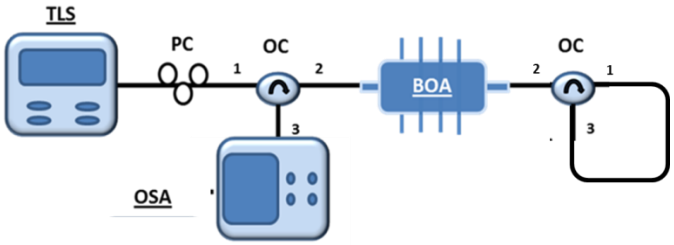

Figure 3.38 Configuration of doublepass BOA

Some of the techniques of producing multiwavelength fiber laser system require the generated signal to be reamplified in the same amplifier. Therefore, the performance of doublepass configuration is vital. The doublepass configuration for BOA assemble

mirror at end of the configuration as illustrated in figure 3.38. For BOA, the result of doublepass configuration is shown in figure 3.39. The mirror is placed at one end of the BOA and the gain is measured by tapping the power using the ocillator placed between the BOA and the TLS.

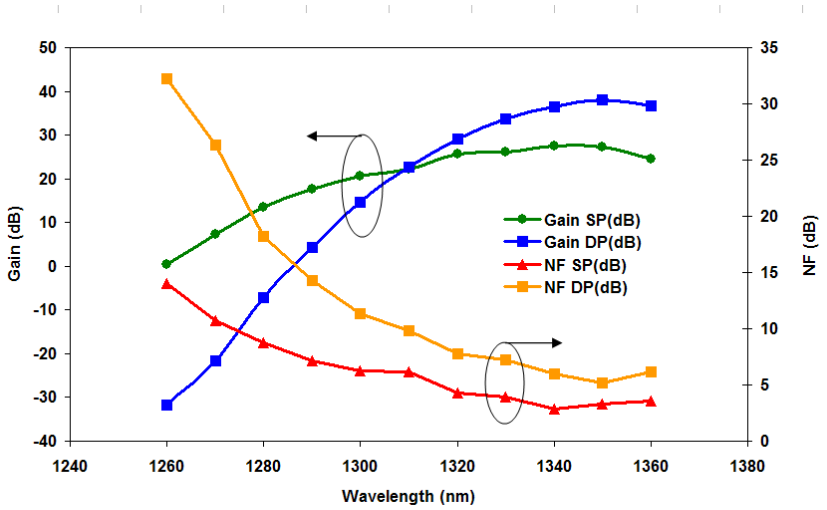

Figure 3.39 Gain spectrum over wavelength for single and doublepass

The result of figure 3.39 shows a comparison being made between a single and doublepass performance. The doublepass BOA configuration produces a maximum of 31 dB gain, however the gain flattening quality is reduced to 40 nm. Moreover the NF of the doublepass BOA configuration is around 3dB higher than singlepass configuration. This means that, in the case of multiwavelength fiber laser with multiple pass amplification for BOA, the gain might be higher at certain wavelength, where an uneven amplification of the channels is shown.

The next chapter will demonstarate the generation of multiwavelength fiber laser utilizing the optical amplifiers. The Booster optical amplifier is utilized as the main amplifier, together with the Raman fiber optical amplifier. The bismuth doped fiber will be used as the nonlinear medium to increase the stability of the multiwavelength fiber laser.

Chapter 4 Generation of O-band Multiwavelength Fiber Laser

4.1 Introduction

There has been much interest in multiwavelength fiber laser (MWFL) with promising applications in the area of fiber optics sensor system (Talaverano, et al. 2001 and Sun, et al. 2010), precision spectroscopy (Denizman, et al. 1993 and Yumoto, et al. 2010), optical testing of components, and as a source for wavelength division multiplexing system (Hurh, et al. 2005 and Tkach, et al. 1989)

There are numerous demonstrations on the multiwavelength fiber laser but mainly in C-band (Peng, et al. 2003), L-band (Zhao, et al. 2002), and lately in S-band (Zulkifli, et al. 2013). The need of generating multiwavelength fiber laser in the O-band region is due to support the possible application in the FTTH project. It is also required in the component testing of devices used in the optical network system. Therefore, this chapter proposes 3 techniques to generate O-band multiwavelength fiber laser and demonstrates its advantages as comparison to the other bands. Various techniques has been proposed and utilized to generate the multiwavelength output namely, the technique of polarization hole burning (PHB) (Chen, et al. 2007 and Yeh, et al. 2008), fiber Bragg grating (Ahmad, et al. 2009 and Liu, et al. 2008), utilizing the arrayed waveguide grating (Latif, et al. 2010) and also the stimulated Brillouin scattering effect in optical fiber (Zhan, et al. 2006).

However, only 3 techniques will be discussed in this chapter. In section 4.2, multiwavelength generation by Stimulated Brillouin Scattering (SBS) effect is proposed where the study of its threshold and the pattern generated with different cavity configuration setup are discussed. Another technique is using interferometer to generate

MWFL. Only two methods using interferometer are adopted namely the Sagnac Loop Mirror (SLM) which is discussed in section 4.3 and Fabry Perot Interferometer in section 4.4.

4.2 Design and Characterization of Multiwavelength O-band Brillouin Fiber Laser (MWBFL)

As discussed in chapter 2, the stimulated Brillouin Scattering (SBS) is one of the nonlinear effects in optical fiber that can generate the multiwavelength fiber laser. The presence of high electric field modifies the refractive index of the medium that changes it into an acoustic phonon which acts like a moving grating. The scattering resulted from the collision between this incident light and acoustic wave is called Brillouin scattering which moves in a backward direction of the incident light. The process last until there is no sufficient Brillouin pump power to produces new laser at shorter wavelength. The multiwavelength fiber laser produce is call as multiwavelength Brillouin fiber laser (MWBFL).

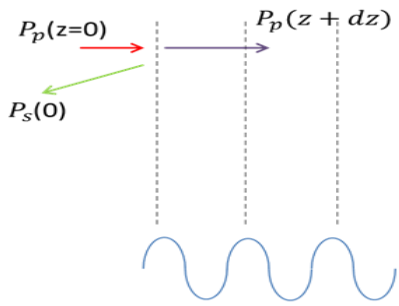

Figure 4.1 Depletion of Brillouin pump and generation of Stokes signal process

There has been greater interest in using the Brillouin effect to generate multiwavelength fiber laser, partly due to its simple approach and its ability to produce multiple wavelengths in a single mode optical fiber. Requirements such as low threshold power and narrow linewidth pump source are attractive area of study (Zhu, et al. 2005, Bakar, et al. 2009 and Al-Mansoori, et al. 2009). However there have been

numerous demonstrations in the literature on the operation of multiwavelength Brillouin fiber laser (MWBFL) in the C-band region (Shirazi, et al. 2008, and Harun, et al. 2007), S-band and also L-band (Al-Mansoori et al. 2007, 2008 and 2009).

In order to generate the MWBFL, the intensity of electric field generated by the laser source has to exceed the Brillouin threshold. Brillouin threshold estimated by neglecting pump depletion of equation 2.4 and equation 2.5 that would be simplified to equation 4.1 and 4.2;

$$I_p(z) = I_p(0)e^{-\propto z} \tag{4.1}$$

$$I_s(O) = I_s(L)exp\left(\frac{g_B P_0 L_{eff}}{A_{eff}} - \propto L\right) \tag{4.2}$$

The depletion of Brillouin pump intensity and the growth of Stokes intensity can be represented as equation 4.1 and 4.2 respectively. Equation 4.2 shows that Stokes is generated in the backward direction. Both equations suggest that the Brillouin threshold can be manifested when the power of the backward scattering Stokes is equal to the initial power of the Brillouin pump. The closest approximation of the non-ideal condition, the Brillouin threshold is estimated at the backward scattering power of 10^{-1} to 10^{-4} of the Brillouin pump power. By considering that the Brillouin gain spectrum to have a Lorentzian shape, the Brillouin threshold power (P_{th}) is defined as;

$$P_{th} = \frac{21A_{eff}}{g_B(v_B)L_{eff}}\left[1 + \frac{\Delta v_P}{\Delta v_B}\right] \tag{4.3}$$

where, A_{eff} is the effective cross section of the fiber used, $g_B(v_B)$ is the peak value of the Brillouin gain coefficient, $\frac{\Delta v_p}{\Delta v_B}$ for is the ratio of frequency linewidth of the pump over the spontaneous Brillouin linewidth (Bayvel, et al. 1990) and L_{eff} is the effective length. The Stokes energy has a slightly lower energy than the Brillouin pump and resulted in a

longer wavelength. The spacing between the BP and the 1st Stokes and subsequently for 2nd, 3rd and so forth, is governed by equation 4.4 as shown below (Agrawal, 1995);

$$f_s = 2nv_a/\lambda \tag{4.4}$$

where n is a group refractive index, v_a is an acoustic velocity, and λ is the wavelength of the BP. Referring to the equation 4.3, the Brillouin threshold depends on L_{eff} and A_{eff} which vary for different wavelength.

4.2.1 Experimental study of the Brillouin threshold.

Measurement of the Brillouin threshold is conducted by observing the backscattered power which represents the Stokes power. Figures 4.2, depicts the experimental setup of measuring the Brillouin threshold.

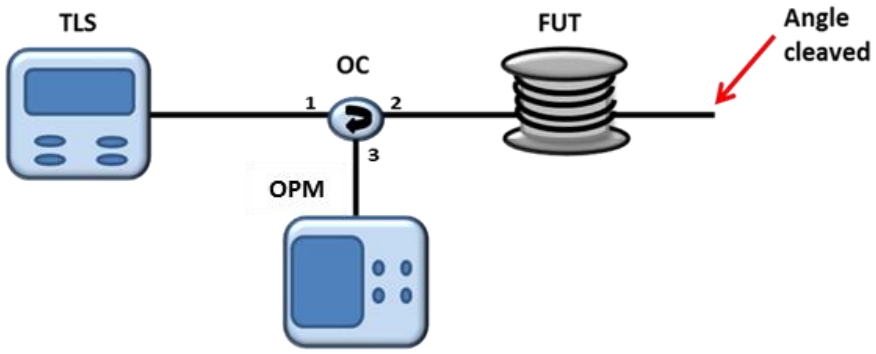

Figure 4.2 Basic setup of measuring the Brillouin scattering backscattered power.

The basic setup of measuring Brillouin scattering consists of a tuneable laser source at 1310 nm (TLS), 3 port optical circulators in the O-band region (OC), fiber under test (FUT) as the Brillouin gain medium and an optical spectrum analyser (OSA) (YOKOGAWA AQ6370) was used to measure the backscattering power with a resolution of 0.015 nm. The tuneable laser source (SANTECTSL510) has a tuning range that spans from1260 nm to1360 nm which covers the entire O-band region with an output power of 12 dBm and a linewidth of 40 MHz. The TLS acts as the Brillouin pump (BP) and the output is connected to port1 of the OC, which then travels to a

spool of nonlinear optical fiber from port 2. The Brillouin pump generates an acoustic wave which acts as a moving grating which then interacts back with the Brillouin pump. This generates a backscattered Stokes signal which travel backwards relative to the Brillouin pump and this is labelled as 1st Stokes. The end of the fiber was angle cleaved to minimize Fresnel reflection. The reflection can affect the measurement of the backscattered power. The backscattered power is measured by optical power meter (OPM) at port 3 of OC. Whenever the backscattered power reach 10% of its BP power, that particular BP power will be considered as the threshold power (P_{th})

The experimental results shows the measurements on FUT for three different types of fibers, namely, the normal single mode optical fiber (SMF-28) of length 50 km, dispersion compensated fiber (DCF) of length 7.7 km and Truewave Reach fiber (TWF) with a length of 20 km. Figure 4.3 shows the backscattered power against the Brillouin pump power for all the three fibers tested.

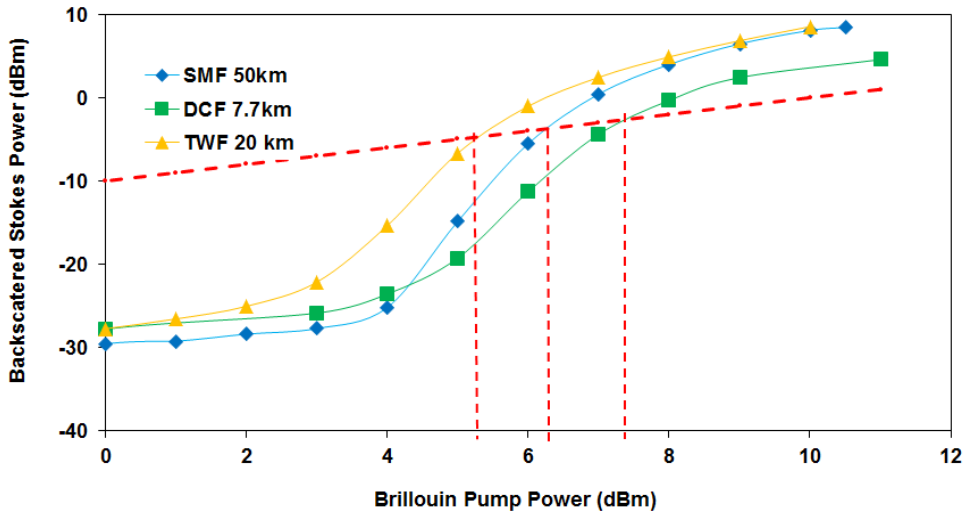

Figure 4.3 Comparison of backscattered stokes power between there different fibers under test.

The red dotted line and dotted vertical lines as indicated in the figure show the points where the backscattered Stokes power readings are 10% of the input power as

defined in equation 4.5. According to the measurements, the Brillouin threshold power is approximately equal to 5.2 dBm for 20 km of Truewave Reach fiber (TWF), 6.2 dBm for 50 km SMF, and 7.5 dBm for a 7.7 km DCF. The P_{th} preferred to be as low as possible to easily generate the SBS effects. Among these three fibers, the TWF has the lowest Brillouin pump threshold. Therefore, this optical fiber is the preferred fiber for the remaining part of the experiment on the Brillouin fiber laser in the O-band region.

Again by referring to equation 4.3, the Brillouin threshold depends on its effective length, effective core area and also the Brillouin gain coefficient. The Brillouin gain coefficient is defined as gain at the peak of Lorentzian spectrum of Brillouin gain spectrum $g_B(\nu_B)$. The peak of the Brillouin gain spectrum is given by equation 4.5;

$$g_p = g_B(\nu_B) = \frac{2\pi^2 n^7 p_{12}^2}{c\lambda_p^2 \rho_0 \nu_A \Gamma_B} \tag{4.5}$$

By using the value measured from the previous experiment of Brillouin threshold, the Brillouin gain coefficient can be obtain mathematically from equation 4.3. Table 4.1 shows parameters of each tested fiber together with calculated Brillouin gain coefficient $g_B(\nu_B)$.

Table 4.1 The parameters for different types of fibers

Type of fiber	**A_{eff} (μm^2)**	**L_{eff} (km)**	**$g_B(\nu_B)$ ($x10^{-1}$m/W)**
SMF	69.40	12.56	2.767
DCF	16.62	5.76	1.102
TWF	55.42	10.00	3.488

The value of $g_B(\nu_B)$ helps to create a numerical study on the effect of the lengths of each fiber towards their Brillouin threshold. The effect is as shown in figure 4.4.

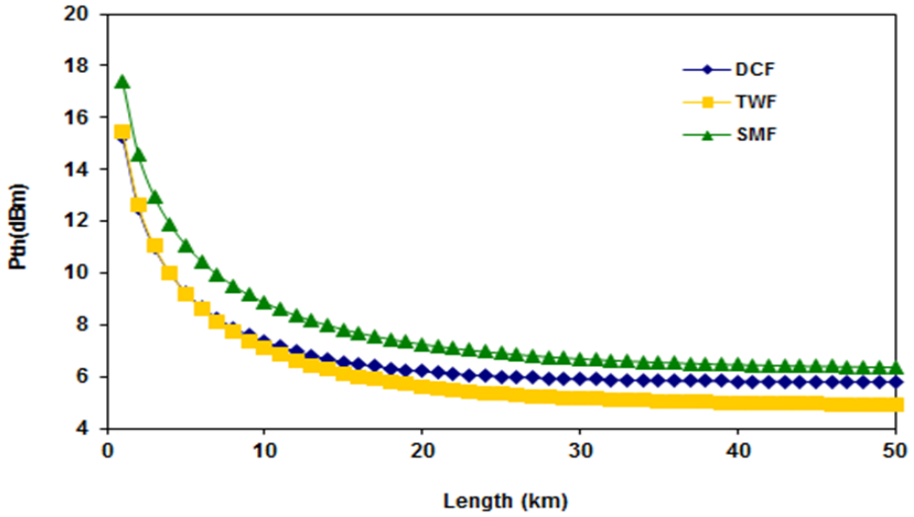

Figure 4.4 Brillouin threshold power over length for different types of fibers

According to figure 4.4, the threshold power for all the 3 fibers decreases with increasing fiber length. The threshold power is high for the first 8km and exponentially decreases before saturation occurs. The TWF has the lowest saturation value compared to others fiber.

Equation 4.3, also shows that the values of Brillouin gain coefficient depend on the Brillouin pump wavelength, which means that at longer wavelength the Brillouin gain coefficient decreases hence it affect the Brillouin threshold. Therefore an experimental comparison between the Brillouin threshold for Stokes generation for 1310 nm (O-band) and 1550 nm (C-band) is demonstrated as indicated in figure 4.5.

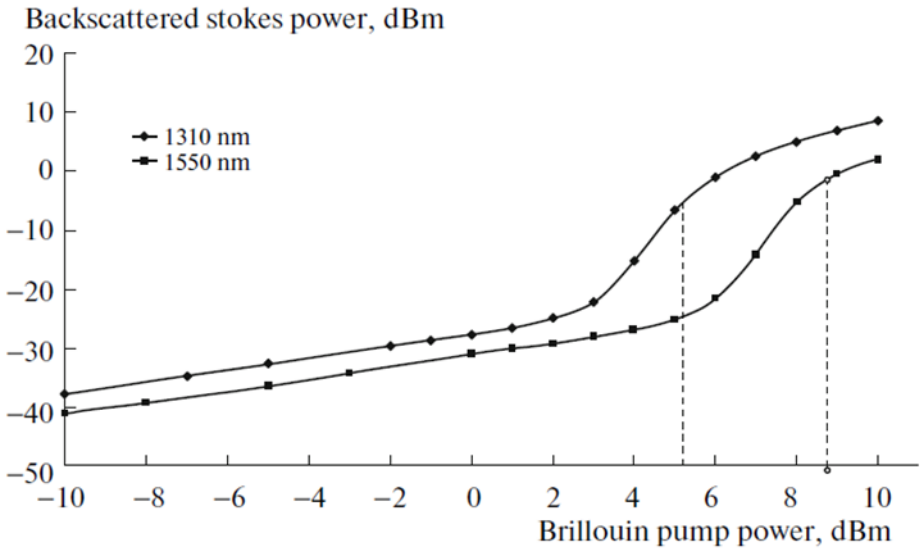

Figure 4.5 Backscattered stokes power for BP wavelength of 1310 and 1550 nm.

By utilizing the same technique and employing 20 km of the TWF, it can be shown that the BP threshold for operation in the 1310 nm is lower than that for 1550 nm with values of 5.2 dBm and 8.5 dBm, respectively.

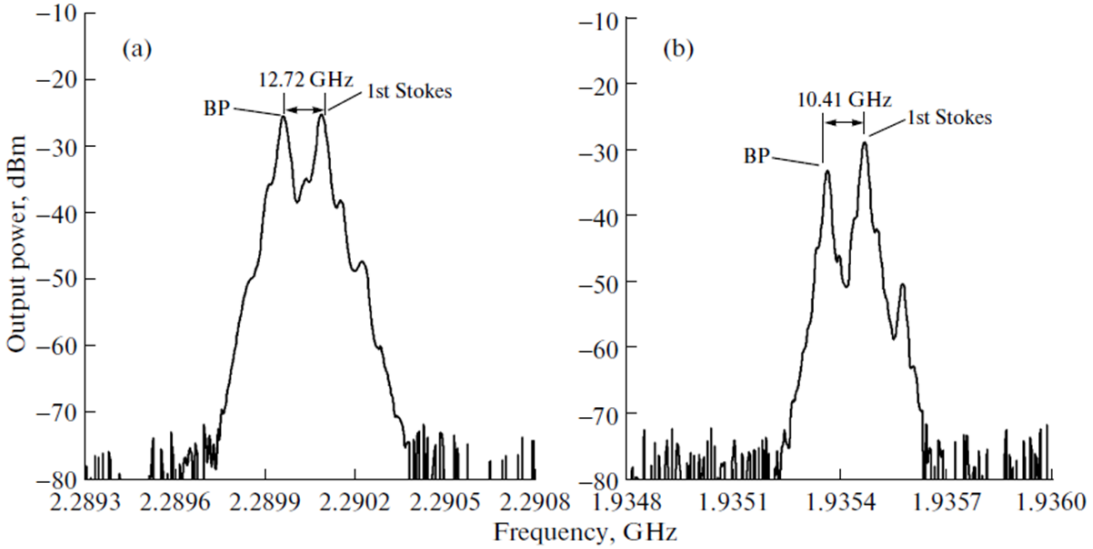

Figure 4.6 Comparison of the line spacing between the BP and its Stokes for (a) O-band and (b) C-band regions.

From figure 4.6, the spacing between the BP and the 1st Stokes is 12.72 GHz for O-band and 10.41 GHz for the C-band. This can be verified using equation 4.4. From

these measurements and the results obtained, the operation of the Brillouin fiber laser in the O-band gives a better performance as compared to the C-band region.

4.2.2 Generating Multiwavelength Brillouin Fiber Laser in Ring Cavity

Once the threshold of Brillouin pump is known, the multiwavelength Brillouin fiber laser can be generated and controlled by manipulating the Brillouin pump power. In this technique, the nonlinear medium is desired to have a high value of Brillouin gain coefficient $g_B(v_B)$ and low threshold power. Therefore, the True wave Reach Fiber (TWF) is selected as the medium to generate multiwavelength Brillouin fiber laser in the following sections. Multiwavelength Brillouin fiber laser is generated by either a ring or linear cavity. Therefore, both configurations are demonstrated in this section starting with the ring cavity configuration as shown in figure 4.7 that allows unidirectional pathway.

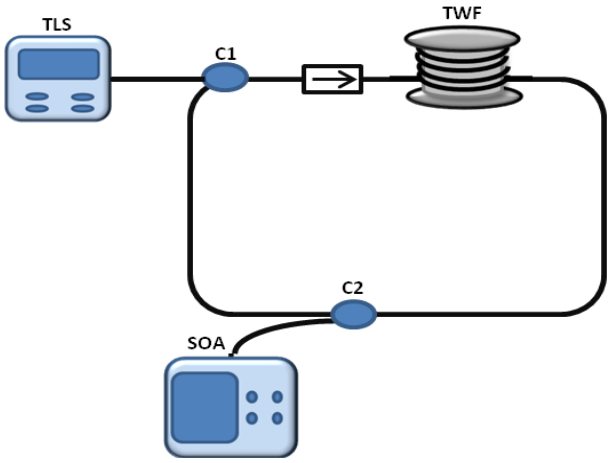

Figure 4.7 The configuration of ring like shaped cavity.

The MWBFL by ring cavity configuration is obtained by using an optical coupler (C1) where the BP signals from TLS enters the C1 and stimulated Brillouin scattering generated from the nonlinear medium of TWF. The generated SBS signals then travel to another coupler of which 10% of its power is tapped to be analysed by the OSA. The remaining signals are then feedback into the TWF through C1. An isolator is placed in between C1 and TWF to prevent any signal from damaging the TLS. By

varying the ratio of C1 with 80:20, 60:40, and 50:50, the spectrum of multiwavelength is observed as shown in figure 4.8.

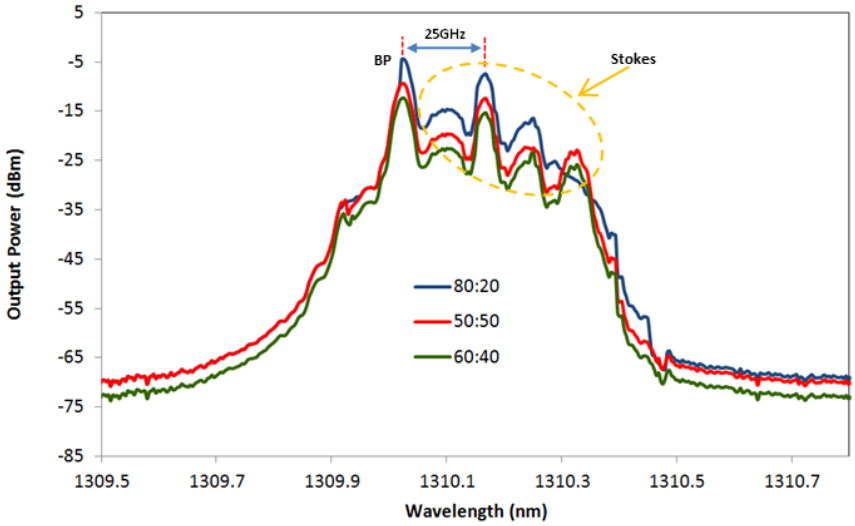

Figure 4.8 Output power for multiwavelength Brillouin fiber laser with ring cavity for different couplers.

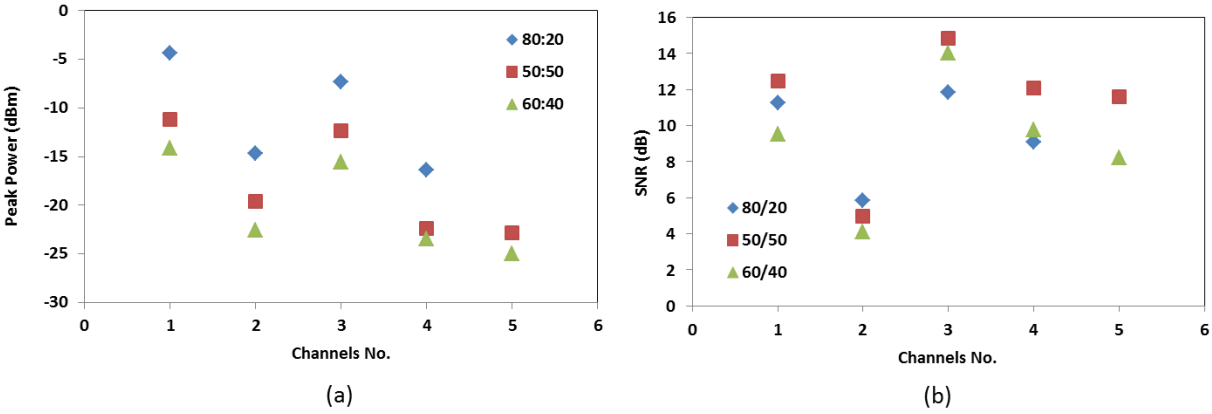

Figure 4.9 The performances of Multiwavelength Brillouin fiber laser with ring cavity for different couplers.

Due to the unidirectional path created by the cavity, preventing the beam generated in opposite direction of signal propagation. Therefore, the odd Stokes suppresses and seems to generate multiwavelength with 25 GHz spacing. Varying the C1 ratio, the connection of the BP power and feedback power is optimised. By setting the BP at 12 dBm at wavelength 1310 nm, the number of channels generated from the ring cavity is 5 for the ratio of 50:50 and 60:40. Meanwhile for C1 80:20 ratio only

generates 4 peaks but with high peak power. The maximum peak powers are -4.35 dBm, -11.14 dBm, and -14.14 dBm with coupler ratio value of 80:20, 50:50 and 60:40 respectively.

4.2.3 Generating Multiwavelength Brillouin Fiber Laser in Linear Cavity

(a) Double pass configuration

Linear cavity allows bidirectional propagations in the nonlinear medium depending on its numbers of passes. Configuration of linear cavity double pass feedback is similar to the configuration of figure 4.9 with addition of optical circulator (OC2) at the end of TWF fiber as reflector as illustrated in figure 4.10. The port 2 of OC2 is connected to the end of TWF while port 3 and port 1 is spliced together to insure the bidirectional position of the signal.

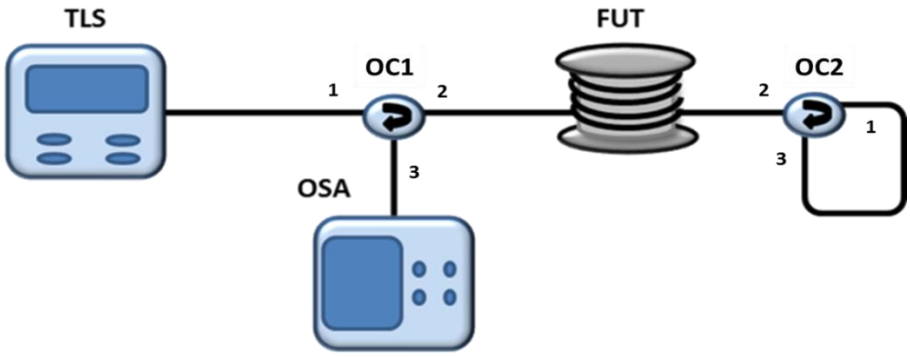

Figure 4.10 Multiwavelength Brillouin fiber laser linear cavity configurations

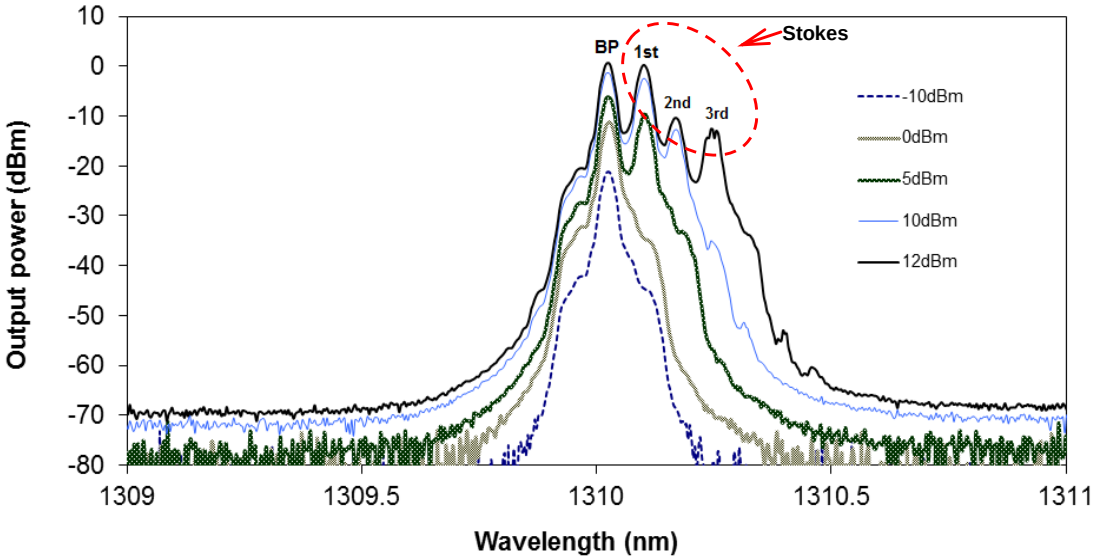

Figure 4.11 Brillouin fiber laser evolves at different Brillouin pump powers for TWF

The dependence of number of Stokes with BP power is shown with varied pump power in figure 4.11. A maximum of four peaks can be generated from this set up with a BP pump of 12 dBm. The first peak is the BP with a wavelength of 1310.2 nm and the second peak is the first backward Stokes (1st Stokes) at 1310.08 nm, 2nd Stokes at 1310.17 nm, and 3rd Stokes at 1310.26 nm. The analysis of important parameter like peak power and the SNR is shown in following figure 4.12.

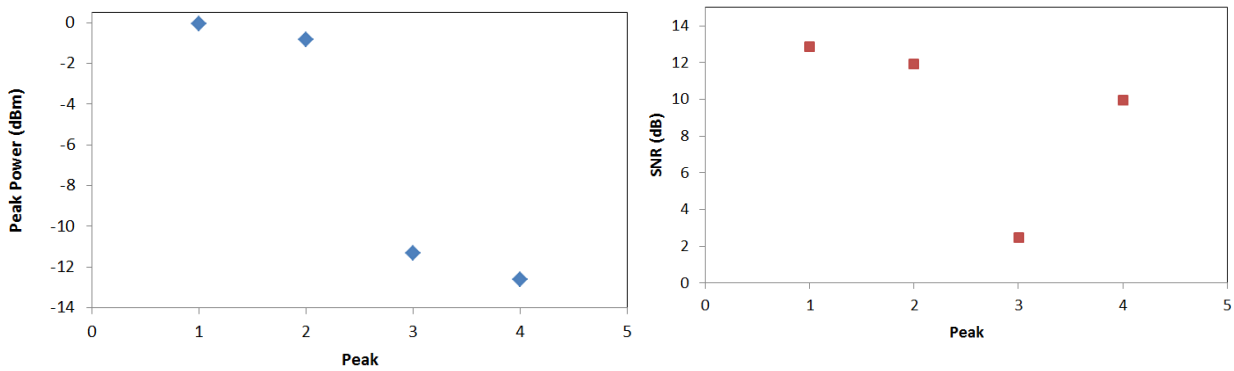

Figure 4.12 The performance of peak power and signal to noise ratio (SNR) of each peaks.

Unfortunately the performance of generated multiwavelength Brillouin fiber laser was unsatisfied where the fluctuation of peak power for all 4 of them is more than 3dB. The same case is found for signal to noise ratio (SNR) in figure 4.12.

(b) Multiple-pass configuration

Multiple-pass configuration allows the backward and forward signals of two interfering multiple times in the nonlinear medium. In order to generate the multiple pass MWBFL another optical circulator OC was inserted at the other ends at the configuration as shown in figure 4.13

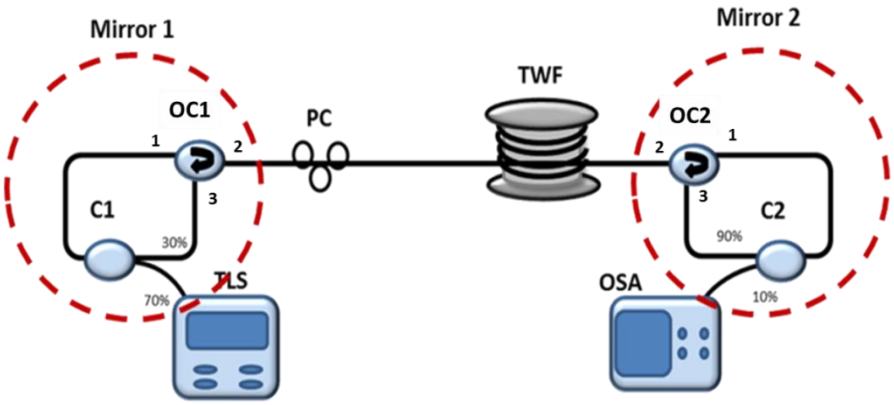

Figure 4.13 The multi pass configuration of multiwavelength Brillouin fiber laser

Multiple pass of MWBFL is generated by two optical circulators (OC1 and OC2) act as mirrors. The two mirrors are constructed using 3 ports optical circulators and 1x2 couplers. For mirror 1, optical circulator OC1 is connected to coupler C1 with a coupling ratio of 70:30. The reflection is created by connecting port 3 and port 1 of OC1 with 30% leg and common leg of C1 respectively. As a result, any signal coming from port 2 that transmitted to port 3 will flow through C1 with transmission of 30% of its power and entered port 1 of OC1 to be transmitted back at port 2. This arrangement will created mirror with 30% reflectivity. Meanwhile, the 70% leg is connected to

external source laser to tunnel the Brillouin pump into the cavity. For mirror 2, the optical circulator OC2 was connected to coupler C2 with coupling ration of 90:10. Port 3 of OC2 was connected to common leg of C2 while its port 1 was connected to 90% leg of C2. Signal that approached from port 2 OC2 will appear at port 3 which then run through common legs of C2 and split its power. Approximation of 90% of its power were transmitted back to port 2 OC2 through its port 1, while another 10% of the signal power used to analysed by connecting it to optical spectrum analyser (OSA).

The configuration mechanism set up 70% of the BP signal transmitted from C1 through port 1 of OC1 which subsequently entered its port 2. Then the BP interacts with the nonlinear medium to generate the 1st Stokes which moving at the opposite direction of BP. The following figures 4.14 shows the generated MWBFL spectrum with multiple-pass configuration by setting the parameters as previous linear cavity configuration.

The performance of MWBFL in linear cavity has shown an improvement of SNR with an average of 20dB as illustrated in figure 4.15. The peak power does not show much comparison with the double-pass configuration but the anti-stokes starts to develop.

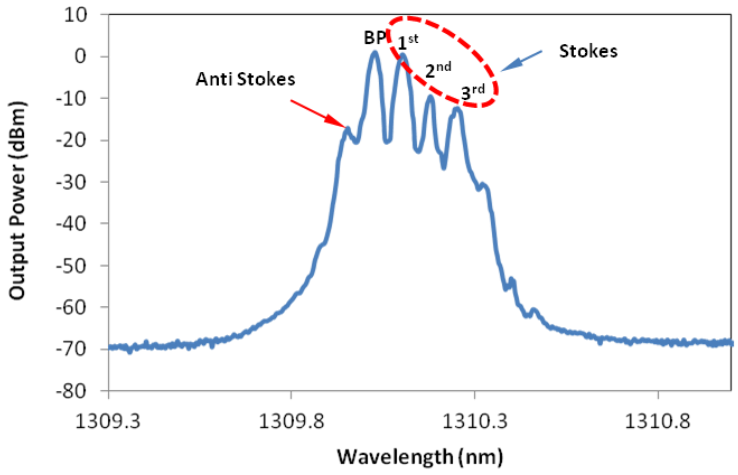

Figure 4.14 The spectrum of MWBFL with multiple pass configuration.

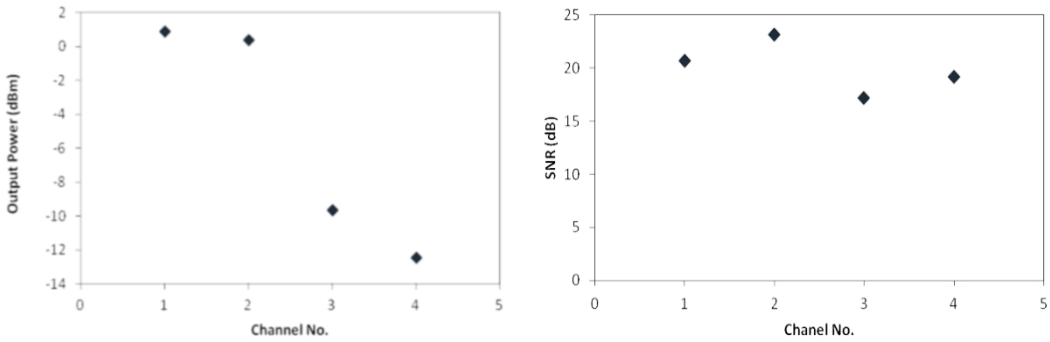

Figure 4.15 The performances of multiwavelength Brillouin fiber laser with multiple-pass configuration.

4.2.4 Generating the MWBFL utilizing BOA as Amplifier

The requirement of good transmission system are sources with high optical signal to noise ratio (OSNR), narrow line width, broad wavelength tune ability, flat or even peak power, and stable lasing output power. Thus far the multiwavelength Brillouin fiber laser demonstrated have poor quality where the SNR measurement is low and has broad line width. The performance could be improved by increasing the Brillouin pump power. Therefore small transformation made not only to boost up the BP power but also to amplify the Stokes signals. The transformation is made by adding amplifier in the configuration.

Previously, chapter 3 demonstrated the performance of 3 types O-band optical amplifier. Among those three, booster optical amplifier (BOA) has produced the highest gain. Hence, in the following section, the BOA will act as an amplifier to improve multiwavelength Brillouin fiber laser performance.

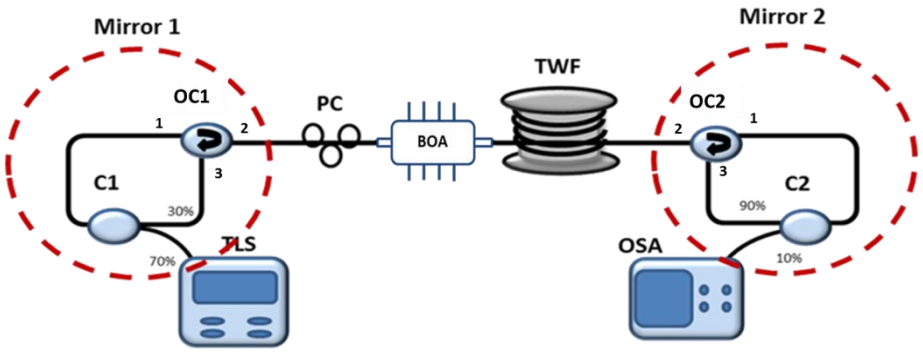

Figure 4.16 Experimental set up of linear cavity for multiwavelength Brillouin/BOA fiber laser.

Besides the amplifier, the transformation is also made to the configuration of cavity where instead of passing only twice before spectrum extracted to be analysed, the BP will pass multiple time by placing another optical circulator as shown in figure 4.16. This multiple pass configuration is chosen according to the performance of high gain of BOA and also to increase the interaction of BP and Stokes signal to the BOA.

Figure 4.16 illustrates linear cavity of multiwavelength Brillouin/BOA fiber laser (MWBBFL). The configurations consists of an external laser source as a Brillouin Pump (BP), O-band BOA to amplify the Brillouin Pump and Stokes that produced from the cavity, a PC to change the polarization of BP, and two mirrors like reflectors at both end of the linear cavity. The nonlinear medium is the 20km TWF.

The mechanism of the configuration is similar to the section 4.2.4 (b) where the beam passes the nonlinear medium and BOA multiple times. The BP signal of 70% transmitted from C1 through port 1 of OC1 which subsequently entered its port 2. The BOA then amplified the BP power where the gain characteristic is as shown in figure 3.32 (a). The amplified BP was then interacts with the nonlinear gain medium TWF to generate the 1st Stokes which moving at the opposite direction of the BP. This generated Stokes, were then amplified by the BOA and moving towards mirror 1, which then reflected only 30% of its power back to the BOA to be amplified again. The amplified

1st Stokes now interacts with TWF as BP to generate 2nd Stokes, this process will continue to take place until the latest Stokes have no sufficient power to be BP for the following Stokes. At the same time, the peak power of the Stokes was amplified by the Brillouin amplifier and until reached its saturated gain. Meanwhile, the remaining BP power that passed through TWF was reflected by mirror 2 and back to TWF, which will generate Stokes if it has sufficient power.

The addition of BOA into the Brillouin fiber laser setup has not only increased the BP power but also the Stokes power. The spectrum obtained for the setup is as shown in figure 4.17 with variation of BP power.

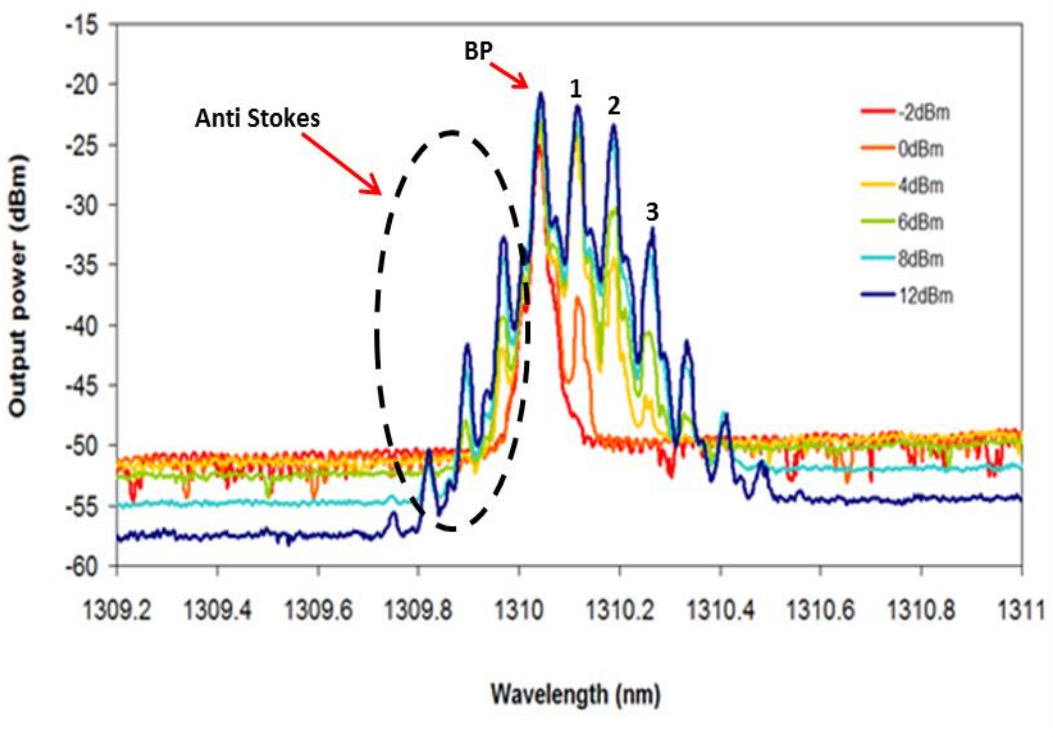

Figure 4.17 Multiwavelength Brillouin/BOA fiber laser

The generated spectrum increase in different channels and there is also appearance of anti-Stokes. The anti-Stokes is generated from the nonlinearity of the BOA according to the structure of the BOA. High nonlinearity has increased its ability to produce four wave mixing effect. Four wave mixing (FWM) is one of the nonlinear refraction effects originated from the third order susceptibility. The FWM is an

intermodulation phenomenon whereby the interaction between two signals generates the third signal which is called an idler. As the BP generates its first Stokes, both of the signals generate the third and the next fourth signals FWM effect. The fourth signal is represented with blue shift and looks like an anti-Stokes of the Brillouin laser. By adding BOA into the cavity it managed to generate 3 anti-Stokes and 4 Stokes with BP power to be set at 12 dBm.

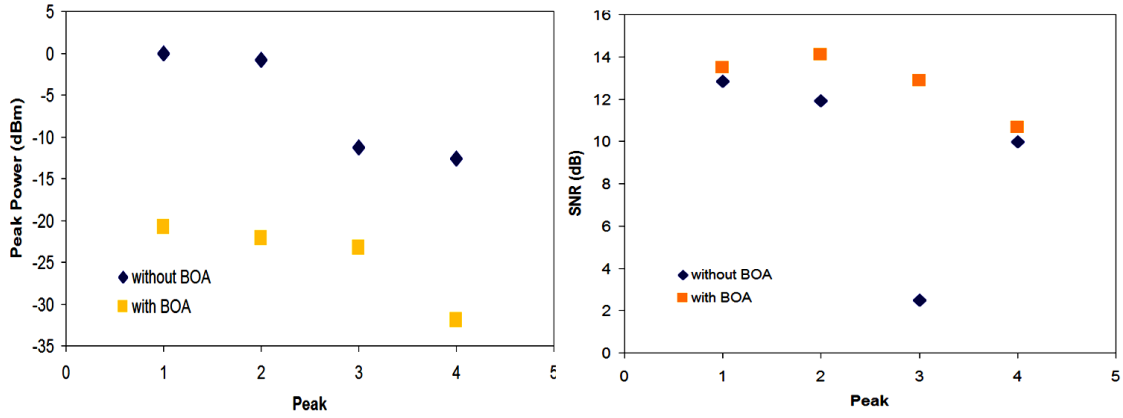

Figure 4.18 Comparison of multiwavelength Brillouin fiber laser for the first 4 peaks with and without BOA

As compared to the previous setup of multiwavelength Brillouin fiber laser, an improvement result is illustrated in figure 4.18 that shows the SNR and the peak power for the first 4 peaks. The SNR shows an improvement on its fluctuation and value but the peak power suffer losses caused by the 10 dB coupler used in this experiment to extract the spectrum.

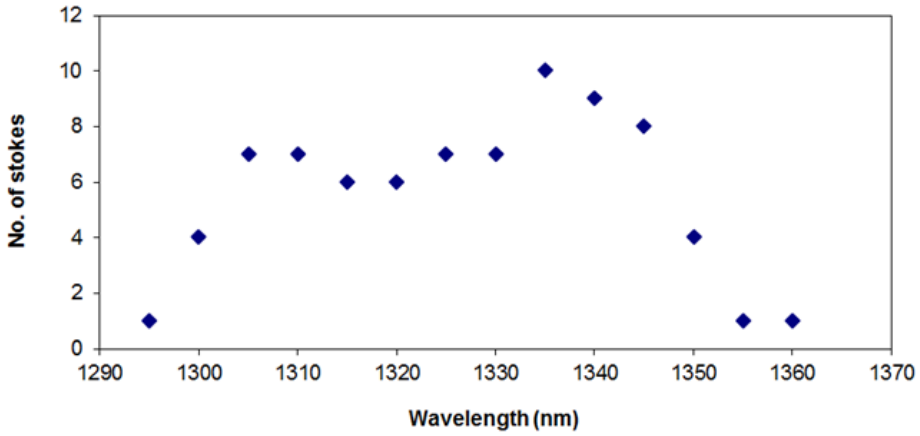

Figure 4.19 Number of Stokes at different wavelength

By utilizing the BOA the numbers of stokes generated will depend on the gain of the BOA. As depicted in figure 4.19, the highest number of peak generated at 1340 nm is compatible with the gain spectrum of the BOA.

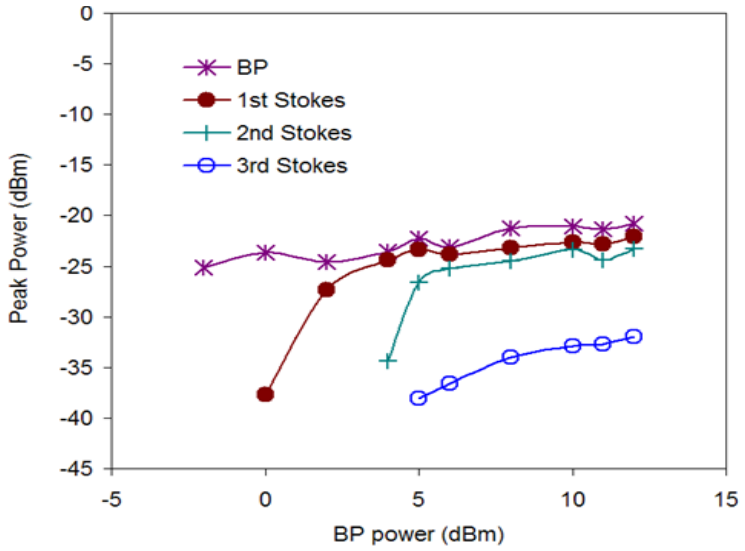

Figure 4.20 peak powers of transmitted Brillouin and the first three Stokes.

As mentioned previously, flatness of the peaks power is one of the requirements of decent multiwavelength laser source. Therefore the details of multiwavelength Brillouin/BOA fiber laser flatness are shown in figure 4.20. Unfortunately the channels show irregularity in peak power. All first 3 Stokes have at least 1 dB separation between each other at 12 dBm BP power and have larger difference for the 3rd Stokes due to

insufficient power of Stokes. Hence improvement shall be made to the flatness of the MWBFL.

4.3 Design and characterization of multiwavelength O-band fiber laser by Sagnac Loop Mirror technique

Another way of producing multiwavelength fiber laser is by utilizing Sagnac Loop Mirror (SLM) technique. The SLM is the assembly of slicing technique, where the SLM acts as comb filter through interferometer principle towards a broad band source such as the ASE used as the signal seed.

The O-band SLM multiwavelegth fiber laser produced by employing the BOA as an ASE source due to its high ASE peak power level and broad bandwidth. As illustrated in figure 4.21, the BOA is placed right before the SLM. Once the ASE of the BOA reach the SLM, the power will split evenly into two beams and both beams will interfere at the PMF. The SLM generate multiwavelength fiber laser due to constructive and destructive interference which resulted from slicing of the ASE. The cavity or resonance architecture can be either ring or linear as shown in figure 4.21(a) and 4.21 (b) respectively.

Linear cavity generated by placed mirrors at the both end of the SLM setup so that the generated beams can pass through the BOA repeatedly for multiple amplifications. As for the ring cavity configuration, the setup is assembled by connecting the end of the 2x2 coupler with the BOA to ensure the feedback of the beams in unidirectional pass. The 10dB coupler in placed between to extract the spectrum generated.

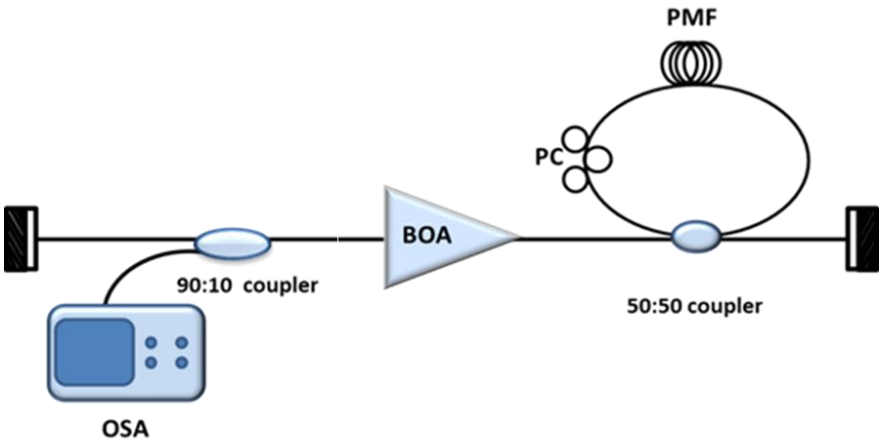

(a)

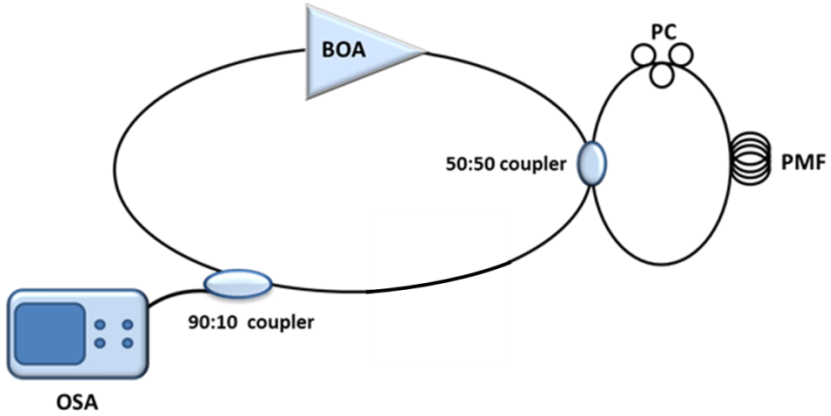

(b)

Figure 4.21 Multiwavelength fiber laser with (a) linear cavity (b) ring cavity SLM fiber laser setup

Both cavities result in different spectrum as shown in figure 4.22. The spectrum generated by taking the length of PMF to be 2m and the BOA power to be set at 400mA.

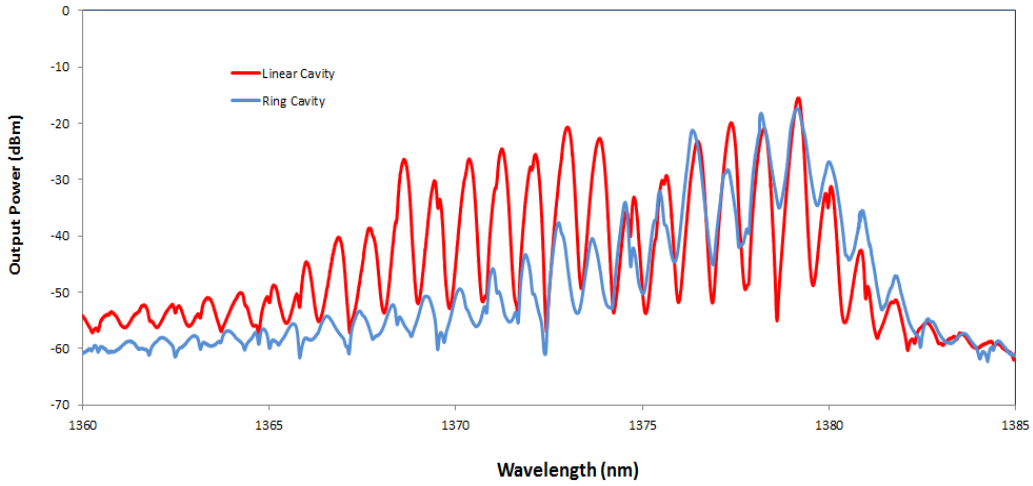

Figure 4.22 The spectrum of the ring cavity and the linear cavity of fiber laser SLM configurations.

The ring cavity generates only few number of channels with poor SNR due to high ASE noise which also been amplified by the BOA as in figure 4.23. The ring cavity generates only 5 high peak channels (>-30 dBm) meanwhile the linear cavity managed to generate more than 10 channels. Linear cavity also generates better performance of SNR which average value is more than 30dB. Due to this improvement, therefore for the next experiment related to SLM fiber laser, linear cavity configuration is utilized.

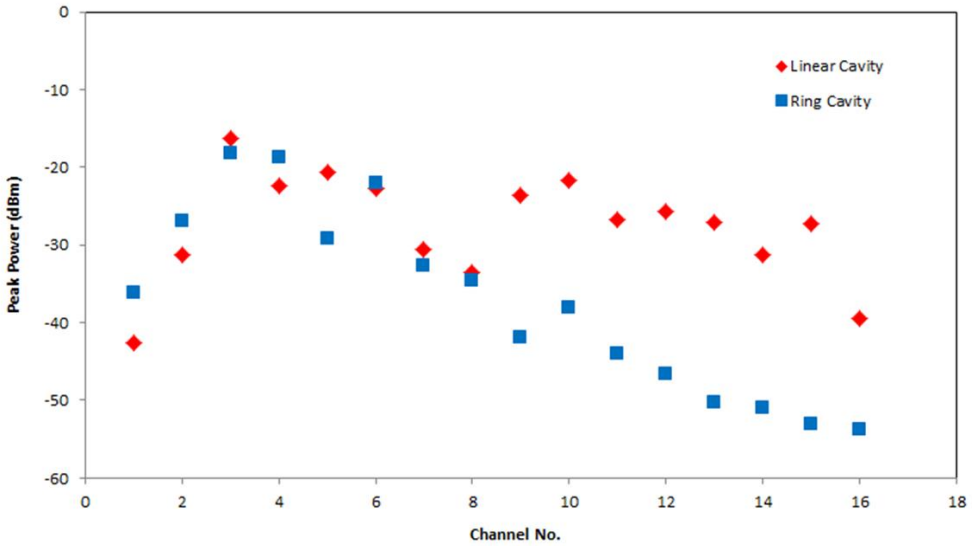

(a)

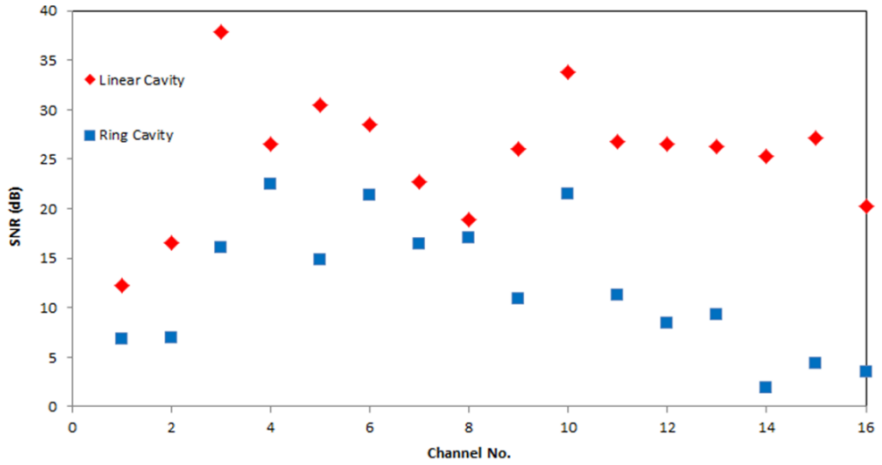

(b)

Figure 4.23 The performance of (a) linear and (b) ring cavity

Both configurations consist of Polarization Controller (PC) that changes the polarization state of the beam that goes through it. By adjusting the PC hence varying the polarization state, different interference patterns were found but the spacing between channels unchanged

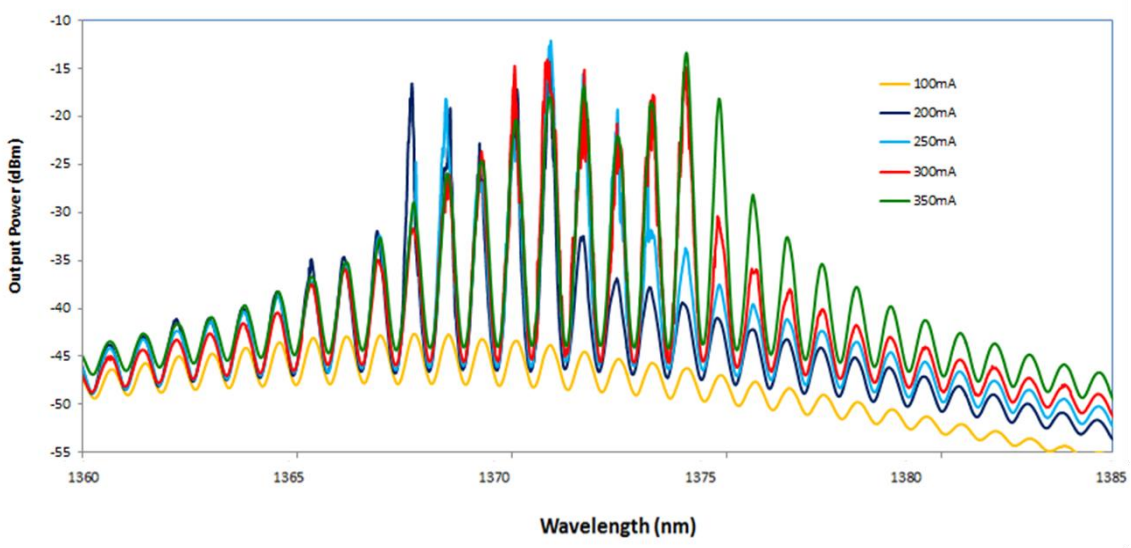

Figure 4.24 The spectrums of multiwavelength fiber laser by Sagnac loop mirror with different BOA power.

4.4 Design and characterization of multiwavelength O-band fiber laser by Fabry Perot Interferometer technique

Another interferometer technique that benefit the multiwavelength fiber laser is Fabry Perot interferometer. In this section, we propose and demonstrate a multiwavelength BOA fiber laser scheme using a Fabry–Perot reflector inside linear cavity. The Fabry-Perot interferometer usually consists of two parallel (highly) reflective surfaces separated by a small gap. The Fabry-Perot interferometer is able to produce sharp interference peaks because it uses multiple beam interference.

The advantage of utilizing this technique was not only for its simple configuration but also its ability to generate higher resolution or SNR. High SNR can be produced by generating multiple pass of beam employing linear cavity as illustrated in figure 4.25. The configuration consists of BOA as the seed source and amplifier, PMF with different length, PC to change the polarization state of the beam, mirror with reflectivity of 90%, coupler 90:10 (C) and OSA. The PMF is the gap where the interference occurs. The seed source of the BOA travels into the PMF where 4% of the light is reflected back due to the Fresnel reflection of air. The reflected beams then interfere with the incidence beam, where the pattern described by the intensity modulation of incident beams which caused by the phase different cause by the PMF. The phase difference is described as in equation 3.2. The channel spacing is predicted to be twice the spacing channel of SLM with similar length of PMF.

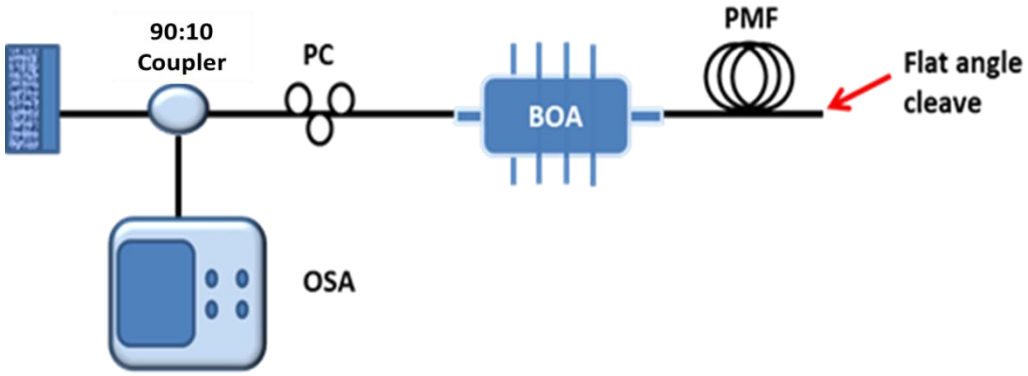

Figure 4.25 Experimental setup of linear cavity Fabry-Perot interferometer

The performance of the multiwavelength fiber laser with Fabry-Perot interferometer using 4 different PMF lengths namely 1 m, 2 m, 3 m and 4 m, is illustrated in figure 4.26. The peaks were generated around wavelength 1345 nm to 1360 nm. The fluctuation is clearly seen for peaks power which is around -10 dBm to -40 dBm

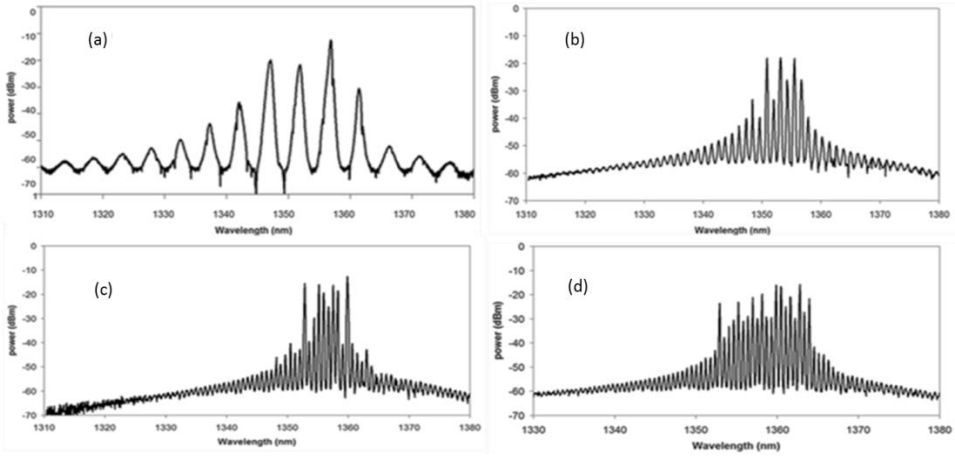

Figure 4.26 Spectrum of multiwavelength fiber laser via Fabry-Perot Interferometer for (a) 1 m, (b) 2 m, (c) 3 m and (d) 4 m.

The spacing between channels or in terms of interference is contingent to the length of the PMF due to the change of phase difference created. As mention in section 2.3.2 and 2.3.3, the interference of two propagated beams in the optical fiber is depend on the phase different, as illustrated in equation 2.10 and 2.11. The birefringence

present as the product of slow and fast indices difference. Birefringence, β can also be interpreted as in equation 4.6

$$\beta = \frac{\lambda}{L_B} \tag{4.6}$$

Where L_B is beat length of the PMF and λ is the incident laser source. The relationship between the channels spacing, $\Delta\lambda$ and phase different, δ is as described in equation 4.7 (Lipson, 1995)

$$\Delta\lambda = \frac{2\pi\lambda}{\delta} \tag{4.7}$$

As mentioned in the previous section the phase difference of the Fabry-Perot interference is twice the Sagnac loop mirror interferometer with the same PMF length. The differences resulted in the channels spacing of the multiwavelength fiber laser Fabry-Perot Interferometer to be twice the spacing of Sagnac Loop mirror refer to figure 4.27. In other words, generating the same channel spacing via Fabry-Perot interferometer only need half of the PMF length than the SLM technique. Hence, the results show that technique is more cost effective than the rest of multiwavelength fiber laser technique demonstrated so far. Another advantage of Fabry-Perot interferometer is an improvement of its SNR as shown in figure 4.28. Even though the value smaller compared to SLM interferometer but it SNR is less fluctuating. Note that the comparison is made by taking PMF length to be 1 m. The 1 m PMF is selected due to less number of channels that make comparison easier.

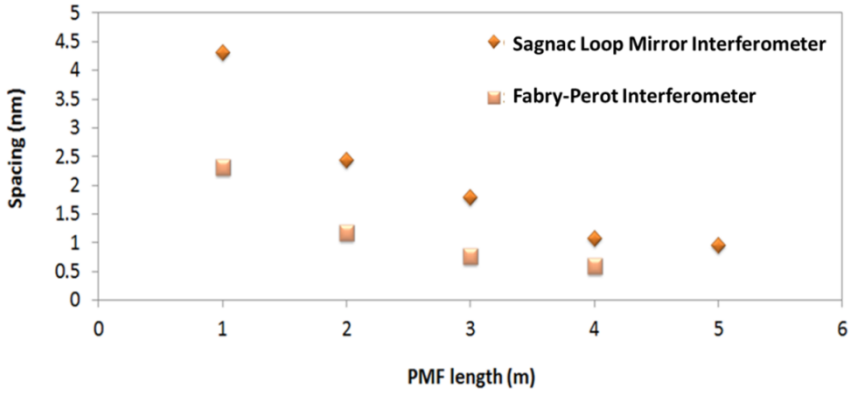

Figure 4.27 The comparison between linear cavity Fabry-Perot interferometer and SLM technique.

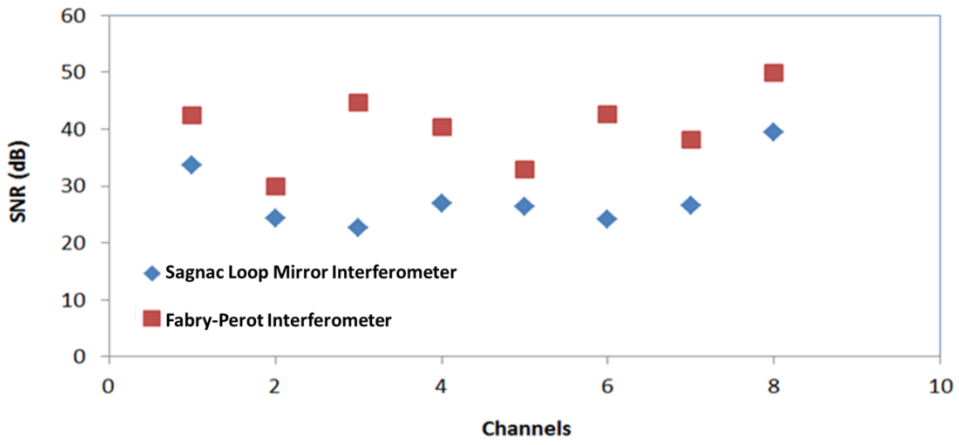

Figure 4.28 The SNR performance of multiwavelength fiber laser with Fabry-Perot interferometer

So far the entire O-band multiwavelength fiber laser demonstrated via 3 conventional techniques fails to meet the requirements of a transmitter. The multiwavelength fiber laser that generated does not have even peak power and ability to vary its channel spacing. Therefore the next chapter will focus on the improvements of MWFL peaks power flatness and variability of channel spacing.

Chapter 5 Improvements of O-band multiwavelength fiber laser (MWFL)

5.1 Introduction

The multiwavelength fiber laser can be useful not only for DWDM system but also for various applications such as sensory system (Venkataraayan, et al. 2011). Unfortunately the required properties of multiwavelength fiber laser for each application are different from each other. One of the requirements is the channels spacing. The channels spacing in multiwavelength Brillouin fiber laser could be obtained by combining the ring and linear configurations. Meanwhile in order to vary spacing for interferometer technique, the phase has to be manipulated (Lee, et al. 2012).

Apart from varying the channel spacing, multiwavelength fiber laser also needs to have even peak power. Even peak power allows better maintenance and calibration especially in the DWDM system. The even peak power for multiwavelength Brillouin fiber laser could be achieved by adjusting the optical amplifier, adding more optical amplifiers or accompanying nonlinear effect such as four waves mixing to levelled the peak power.

5.2 Improvement of O-band multiwavelength Brillouin fiber laser (MWBFL)

As demonstrated in section 4.2.4, the generated multiwavelength Brillouin fiber laser consist of spectrum with uneven peak power fluctuating from 3 dB to 20dB. A key concern in operating communication system as mentioned previously is to have source with even peak power and less fluctuating in order to provide stable data transmission performance. Synchronous signals are also important for DWDM calibration process. This gives motivation to run an experiment to improve the flatness of output spectrum BFL. There are few ways discussed in this section to generate flatter peak power

multiwavelength Brillouin fiber laser including relocating amplifier, utilizing highly nonlinear fiber and hybrid amplifier.

5.2.1 Design and characterization to improve flatness of MWBFL

(a) Relocating the amplifier

In the conventional MWBFL setup in section 4.2.4, the BOA was used to amplify the power of BP and Stokes signal was generated from the setup. The BP was the first to be amplified by the BOA, then followed by generation of Stokes, where the number of Stokes depending on the power of BP. By the time Stokes reaches the BOA, the amplification of BOA was dominated by the BP signals. Hence, the multiwavelength spectrum resulted in uneven peak power

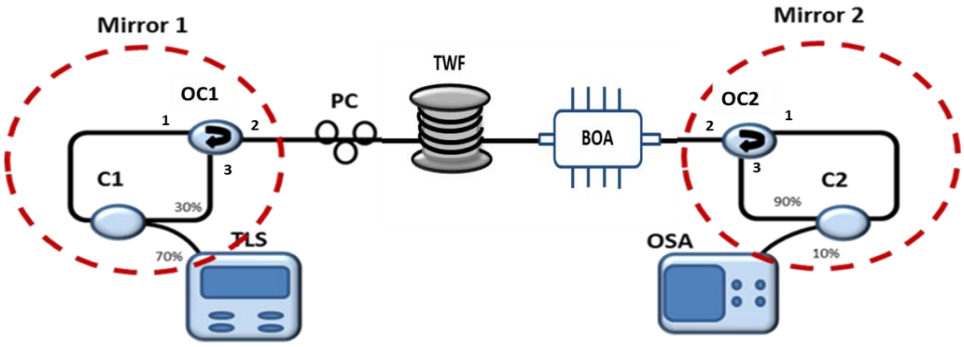

Figure 5.1 Experimental setup of linear cavity of multiwavelength Brillouin/BOA fiber laser.

Therefore an investigation on the effect of amplifier location in the Brillouin fiber laser system to the output flatness was conducted. The BOA was relocated after the TWF as depicted in figure 5.1. Thus, the BP will interact with TWF initially to produce 1st Stokes before it was amplified by the BOA. At that point, the BP power has less power and Stokes already started to grow, therefore the BOA amplification is no longer dominated by the BP but the 1st stokes.

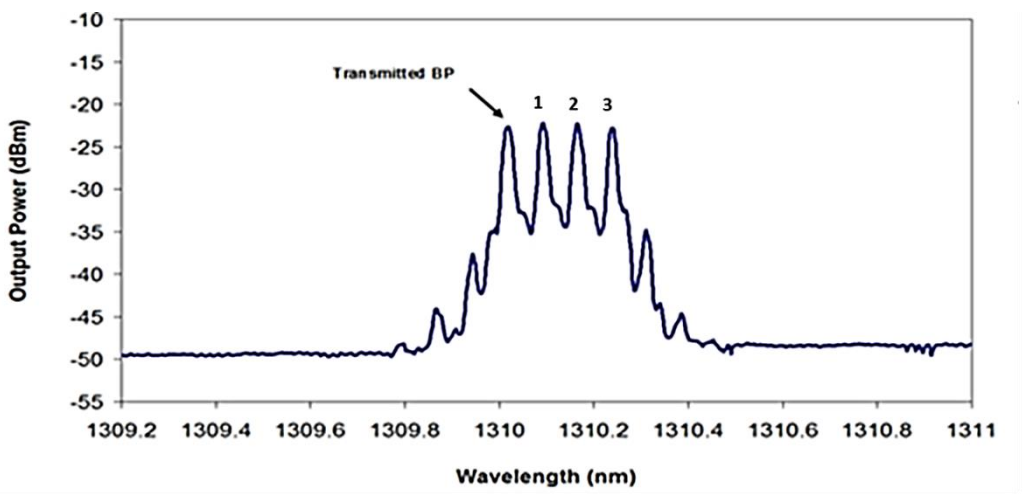

Figure 5.2 Spectrum of Multiwavelength Brillouin Fiber Laser with even peak power.

Even peak power is generated, as shown in following figure 5.2. There are 9 peaks generated by maintaining the BP power at 12 dBm at a wavelength of 1310 nm and BOA current at 400 mA. Between these 9 peaks, 4 peaks including the BP have even peak power with fluctuation of less than 1dB. Moreover, this setup reduces the effect of FWM due to low power of BP and Stokes entering the BOA. The growth of the transmitted BP and the first 3 Stokes is shown in figure 5.3

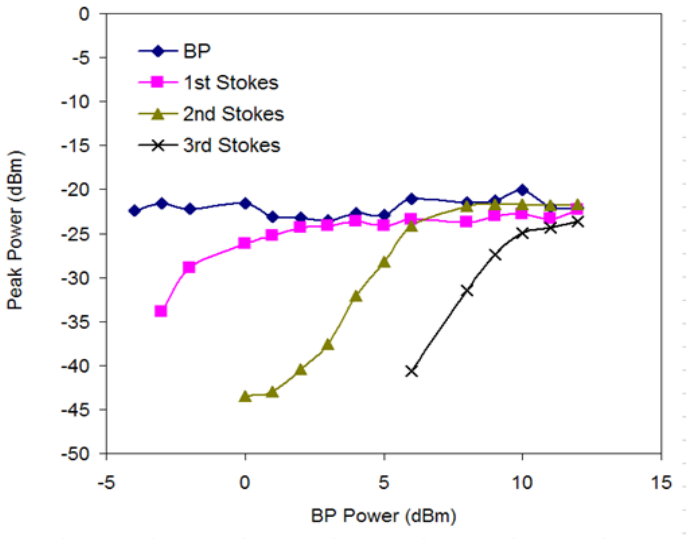

Figure 5.3 Peaks powers of transmitted Brillouin and the first 4 stokes

The result shows that each Stokes has its own threshold BP power. The 1st Stokes generated together with the transmitted BP as low as -5 dBm, and once the 1st

Stokes reach around -26 dBm with the BP power set at 0 dBm, the 2nd Stokes start to generate with power at -45 dBm. This condition is applied to all other Stokes. The 3rd Stokes emitted at 5dBm soon after the 2nd Stokes reach -25 dBm. Meanwhile, the transmitted BP experienced drop of power to -24 dBm when the 2nd Stokes was generated. By the time BP power reach 12 dBm all 4 peaks have less than 1dB difference nearly the same at -22 dBm. It can also be concluded that the power needed for the Stokes to generate following Stokes have to be higher than -26 dBm. The flatness of multiwavelength Brillouin fiber laser was easily achieved by having the BOA to place as an amplifier of all signal and not just booster for BP signal. It also manages the waste of energy of BOA saturated by high power BP from the earlier configuration.

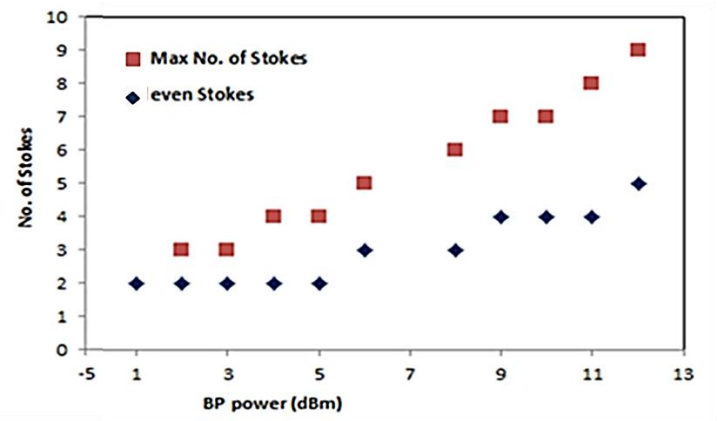

Figure 5.4 Number of Stokes with different BP power

The number of generated Stokes and number of flat Stokes at different input power is as shown in figure 5.4, where the BP wavelength is fixed at 1310 nm. The even Stokes was represented at least half of the maximum number of Stokes generated from the configuration.

The variability of multiwavelength Brillouin fiber laser over the BP wavelength is illustrated in figure 5.5. The BP power was fixed at the 12 dBm and BOA current at 400 mA.

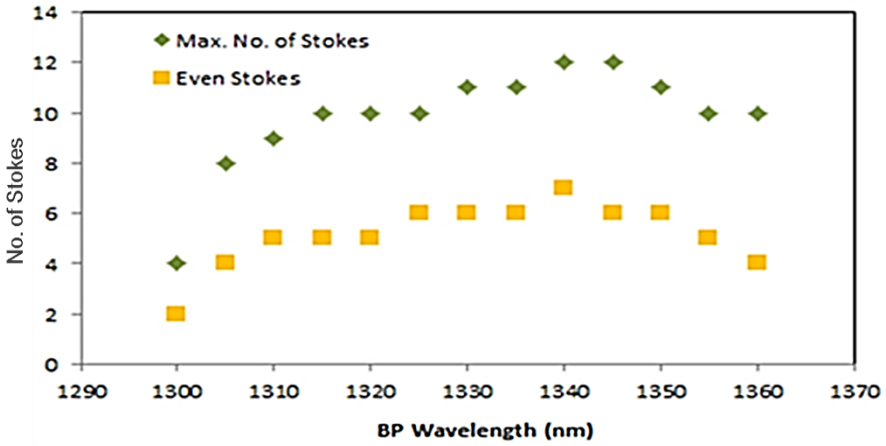

Figure 5.5 Number of Stokes at different BP wavelength

The maximum number of Stokes generated is 12 at BP wavelength of 1340 nm and 1345 nm. The maximum even peak power of Stokes is at BP wavelength of 1340 nm with 6 peaks. The pattern of number of Stokes for MWBFL is compatible with the BOA gain spectrum. The ratio of even Stokes with maximum number of Stokes is also more than half along the available BP wavelength.

5.2.1(b) Utilizing the Bismuth Doped Fiber (BiDF)

Other ways of achieving even peak power is by employing nonlinear effect into the configuration. The nonlinear effect could generate more lines through the four wave mixing effects. By adding nonlinear medium, the FWM effect will be stronger. In chapter 3, Bismuth doped fiber shows high nonlinear coefficient value at 1310 nm region, due to the location of zero dispersion wavelength.

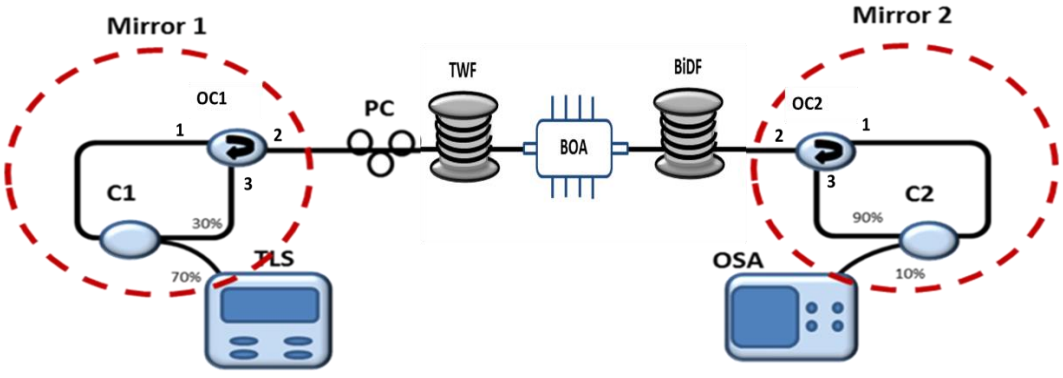

Figure 5.6 Multiwavelength Brillouin/BOA fiber laser with additional nonlinear medium.

The BiDF was placed after the BOA as illustrated in figure 5.6. As in section 5.2.1(a), this experiment is repeated without changing any setup parameter, where the BOA is driven by the same current with same BP power and all parameters are left intact. The only difference is the 4m BiDF was placed after BOA to induce the FWM effect. The BP generates Stokes at the TWF and then amplified by the BOA. Both of the peaks then enter the BiDF which generates FWM which then emits new channels with the same spacing. All the channels bounce inside the cavity and generate more new signals. The spectrum of the multiwavelength Brillouin/BOA fiber laser with an additional nonlinear medium is as shown in figure 5.7. The spectrum shows an increase of anti-Stokes which are tagged as the 6th and the 7th Stokes and also the increasing of the 5th Stokes.

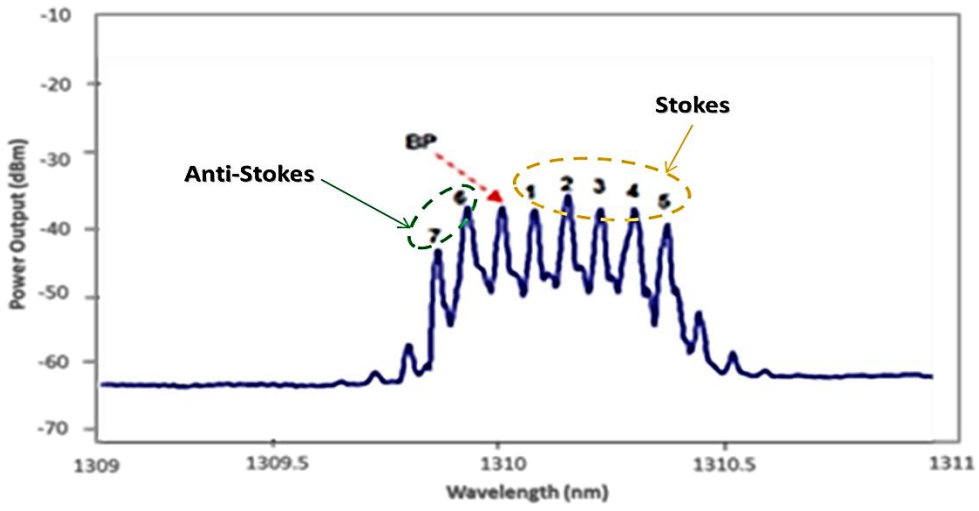

Figure 5.7 Multiwavelength Brillouin/BOA fiber laser with BiDF

All 7 peaks show even peak power in figure 5.8 with lower average peak power of -32 dBm and the fluctuation less than 3 dB. Lower peak power resulted from the loss contributed by the BiDF with amount of 4-5 dB/m.

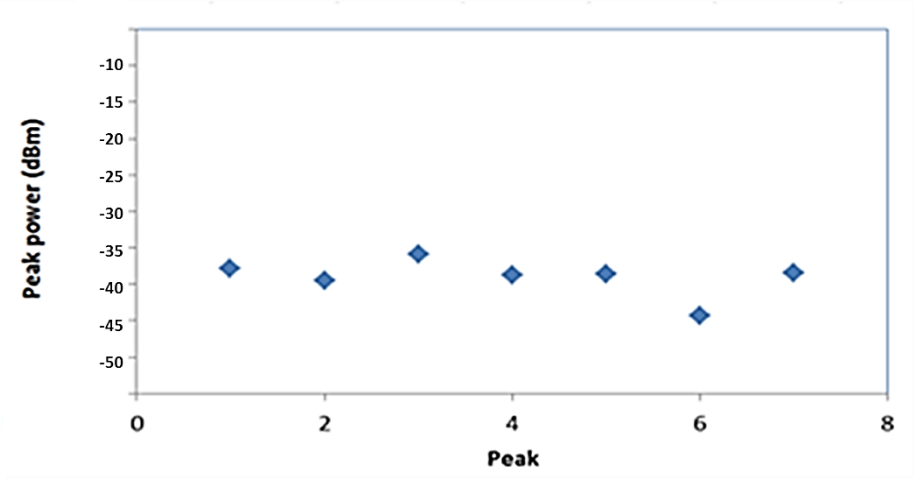

Figure 5.8 Properties of peak power for multiwavelength Brillouin/BOA fiber laser with BiDF

5.2.1(c) Multiple optical amplifiers

Other method of generating more channels and even peaks is by adding another amplifier in the configuration. An extra amplifier not only increases channels and flattening the peak power, but also it increases the peak power level. An amplifier that suitable for this task is Raman fiber amplifier (RFA). The RFA can be added into the setup by inserting a Raman Pump1250 nm in between TWF and BOA. No extra fiber needed to create RFA as shown in figure 5.9.

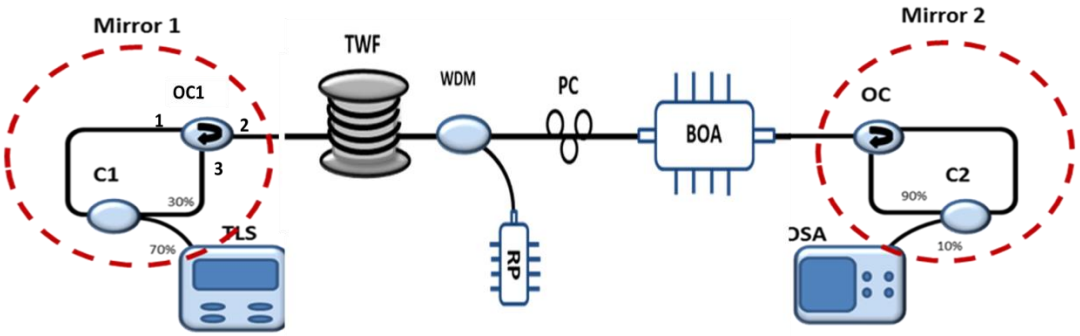

Figure 5.9 Multiwavelength Brillouin/BOA fiber laser with addition of RFA

By adding the RFA, the initial signal BP that enters the TWF will not only generate first Stokes but also amplifies the BP and Stokes simultaneously. Therefore the BP is continuously be amplified and continues to generate more signals before being re-amplified by the BOA. As the previous setup, the recent Stokes will develop new Stokes until it no longer has sufficient power to generate more Stokes. Spectrum generated from the setup is shown in figure 5.10 with BP at 1310 nm and power of 12 dBm. The setup successfully generated more than 8 channels with high peak power and with fluctuation of less than 3 dB.

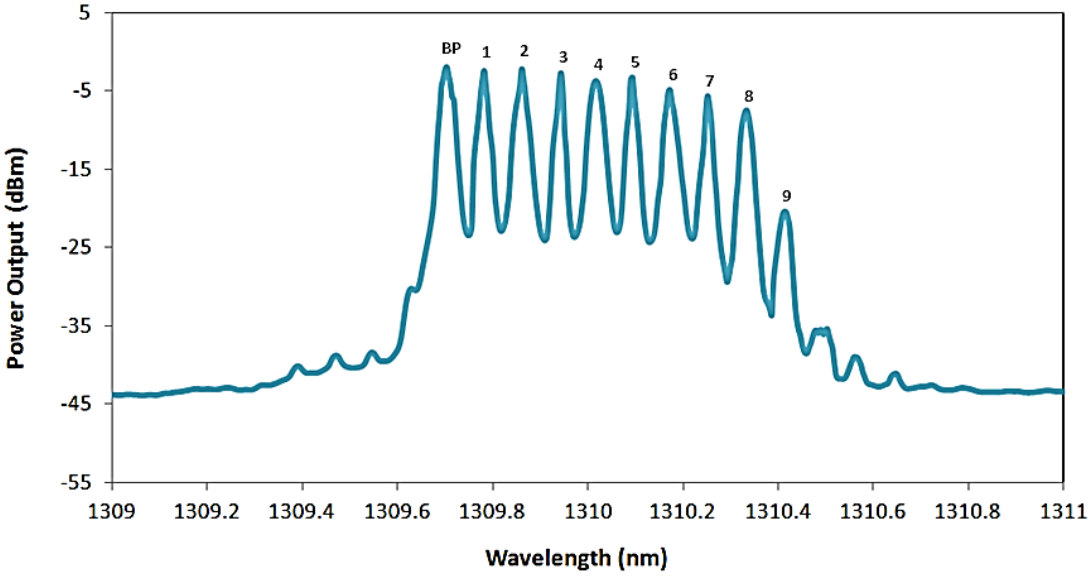

Figure 5.10 Multiwavelength Brillouin/BOA/RFA fiber laser.

From figure 5.11, the improvement of peak power and SNR for every peak was validated. There were 8 channels with average peak power of -2.5 dBm and SNR of more than 18 dB.

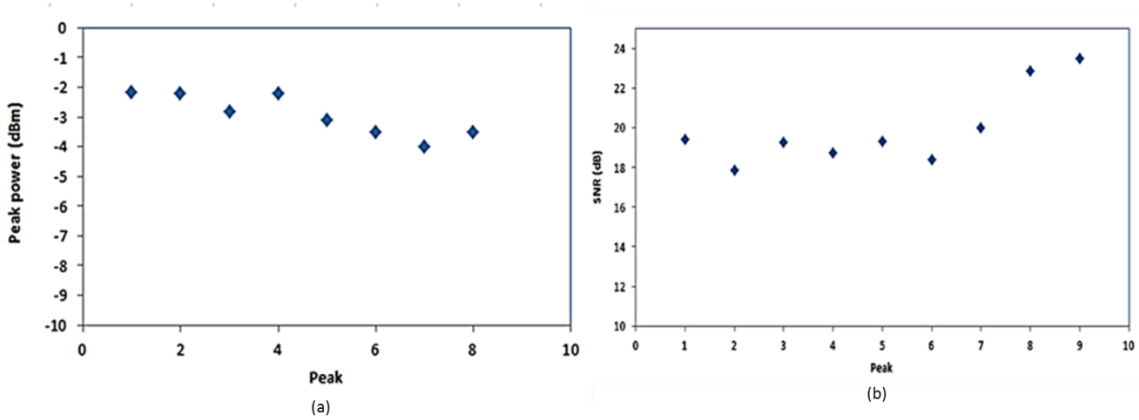

Figure 5.11 Characteristic of multiwavelength Brillouin/BOA/RFA fiber laser (a) peak power (b) SNR.

The combination of 2 amplifiers increased the variability along the BP wavelength. According to figure 5.12, the number of even Stokes that is generated is approximately 8 from 1311 nm to 1350 nm with highest number of even Stokes of 12 at wavelength 1340 nm.

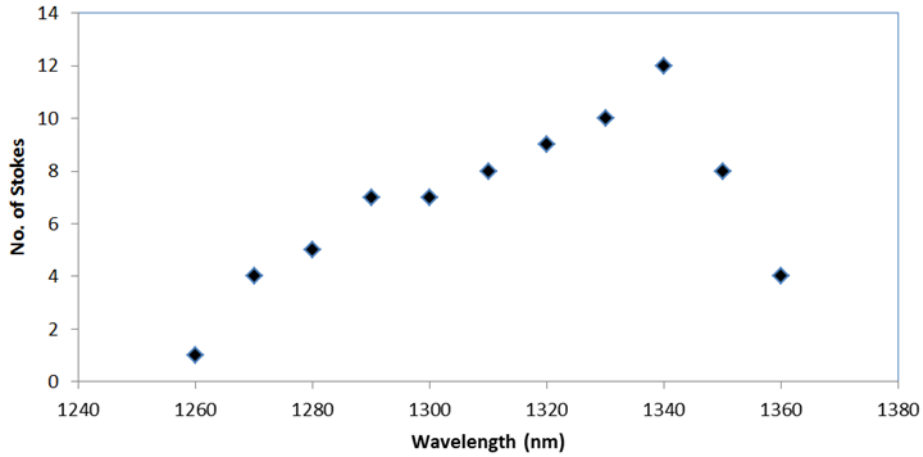

Figure 5.12 Number of Stokes through out O-band wavelength

Therefore, it could be concluded that generating a MWBFL is much more effective by combining 2 amplifier or by increasing gain performance of BOA.

5.2.2 Design and characterization of varied channel spacing of MWBFL

Another concern in designing a multiwavelength fiber laser source is variability in the channels spacing. The multiwavelength Brillouin fiber laser configuration with variable channel spacing is demonstrated by combining two cavities in a configuration.

According to equation 4.6, the spacing of the multiwavelength Brillouin fiber laser was depends on its BP wavelength. However the spacing is not significantly visible (2 GHz) in the transmission region. Therefore a new technique should be proposed to generate varieties of channel spacing for multiwavelength Brillouin fiber laser.

Different spacing was demonstrated for different cavity configurations in section 4.2. Hence by combining both of the configurations the variability of channel spacing could be obtained.

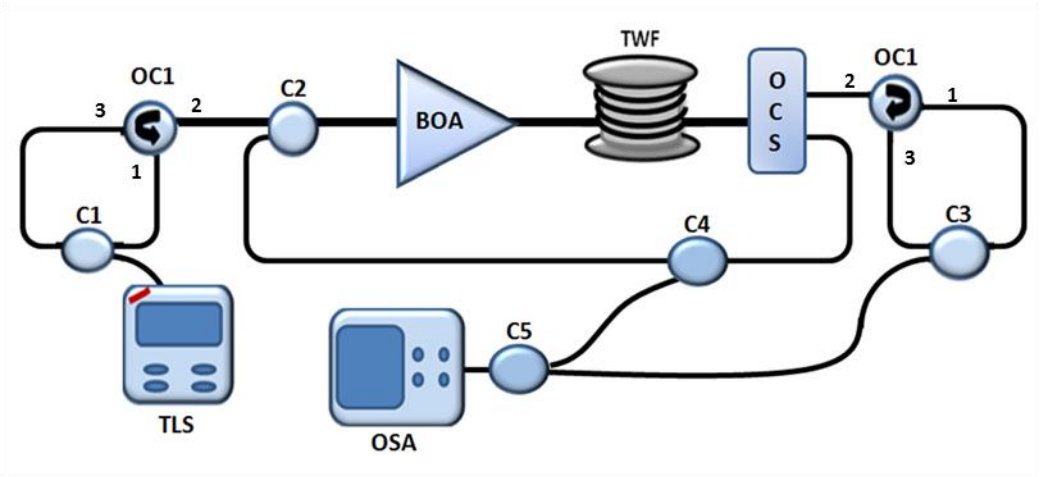

Figure 5.13 Configuration of tuneable multiwavelength Brillouin fiber laser

The variable spacing multiwavelength Brillouin fiber laser setup is built by combining ring cavity and linear cavity with a switch component. The BP generated from TLS is connected to 70% port of C1 and is amplified by BOA after pass through port 3 and 2 of optical circulator OC1 and 3dB of coupler C2. The Amplified BP then generates the Stokes which then travels to optical channel selector (OCS). The OCS is an optical switch that changes the routes of the Brillouin pump and generation of

Stokes. By changing the route it creates different cavity can be created. On channel 1, the OCS is connected to the OC2 which looped the beam back into the nonlinear medium and form linear cavity. The 10% of its power is tapped by coupler C3 to be analysed by the OSA. Meanwhile, channel 2 of the OCS is linked to coupler C2 creating the ring cavity configuration with power observation by 20%. The spectrum losses it power due to the insertion of the OCS.

The spectrum of multiwavelength Brillouin fiber laser is dependent on the channel selected by the OCS. The figure 5.14 shows the spectrum generated by both of the channels.

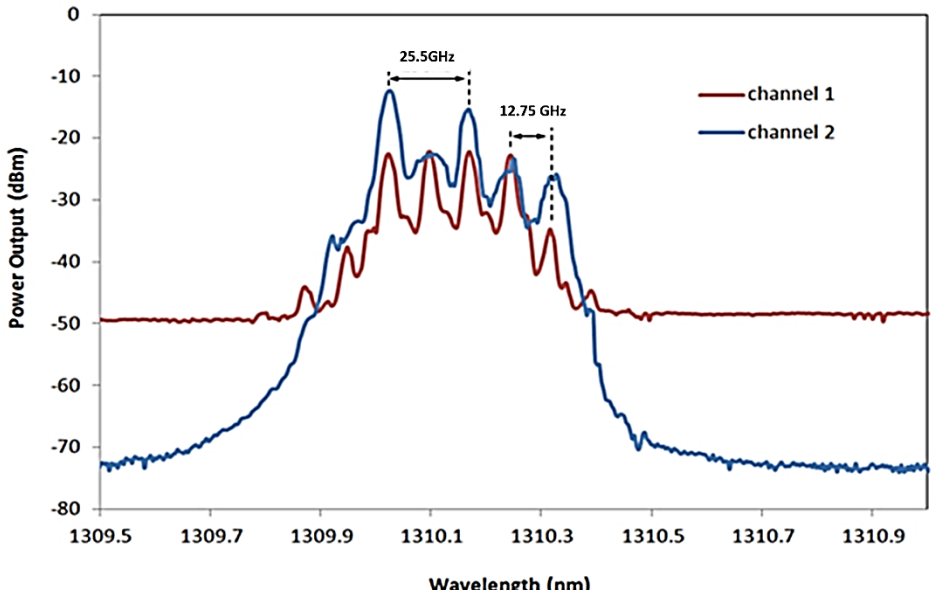

Figure 5.14 Spectrum of tuneable multiwavelength Brillouin fiber laser

Figure 5.14 shows the overlapped of the spectrum results from 2 OCS channels. The variability of MWBFL is limited to two channel spacing which is 0.072 nm/ 12.75 GHz and 0.144 nm/ 25.50 GHz.

5.3 Improvement for O-band Multiwavelength fiber laser of Sagnac Loop Mirror technique

5.3.1 Design and characterization of improved flatness of MWFL via SLM

Generation of even peak power of multiwavelength fiber laser by Sagnac Loop Mirror (SLM) can be achieved by utilizing nonlinear effect which is by adding 4m BiDF in the cavity. The BiDF was placed in between coupler and the PC. High nonlinearity of BiDF generates four wave mixing effect that helps to improve the quality of multiwavelength fiber laser (Cholan et al. 2012).

By maintaining the parameter from the previous setup of the multiwavelength Fabry-Perot Interferometer fiber laser, the performance is as shown in figure 5.15. The performance of the peak power is more stable. Meanwhile, number of channels above power of -50 dBm has increased. The uniformity of peak power is shown in figure 5.16 by comparing the performance of 1m PMF with and without BiDF. The peaks powers are stable with BiDF show stability at -17 dBm with fluctuation less than 3 dB.

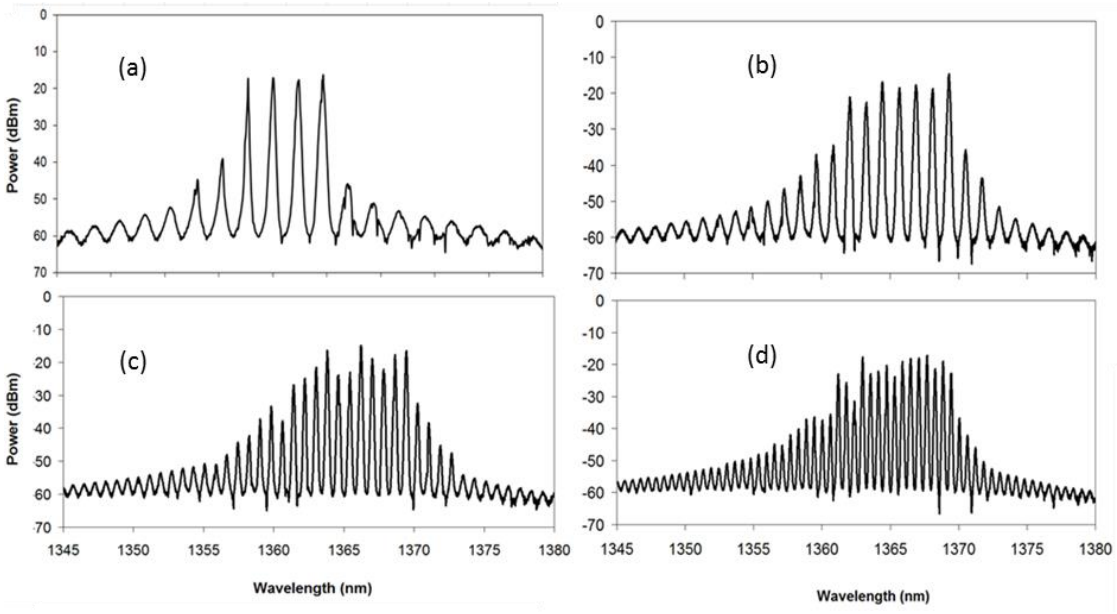

Figure 5.15 Performance of multiwavelength fiber laser SLM with different spacing for (a) 1m, (b) 2m, (c) 3m and (d) 4m

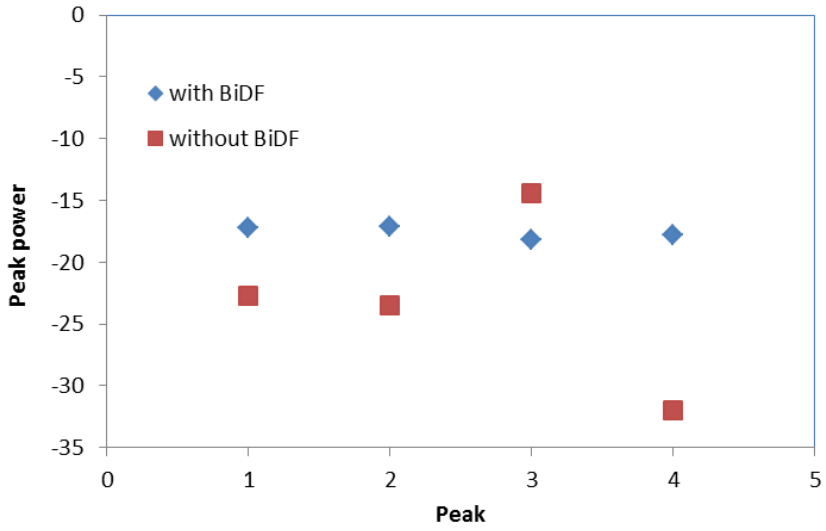

Figure 5.16 The peak power performance of Fabry Perot interferometer with and without BiDF.

5.3.2 Design and characterization of varied channel spacing of MWFL by SLM

Both configurations consist of PC that changes the state polarization of the beam. Adjusting the PC and varying the polarization states only give different interference patterns, but not the spacing between the channels. In order to build variable spacing multiwavelength fiber laser SLM, the PMF length should be varied. The channel spacing is inversely proportional with PMF length (L) as described in equation 4.6. By utilizing linear cavity the tuneable multiwavelength SLM fiber laser is obtained by varying 4 different PMF lengths, 1 m, 2 m, 3 m, and 4 m as illustrated in figure 5.17

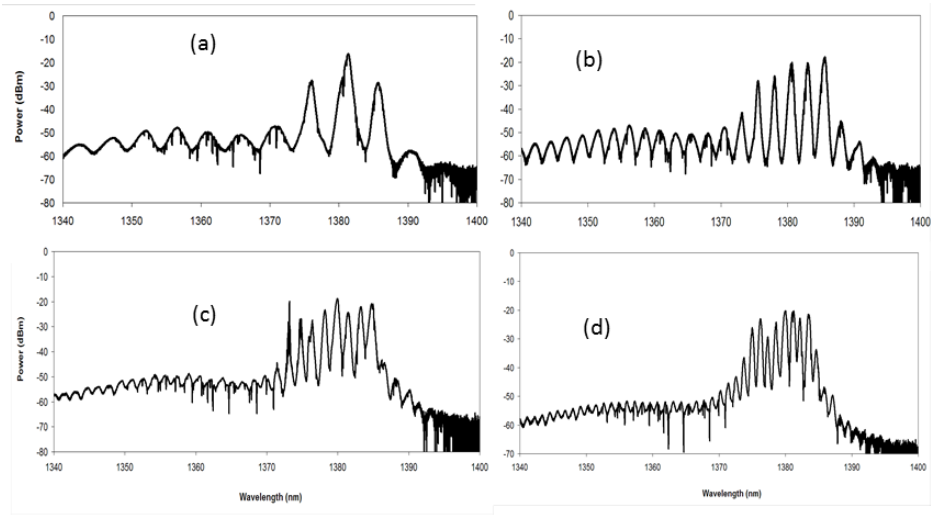

Figure 5.17 Demonstration of multiwavelength fiber laser SLM with different PMF length for (a) 1m, (b) 2m, (c) 3m and (d) 4m.

As in equation 4.7, the spacing can be calculated if the value of the phase difference is known. As shown in figure 5.18, with the beat length of PMF given by the fiber manufacturer to be 3.5 mm, the calculated spacing over length of PMF is approximately equal to the channel spacing from the experimental result. The peak and SNR analysis is plotted in figure 5.19 for 2 m PMF performance for the highest six peaks.

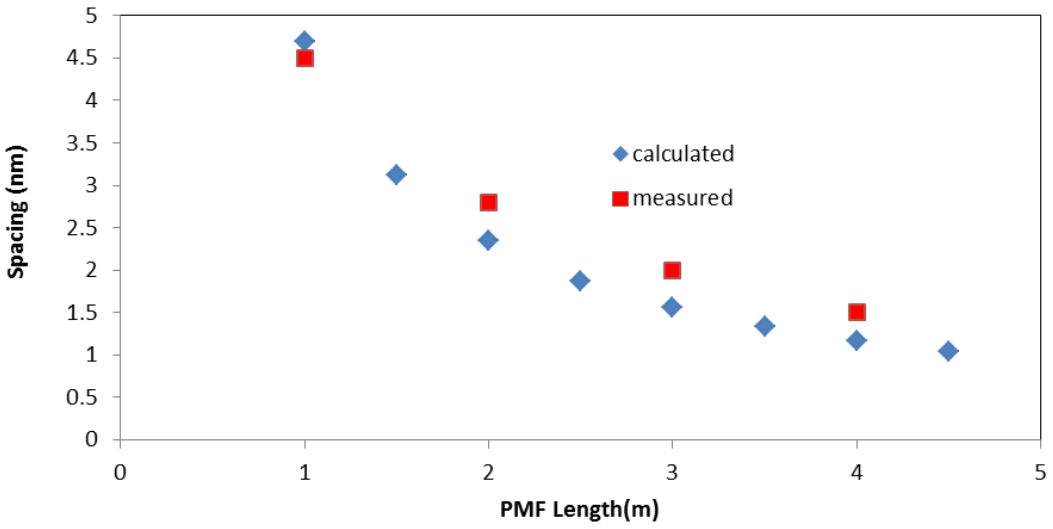

Figure 5.18 Channel spacing over PMF length

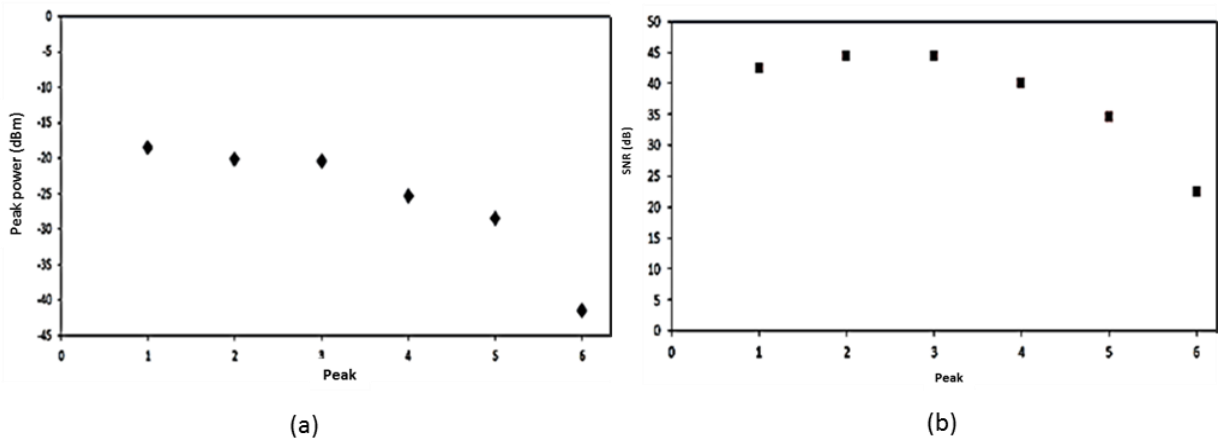

Figure 5.19 Performance of (a) peak power and (b) SNR of multiwavelength fiber laser SLM

The variability of multiwavelength fiber laser SLM was demonstrated but unfortunately this technique required manual adjustment to the configuration. Direct adjustment might interrupt its actual performance as multiwavelength fiber laser.

5.4 Improvement for O-band Multiwavelength fiber laser of Fabry Perot Interferometer technique

5.4.1 Design and characterization of flatness of MWFL via Fabry Perot Interferometer

In generating uniform peak power of the MWFL by FPI again utilizing the BiDF in the configuration to induces the nonlinear effects. The BiDF was inserted before the BOA to insure that the generated multiwavelength fiber laser FPI to be amplified first by the BOA as illustrated in figure 5.20. The nonlinear BiDF was inserted between the mirror and the BOA.

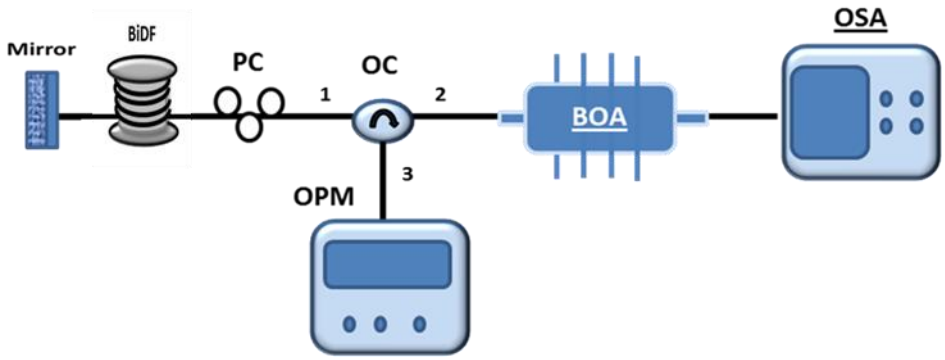

Figure 5.20 The flattening multiwavelength fiber laser FPI

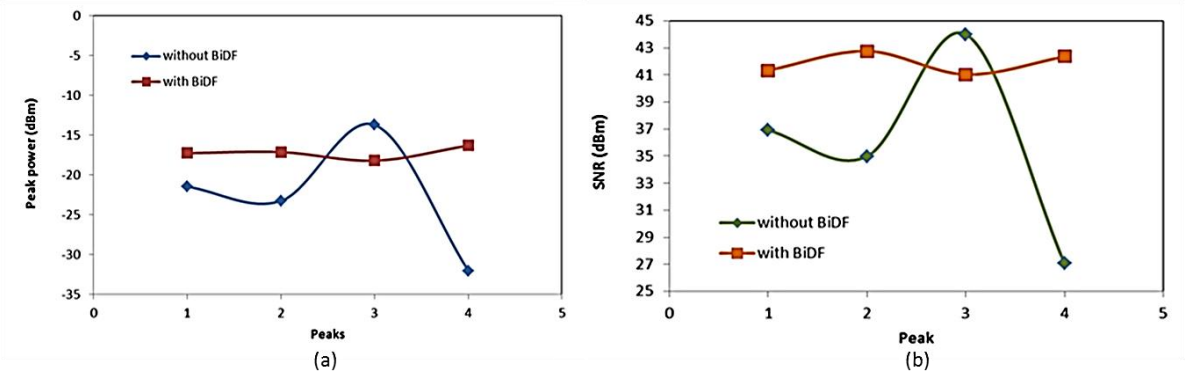

Figure 5.21 Performance of even multiwavelength fiber laser FPI (a) peak power and (b) SNR.

Comparison made between multiwavelength fiber laser FPI with and without BiDF as in figure 5.21. The result is for 1m PMF length. The peaks powers have less than 1 dB of fluctuation and higher SNR. Even though the peaks power for multiwavelength fiber laser FPI without the BiDF is much higher but the peaks with BiDF are more stable.

5.4.2 Design and characterization of varied channel spacing of MWFL via FPI.

As any interferometer, the spacing between FPI multiwavelength fiber laser channels depends on its phase change. Therefore to obtain different channel spacing, the PC was placed at the end of the PMF or simply creating the half plate rotator by using the PMF.

By placing the PC at the end of the PMF, the beam from the Fresnel reflection will have different polarization state which resulted in change of channel spacing. Phase difference change simultaneously with the change of polarization state therefore, different channels spacing produce.

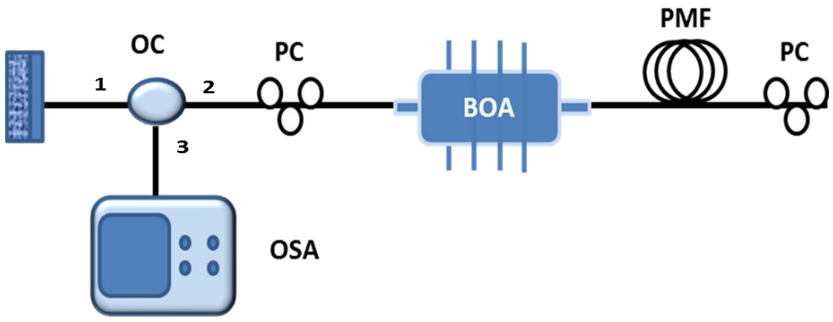

Figure 5.22 The configuration of the multiwavelength fiber laser FPI with even peaks power.

The 4 m PMF is used in these demonstration due to its performance on producing the smallest spacing. The spacing channel was successfully varied from 5.0 nm to 1.25 nm around the region of 1350 nm to 1370 nm as shown in figure 5.23. This technique is non-invasive and cost effective where changes were only made without changing the PMF length physically.

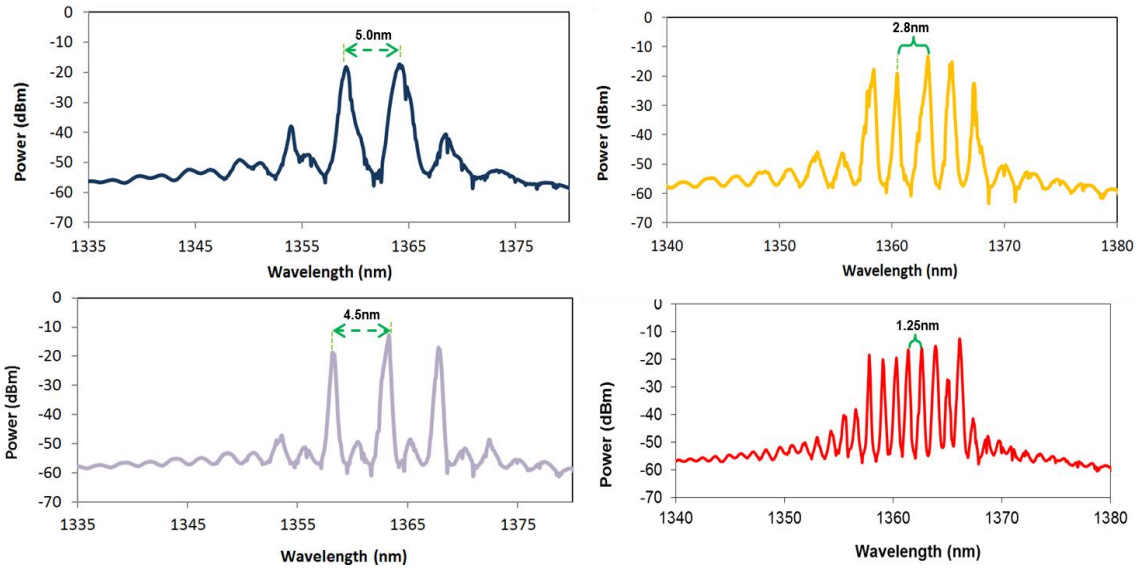

Figure 5.23 Multiwavelength fiber laser FPI with varied channel spacing

Chapter 6 Conclusion and Future Works

6.1 Thesis Summary

The demonstration and findings of the research work are summarized and discuss in this chapter. The works focused on the research on the multiwavelength O–band fiber laser for the WDM use. These research works are necessary to cater the exponential growth in the transmission capacity. In order to overcome the issue, the transmission window must be expanded from C-band to O-band.

The research works start with the characterization of the O-band optical amplifier. The optical amplifier is a crucial component to generate the multiwavelength fiber laser and also help to boost up the power of generated signals. There are 3 types of optical amplifier tested in this work. The first optical amplifier tested is Bismuth doped fiber laser (Bi-DF) that could amplify throughout the entire available transmission windows. The ASE of BiDF cover wide range of transmission window, unfortunately the gain generated from this amplifier is very low which is around ~2 dB. The BiDF also measured for its nonlinearity effects. The next optical amplifier that was tested is the nonlinear effect which called Raman fiber amplifier (RFA) where its performance depends on the gain medium used. Another type of optical amplifier is the semiconductor amplifier that provides the highest performance among all three types. Therefore semiconductor optical amplifier is selected for the generation of multiwavelength fiber laser setup.

The optical amplifier is a vital component in communication systems. Conventionally the optical amplifier only used to amplify signal. However the development in laser and optical fiber industries provides more capabilities to the

optical amplifier such as seed source for fiber laser, and gain controller. Therefore, the characteristics, and parameters of the amplifier needs to be verified.

The Bismuth doped fiber amplifier is claimed to provide wide amplification from 1260 nm to 1620 nm. Unfortunately, the tested BiDF provided low power around 2 dB at O-band wavelength and negative gain at other transmission windows even the ASE shows wide coverage of O to L band. The Bismuth doped fiber had been tested for the nonlinearity effect via four wave mixing effect. High nonlinear coefficient of BiDF was measured as 13.98 W^{-1} km^{-1}, and nonlinear refractive index was calculated to be $0.917x10^{-20}$ m^2/W.

Another type of optical amplifier is by manipulating the nonlinear effect of optical fiber. The amplification using nonlinear effect could be generated using various configurations but only the stimulated Raman scattering (SRS) was used in this work. Raman fiber amplifier has advantages especially in the flexibility of amplification region. The Raman fiber amplifier was tested on 4 different optical fibers. Dispersion compensated fiber (DCF) of 7.7 km length required less power to create the Raman scattering due to high Raman gain coefficient and low threshold power. The 1250 nm pump power was used to generate the amplification around O-band region, which is 12 dB at a wavelength of 1340 nm.

The booster optical amplifier (BOA) is an example of integrated optical amplifier. The BOA demonstrated very good performance of amplification with gain of 28 dB at 1350 nm along a spectrum of 90 nm (1270 nm to 1360 nm). This is higher than the conventional integrated optical amplifier (~16 dB). However this performance can only be achieved with the inclusion of angle connectors to minimize the feedback signal. Meanwhile the double pass configuration gives improvement in gain (~31 dB) but decrease the spectrum width to 40 nm. Hence due to the high amplification power

provided by the BOA, the multiwavelength fiber laser was demonstrated using the BOA as the optical amplifier and as seed source.

The multiwavelength fiber laser had been demonstrated by 3 different techniques; Brillouin scattering effect, Sagnac Loop mirror and Fabry Perot Interferometer. The multiwavelength Brillouin fiber laser (MBFL) will be generated whenever the incident source or Brillouin pump power equals or exceed its Brillouin threshold. The Brillouin threshold was measured for different types of fiber and shows that the 20 km True Wave Reach fiber (TWF) required lowest power to generate the Brillouin effect of 5.2 dBm. The Brillouin threshold studies was also extended by comparing the Brillouin threshold for O and C band, which shows that the O-band has small Brillouin threshold compared to C band. The MBFL was generated from 2 cavity setup, namely ring and linear cavity configurations. Both cavities generate 4 Stokes channels but linear cavity provides much higher peak power and narrower spacing between channels which is ~0 dBm and 12.5 GHz respectively. By inserting the BOA into the multiple pass configuration the channels peaks power lowered to -20 dBm but adds 3 anti-Stokes channels into the linear spectrum. The multiwavelength fiber laser utilizing the Sagnac loop mirror (SLM) also demonstrated in 2 pattern of cavity, and shows better performance from linear cavity where the number of channels generated are 16 with even peak power of -20 dBm. Meanwhile another multiwavelength fiber laser generated from basic interferometer technique is the Fabry Perot Interferometer (FPI). The FPI was demonstrated using the end face reflector. The channel spacing was twice the value generated from multiwavelength fiber laser of SLM for same length of gain medium.

The improvements of the multiwavelength fiber laser were also demonstrated. The improvements include the flatness of peak power and varying channel spacings. The peaks power of multiwavelength Brillouin fiber laser was levelled by utilizing three

different techniques, which are relocating the optical amplifier, utilizing the BiDF, and adding an extra amplifier. Locating the BOA after the nonlinear medium reduced the effect of FWM and enables the Stokes to be amplified when the BOA is not saturated with the BP signal. Then another nonlinear effect is applied by adding the 4m BiDF. The even peak power obtained was the result of the four waves mixing effect generated in the BiDF. Another proposed technique is by adding additional RFA, which minimizes the absorption loss of the TWF fiber and also amplified the generated signals all in one fiber. The improvements of levelling the peaks power of multiwavelength fiber laser using Sagnac Loop Mirror and Fabry Perot Interferometer were demonstrated by utilizing the BiDF techniques. The BiDF was placed before the BOA to ensure that the powers of the generated signals are amplified to generate FWM effect.

Due to the various applications, which required different specific spacing, the multiwavelength fiber laser should be able to vary its channels spacing. The spacing of multiwavelength Brillouin fiber laser could be changed between 12.5 GHz to 25 GHz, by combining two cavities into one configuration with an optical switch included to adjust the spacing. Meanwhile for multiwavelength fiber laser that use interferometer technique, the change of phase is important to vary the multiwavelength fiber laser spacing. The change of phase for Sagnac loop mirror was obtained by changing the length of PMF. Utilizing 1 m, 2 m, 3 m and 4 m PMF length the channel spacing varied from 0.8 nm to 4.5 nm. As for the Fabry Perot Interferometer, the channel spacing was varied by inserting the PC at the fiber end to change its phase. The spacing varied from 5.0 nm to 1.25 nm around the region of 1350 nm to 1370 nm by utilizing the 4 m PMF.

6.2 Future Works

The mutiwavelength fiber laser in O-band have demonstrated in this thesis work could be futher improved in few ways including;

Expanding the transmission capacity

The extension of the research work of the multiwavelength fiber laser with conbination of all available tranmission windows to study the effectiveness of transmitting signals in multiple communication bands simultaneously. The combination might required numerous components combinations to producing the multiwavelength fiber laser for each windows. This increase the complexity of the configuration and the maintance. Therefore, further study should be undertake to propose new components that are compatible to all transmission windows. The example is by usingBismuth doped fiber. Detailed analysis should be made to overcome the Bismuth doped fiber problem, where there is still no sign of successful broad optical amplifier, BiDF at the moment.

Commercialization the O-band transmission window

Since the thesis only proposed the techniques of generating multiwavelength in O-band, a complete system that uses this multiwavelength fiber laser could be further investigated. Furthe research of should be include to utilize the proposed multiwavelength fiber laser in the CWDM or DWDM transmission system. This study includes the data test such as eye diagrams, jitter performance, BER tests, and optical modulation analysis.

References

1. K.C. Kao and G.A. Hockham, “Dielectric-Fibre Surface Waveguides for optical frequencies” Proc. IEEE. 113(3), 1151-1158 (1966).
2. T. Miya, Y. Terunuma, T. Hosaka, and T. Miyashita,” Ultimate low-loss single-mode fiber at 1.55 μm” Electron. Lett. 15, 106-108 (1979)
3. D. Gloge “Weakly guiding fibers” Appl. Opt. 10, 2252-2258 (1971)
4. H. Huang, “ Microwave approach to highly-irregular fiber optics” Wiley, New York (1998)
5. K. Inoue, H. Toba, “Wavelength conversion experiment using fiber four-wave mixing”, IEEE Photon. Technol. Lett. 14 (1) pp. 69-72 (1992).
6. D. Hillerkuss, R. Schmogrow, T. Schellinger, M. Jordan, “26Tb/s line rate super channel transmission utilizing all optical fast Fourier transform processing” Nature Photonics, 5, pp. 356-371 (2011)
7. Tadashi Kasamatsu, Yutaka Yano, and Takashi Ono, “1.49-μm -Band Gain-Shifted Thulium-Doped Fiber Amplifier for WDM Transmission Systems” , Journal of Lightwave Technology, Vol. 20, Issue 10, pp. 1826-1829 (2002)
8. E. Desurvire, J.R. Simpson and P.C. Becker, “High-gain erbium-doped traveling-wave fiber amplifier” Optics letters, 12, (11), (1987)
9. T. Yamamoto, M. Nakazawa, “Highly efficient four-wave mixing in an optical fiber with intensity dependent phase matching” , IEEE Photon. Technol. Lett. 9 (3), 327-329 (1997).
10. M. R. Shirazi, N. S. Shahabuddin, S. N. Aziz, K. Thambiratnam, S. W. Harun, and H. Ahmad, “A linear cavity Brillouin fiber laser with multiple wavelengths output”, Laser Phys. Lett. 5(5), 361-365 (2008).

11. M. R. Shirazi, S. W. Harun, M. Biglary, and H. Ahmad, "Linear cavity Brillouin fiber laser with improved characteristics" Opt. Lett. 33(8), 770-772 (2008).
12. S. Song, C.T. Allen, K.R. Demarest, R. Hui, "Intensity-Dependent Phase-Matching Effects on Four-Wave Mixing in Optical Fibers", J. Lightwave Technol. 17 (11), 2285-2289 (1999)
13. H. Chen, "Simultaneous measurements of non-linear coefficient, zero-dispersion wavelength and chromatic dispersion in dispersion-shifted fibers by four wave mixing", Optics Communications 220 (2003) 331-335.
14. M.L.F. Mollenauer, P.V. Mamyshev, M.J. Nuebelt, "Method for facile and accurate measurement of optical fiber dispersion maps"Opt. Lett. 21(21), 1724-1726 (1996).
15. C. Vinegoni, H. Chen, M. Leblanc, G. Schinn, M. Wegmuller, N. Gisin, "Distributed measurements of chromatic dispertion and non-linear coefficient in DSF fiber with non-negligible values of PMD", Paper WA5, OFC_2002, Anaheim,CA, USA.
16. IEEE Journal Of Selected Topics In Quantum Electronics, Vol. 15, No. 2, March/April 2009 415 Novel Multiwavelength L-Band Brillouin–Erbium Fiber Laser Utilizing Double-Pass Brillouin Pump Preamplified Technique Mohammed Hayder Al-Mansoori, Mohd Adzir Mahdi, and Malin Premaratne
17. H. Ahmad , n. S. Shahabuddin, s. S. W. Harun" Multi-Wavelength Source Based On SOA And Loop Mirror" Optoelectronics And Advanced Materials – Rapid Communications, 3(1) 1 – 3 (2009)
18. H. Ahmad, S. F. Norizan, M. Z. Zulkifli & S. W. Harun "Dual-Wavelength Erbium Fiber Laser In A Simple Ring Cavity" Fiber And Integrated Optics, 28(6), 430-439 (2009)

19. D.N. Wang, F.W. Tong , Xiaohui Fang, W. Jin,P.K.A. Wai, J.M. Gong,“ Multiwavelength Erbium-Doped fiber Ring Laser Sourcewith A Hybrid Gain Medium” Optics Communications 228, 295–301 (2003)

20. M. Naftaly, A. Jha, "Nd^{3+}-Doped Fluoroaluminate Glasses For A 1.3 μm Amplifier," Journal Of Applied Physics , 87(5),2098-2104, (2000)

21. Yasutake Ohishi, Terutoshi Kanamori, Takeshi Kitagawa, Shiro Takahashi, Elias Snitzer, And George H. Sigel, Jr. , “Pr^{3+}-Doped Fluoride Fiber Amplifier Operating At 1.31 μm” Optics Letters, 16(22),1747-1749 (1991)

20. M. Dianov, D. G. Fursa, A. A. Abramov, M. I. Belovolov, M. M. Bubnov, A. V. Shipulin, A. M. Prokhorov, G. G. Devyatykh, A. N. Gur'yanov and V. F. Khopin “Raman Fibre-Optic Amplifier Of Signals At The Wavelength Of 1.3 μm” Quantum Electronics, 24(9) 749-751, (1994)

21. A. Assadihaghi, H. Teimoori, R. Millett, A. Benhsaien, V. Tolstikhin, T. Hall, K. Hinzer, "O-Band Semiconductor Optical Amplifier Design For CWDM Applications," presented at Microsystems and Nanoelectronics Research Conference, 89-92,(2008)

22. Fujimoto, Y., Matsubara, H. ,Nakatsuka, M., "New Fluorescence From Bi-Doped Silica Glass And Its 1.3-Mm Emission With 0.8-Mm Excitation For Fiber Amplifier," The 4th Pacific Rim Conference On Lasers And Electro-Optics, 2001. CLEO/Pacific Rim 2001., 2, 462-463(2001)

23. X. S. Cheng, R. Parvizi, H. Ahmad, S. W. Harun “Wide-Band Bismuth-Based Erbium-Doped Fiber Amplifier With a Flat-Gain Characteristic”, IEEE Photonics Journal, 1(5) (2009)

24. Ju Han Lee, Tatsuo Nagashima, Tomoharu Hasegawa, Seiki Ohara, Naoki Sugimoto, and Kazuro Kikuchi, “Bismuth-Oxide-Based Nonlinear Fiber With a High SBS Threshold and Its Application to Four-Wave-Mixing Wavelength Conversion Using a Pure Continuous-Wave Pump”, Journal of Lightwave Technology, 24(1), 22-25(2006)

25. Sugimoto, N.; Nagashima, T.; Hasegawa, T.; Ohara, S. , "Bismuth-based optical fiber with nonlinear coefficient of 1360 W/sup -1/ km/sup -1/," Optical Fiber Communication Conference, 2004. OFC 2004 , vol.2, no., pp.3 pp. vol.2, 23-27 Feb.

26. Yasushi Fujimoto and Masahiro Nakatsuka 2001 Jpn. J. Appl. Phys. 40 L279 doi:10.1143/JJAP.40.L279Infrared Luminescence from Bismuth-Doped Silica Glass

27. F. G. Omenetto, N. A. Wolchover, M. R. Wehner, M. Ross, A. Efimov, A. J. Taylor, V. V. R. K. Kumar, A. K. George, J. C. Knight, N. Y. Joly, and P. St. J. Russell, “Spectrally smooth supercontinuum from 350 nm to 3 μm in sub-centimeter lengths of soft-glass photonic crystal fibers,” Optics Express Vol. 14, pp. 4928-4934, 2006.

28. Seongwoo Yoo, Mridu P. Kalita, Johan Nilsson, And Jayanta Sahu, “Excited State Absorption Measurement In The 900–1250 Nm Wavelength Range For Bismuth-Doped Silicate Fibers”, Optics Letters / Vol. 34, No. 4 / February 15, 2009

29. Young-Seok Seo, Changwan Lim, Yasushi Fujimoto, And Masahiro Nakatsuka, 9.6 Db Gain At A 1310nm Wavelength For A Bismuth-Doped Fiber Amplifier, Journal Of Optical Society Of Korea, Vol. 11, No. 2, June 2007, Pp. 63-66.

30. J. B. Rosolem, A. A. Juriollo, R. Arradi, A. D. Coral, J. C. R. F. Oliveira, And Murilo A. Romero, “All Silica S-Band Double-Pass Erbium-Doped Fiber Amplifier,” IEEE Photonics Technology Letters, Vol. 17, No. 7, July 2005 1399

31. S. Nishi, K. Ainda, And K. Nakagawa, “Highly Efficient Configuration Of Erbium Doped Fiber Amplifier,” In Eur. Congress Optical Communication (ECOC), Vol. 1, Amsterdam, The Netherlands, 1990, Pp. 99–102.

32. S. W. Harun, N. Tamchek, P. Poopalan, And H. Ahmad, “Double-Pass L-Band EDFA With Enhanced Noise Figure Characteristics,” IEEE Photon. Technol. Lett., Vol. 15, No. 8, Pp. 1055–1057, Aug. 2003.

33. S. Aozasa, H. Masuda, T. Sakamoto, K. Shikano, And M. Shimizu, “Gain Shifted TDFA Employing High Concentration Doping Technique With High Internal Power Conversion Efficiency De 70%,” Electron. Lett., Vol. 38, No. 8, Pp. 3612–3613, Apr. 2002.

34. Mridu P. Kalita, Seongwoo Yoo, And Jayanta K. Sahu, "Influence Of Cooling On A Bismuth-Doped Fiber Laser And Amplifier Performance," Appl. Opt. 48, G83-G87 (2009)

35. Hasegawa, T.; Nagashima, T.; Ohara, S.; Sugimoto, N., "High Nonlinearity Bismuth Fibers And Their Applications," Optical Fiber Communication Conference, 2006 And The 2006 National Fiber Optic Engineers Conference. OFC 2006 Vol., No., Pp.3 Pp., 5-10 March 2006.

36. M.L.F. Mollenauer, P.V. Mamyshev, M.J. Nuebelt, Opt. Lett. 21 (1996) 1724.

37. Zhao, Yu; Jin, Yongxing; Wang, Jianfeng; , "Measurement Of The Raman Gain Coefficient In Optical Fibers By Using The Spontaneous Technique," Photonics

And Optoelectronic (SOPO), 2010 Symposium On , Vol., No., Pp.1-3, 19-21 June 2010

38. L. Talaverano, S. Abad, S. Jarabo, and M. López Amo, “Multiwavelength fiber laser sources with Bragg-grating sensor multiplexing capability” J. Lightwave Technol. 19, 553-558 (2001).
39. Z. Sun, D. Liu, H. Liu, and Q. Sun, “ The Design of SOA-based Multiwavelength Fiber Ring Laser for Fiber Sensing”, Network Comp. Inform. Sci. 3, 41 (2010).
40. L. Denizman, T. Koktay, M. Hack, and T. Eker, “Multi-wavelength spectroscopy of the stable shell star HD 193182”Astrophys. Space Sci. 208(1), 135-151 (1993).
41. M. Yumoto, Y. Maeda, N. Saito, T. Ogawa, M. Yamashita, and S. Wada, “Multi-Wavelength Spectroscopic Application Using Rapid and Random Wavelength-Tuned Mid-Infrared Light Source” Jpn. J. Appl. Phys. 49, 010209 (2010).
42. Y. S. Hurh, G. S. Hwang, J. Y. Jeon, K. G. Lee, K. W. Shin, S. S. Lee, K. Y. Yi, and J. S. Lee, IEEE Photon. Technol. Lett. 17, 696 (2005).
43. Peng-Chun Peng, Hong-Yih Tseng, and Sien Chi A Tuneable Dual-Wavelength Erbium-Doped Fiber Ring Laser Using a Self-Seeded Fabry–Pérot Laser Diode IEEE Photonics Technology Letters, 15(5), 61-663 (2003)
44. Chun-Liu Zhao, Shiquan Yang, Hongyun Meng, Zhaohui Li, Shuzhong Yuan,
45. Kai Guiyun, Xiaoyi Dong Efficient multi-wavelength fiber laser operating in L-band Optics Communications 204 (2002) 323–326

46. Zulkifli MZ1, Ahmad H, Taib JM, Muhammad FD, Dimyati K, Harun SW. "S-band multiwavelength Brillouin/Raman distributed Bragg reflector fiber lasers", Optics Communications 52 (2013) 3753-3756

47. R. W. Tkach, A. R. Chraplyvy, R. M. Derosier, "Performance of WDM network based on stimulated Brillouin scattering," IEEE Photon. Technol. Lett. 1, 111–113 (1989)

48. D. Chen, "Stable multi-wavelength erbium-doped fiber laser based on a photonic crystal fiber Sagnac loop filter" Laser Phys. Lett., 4(6), 437-439 (2007).

49. C. H. Yeh, F. Y. Shih, C. T. Chen, C. N. Lee, and S. Chi, "Multiwavelength erbium fiber ring laser using Sagnac loop and Fabry-Perot laser diode" Laser Phys. Lett. 5, 210-212 (2008).

50. H. Ahmad, S. F. Norizan, M. Z. Zulkifli, and S. W. Harun, Fiber Integrat. Opt. 28, 430 (2009).

51. Z. Y. Liu, Y. G. Liu, J. B. Du, S. Z. Yuan, and X. Y. Dong, "Channel-spacing and wavelength switchable multiwavelength erbium-doped fiber laser using sampled Hi-Bi fiber grating and photonic crystal fiber loop mirror "Laser Phys. Lett. 5, 122-125 (2008).

52. A. Latif, M. Z. Zulkifli, N. A. Hassan, S. W. Harun, Z. A. Ghani, and H. Ahmad, "A compact O-plus C-band switchable quad-wavelength fiber laser using arrayed waveguide grating" Laser Phys. Lett. 7, 597-602 (2010).

53. L. Zhan, J. H. Ji, J. Xia, S. Y. Luo, and Y. X. Xia, Opt. Express. 14, 519 (2006).

54. Z. Zhu, D. J. Gauthier, Y. Okawachi, J. E. Sharping, A. L. Gaeta, R. W. Boyd, and A. E. Willner, J. Opt. Soc. Am. B 22, 2378 (2005).

55. A. A. Bakar, M. H. Al Mansoori, M. A. Mahdi, M. S. Zainal Abidin, and M. A. Mohd Azau, "Fiber break location technique utilizing stimulated Brillouin scattering effects in optical fiber "Laser Phys. Lett. 6, 59-62 (2009).

56. M. H. Al Mansoori, M. K. Abd Rahman, F. R. Mahamd Adikan, and M. A. Mahdi, "Widely tuneable linear cavity multiwavelength Brillouin-Erbium fiber laser", Opt. Express 13, 3471-3476 (2005).

57. M. R. Shirazi, N. S. Shahabuddin, S. N. Aziz, K. Thambiratnam, S. W. Harun, and H. Ahmad, "A linear cavity Brillouin fiber laser with multiple wavelengths output", Laser Phys. Lett. 5, 361-363 (2008).

58. S. W. Harun, S. D. Emami, F. Abd Rahman, S. Z. Muhd Yassin, M. K. Abd Rahman, and H. Ahmad, "Multiwavelength Brillouin/Erbium-Ytterbium fiber laser",Laser Phys. Lett. 4, 601-603 (2007).

59. M. R. Shirazi, S. W. Harun, M. Biglary, and H. Ahmad, "Linear cavity Brillouin fiber laser with improved characteristics" Opt. Lett. 33, 770-772 (2008).

60. M. H. Al Mansoori and M. A. Mahdi, "Multiwavelength L-Band Brillouin–Erbium Comb Fiber Laser Utilizing Nonlinear Amplifying Loop Mirror"J. Lightwave Technol. 27(22), 5038-5044 (2009).

61. M. H. Al Mansoori, M. A. Mahdi, and A. K. Zamzuri, "Tuneable multiwavelength Brillouin-Erbium fiber laser with intra-cavity pre-amplified Brillouin pump" Laser Phys. Lett. 5, 139 (2008).

62. M. H. Al Mansoori, A. W. Naji, S. J. Iqbal, M. K. Ab dullah, and M. A. Mahdi, "L-band Brillouin-Erbium fiber laser pumped with 1480 nm pumping scheme in a linear cavity", Laser Phys. Lett. 4, 371-375 (2007).

63. P. Bayvel and P. M. Radmore, Elect. Lett. 7, 434 (1990).

64. T. Shimizu, K. Nakajima, K. Shiraki, K. Ieda, and I. Sankawa, "Evaluation methods and requirements for the stimulated Brillouin scattering threshold in a single-mode fiber", Opt. Fiber Technol. 14, 10-15 (2008).

65. G. P. Agrawal, Nonlinear Fiber Optics, 2nd ed. (Academic, San Diego, 1995), p. 356.

66. Venkataraayan, K.; Askraba, S.; Alameh, K.E.; Smith, C.L., "Optical-Cavity-Based Multiwavelength Sensor for Spectral Discrimination and Object Position Detection," Lightwave Technology 29(16), pp. 2365-2371, (2011)

67. B. H. Lee, Y. H. Kim, K. S. Park, J. B. Eom, M. J. Kim, B. S. Rho, H. Y. Choi "Interferometric fiber optic sensors", Sensors, 12(3), pp. 2467-2486 (2012)

68. Bunch, Bryan H; Hellemans, Alexander "The History of Science and Technology", Houghton Mifflin Harcourt. pp. 695. (April 2004).

69. Chun Jiang "Modelling a Broadband Bismuth-Doped Fiber Amplifier", IEEE Journal Of Selected Topics In Quantum Electronics, Vol. 15, No. 1, pp. 79 (Feb 2009)

70. Mrinmay P; Somanath B; Palas B; Rimlee D; Paul M.C; Rajan s; Kamal D; Bhadra S.K. " Study of gain flatness for multi-channel amplification in single stage EDFA for WDM applications" Optics Quantum Electronics 39 pp. 1231-1243 (2007)

71. Nusinsky I and Amos A. Hardy "Multichannel Amplification in Strongly Pumped EDFAs" Journal of Lightwave Technology, 22, No. 8, pp. 1946 (Aug 2004)

72. Gumenyuk R.; Golant K.; Okhotnikov O.G. " Energy transition characterization of 1.18 and 1.3 μm bands of Bismuth fiber by spectroscopy of the transient oscillations" Applied Physic Letter 98, No. 19 pp. 191108 (2011)

73. D.W. Stowe, D. R. Moore, and R. G. Priest, "Polarization fading in fiber interferometric sensors," IEEE J. Quantum Electron., QE-18, pp. 626-665 (1982).

74. Lipson, S.G.; Lipson, H.; Tannhauser, D.S. (1995). *Optical Physics* (3rd ed.). London: Cambridge U.P. pp. 248

75. M . Gospodinov , P . Sveshtarov , N . Petkov , T . Milenov , V . Tassev , and A . Nikolov , ''Growth of Large Crystals of Bismuth-Germanium Oxide and Their Physical Properties , '' Bulgarian J . Phys . 16 : 520 – 522 (1989) .

76. A. Cholan, M. H. Al-Mansoori, A. S. M. Noor, A. Ismail and M. A. Mahdi "Flattening effect of four wave mixing on multiwavelength Brillouin-erbium fiber laser", Appl. Phys. B, pp. 112-215 (2013)

List of Publications

Publications related to the thesis title:

1. H. Ahmad, S. F. Norizan, M. Z. Zulkifli, Z. A. Ghani and S. W. Harun, Operation of Brillouin fiber laser in the O-band region as compared to that in the C-band region, Laser Physics, Vol. 21, No. 1, pp. 1-5 2011.

2. H. Ahmad, S. F. Norizan, M. Z. Zulkifli, C. H. Pua, Z. A. Ghani and S. W. Harun, Investigation of O-band Brillouin Fiber Laser Flatness at Different SOA Location, Journal of Modern Optics, Vol. 58. No.7, pp.580-586 2011

3. S. F.Norizan, W. Y. Chong, S. W. Harun, H. Ahmad, O-Band Bismuth-Doped Fiber Amplifier With Double-Pass Configuration, IEEE Photonics Technology Letters Vol. 23 Issue 24 pp. 1860-1862 (2011)

4. H. Ahmad, S. F. Norizan, N.A. Awang , Tunable Microwave Photonic Frequencies Generation Based on Stimulated Brillouin Scattering Operating in the L-Band Region, Microwave and Optical Technology Letters Vol.53, Issue 8, pp. 1710-1713 (2011)

Other publications:

1. H. Ahmad, S. F. Norizan, M. Z. Zulkifli, S. W. Harun, Dual-Wavelength Erbium Fiber Laser in a Simple Ring Cavity, Fiber and Integrated Optics, Vol. 28, Issue 6 pp. 430 – 439, 2009

2. H. Ahmad, M. Z. Zulkifli, S. F. Norizan, and A. A. Latif, Controllable Wavelength Channels for Multiwavelength Brillouin Bismuth/Erbium Based Fiber Laser, Progress In Electromagnetics Research Letters, Vol. 9, 9 18, 2009

3. Ahmad, H., S. F. Norizan, A. Hamzah, and S. W. Harun, Double-pass Raman amplifier for gain enhancement and gain clamping, Optoelectronics and Advanced Materials Rapid Communication, Vol. 3, No. 9, 924-926, 2009.

4. H. Ahmad, M.Z. Zulkifli, K. Thambiratnam, S.F. Norizan, S.W. Harun, High power and compact switchable bismuth based multiwavelength fiber laser, Laser Physics Letters, Volume 6 Issue 5, pp 380 – 383**,** **(**2009).

5. N.A. Awang, M. Z. Zulkifli, S. F. Norizan, S. W. Harun, Z. A. Ghani, H. Ahmad, Highly Efficient and High Output Power of Erbium Doped Fiber Laser in a Linear Cavity Configuration, Laser Physics, Vol. 20, Issue 10, pp. 1894-1898, 2010.

6. H. Ahmad**,** A.A. Latif**,** S.F. Norizan**,** M.Z. Zulkifli **and** S.W. Harun**,** Flat and compact switchable dual wavelength output at 1060 nm from ytterbium doped fiber laser with an AWG as a wavelength selector, Optics & Laser Technology, Vol. 43, Issue 3, pp.550-554, 2011.

7. S. Shahi, S.W. Harun, S.F Norizan, H. Ahmad, Brillouin–Raman Multi-Wavelength Laser Comb Generation Based On Bi-Edf By Using Dual-Wavelength In Dispersion Compensating Fiber Journal Of Nonlinear Optical Physics & Materials, Vol. 19, Issue. 1 pp. 123-130 (2010)

8. H. Ahmad, M.Z. Zulkifli, S. F. Norizan, M. H. Jemangin, and S. W. Harun, S-band multiwavelength Brillouin Raman Fiber Laser, Optics Communications Vol. 284 Issues 20 pp. 4971-4974 (2011)

9. Electrically Tunable Microfiber Knot Resonator Based Erbium-Doped Fiber Laser, IEEE Journal of Quantum Electronics, Vol. 48, Issues 4, pp. 443-446 (2012)

10. A.Sulaiman, S.W. Harun, F. Ahmad, S.F. Norizan, H. Ahmad, Tunable laser generation with erbium-doped microfiber knot resonator, Laser Physic, Vol. 22 Issue 3 pp. 588-591 (2012)

List of Awards

1. Silver Medal "Tunable Multiwavelength Fiber Laser using AWG and FBG" University of Malaya, Research and Invoation Expo 2009 (UMEXPO)

2. Gold Medal "An All-Optical Frequency Up/Down Converter Utilizing Stimulated Brillouin and Raman Scattering in Truewave Reach Fiber and Dispersion Compensating Fiber for Radio Over Fiber Application" University of Malaya, Inovation and Creativity Expo 2010

3. Bronze "Low Cost Tunable Laser Diode" University of Malaya, Inovation and Creativity Expo 2010